Appendix D

Calibration of historical earthquakes for the earthquake catalogue of Switzerland (ECOS-09)

Sonia Álvarez-Rubio, Philipp Kästli, Donat Fäh, Souad Sellami
(March 2010)

Content

1 Introduction

The macroseismic intensity is a semi-empirical measure for earthquake effects, and indirectly, earthquake size. When assessed at a sufficiently large number of sites (usually settlements or zip code areas), it can show regular regional patterns that can be related to earthquake size, variation of energy dissipation and absorption, site response, and focal depth. In this work the macroseismic field is used to parameterize historical earthquakes, assessing earthquake parameters such as location, magnitude, and, if possible, depth.

The final calibration of historical earthquake parameterization in ECOS-09 follows the same strategy as that applied in ECOS-02 (Swiss Seismological Service, 2002; Fäh et al., 2003). This is an approach that determines earthquake source parameters, location and magnitude directly through a continuous regression of individual intensity observations. The method is generally known as the “Bakun-Wentworth method” (hereafter referred as the *BW method*) (Bakun and Wentworth, 1997). The main issue is that the coefficients defining the intensity attenuation model require calibration. This calibration procedure is one of the main steps in establishing a regional model (Bakun and Wentworth, 1997; Hinzen and Oemisch, 2001; Bakun and Scotti, 2006; Musson et al., 2008). In principle, a point source model is assumed with a certain focal depth *h* and an appropriate relation for intensity attenuation with source distance:

$$I = f\left(M, d\right) \qquad (1)$$

where *d is* distance from the source to the intensity data points (IDPs), and *M* stands for the magnitude. The coefficients defining the relation are obtained from the calibration process; using events with well constrained moment magnitudes and source locations derived from instrumental data along with their related macroseismic observations. Once the relation is implemented in the BW method, a residual minimization technique is applied over a search grid, taking the magnitude as an unknown variable. Each grid point is treated as a potential epicenter where, given equation (1), its mean magnitude (as inferred from individual intensity assignments) is calculated. The root mean square (RMS) of model deviations for individual intensity points is used as the penalty function to assess location quality. The results of this minimization are a probability distribution function that characterizes the likelihood of an epicenter being at a given location, and a second surface that, assuming the epicenter is at a given location, shows its preferred magnitude. With a consistent dataset, the locations of the minimum RMS and inferred magnitude are expected to be co-located. However, as a result of, for instance, incomplete intensity fields, radiation effects, and site effects, they may diverge. Further details about the application of this technique are given in the aforementioned references. In ECOS-09 we assessed location and magnitude using expert judgment that was based on the distributions of RMS and magnitude, as well as on a priori knowledge of the seismotectonic setting and from historical sources. We also addressed depth as a variable of the intensity attenuation model, and estimated parameter uncertainty.

In this work, we present the different stages of the ECOS-09 calibration initiative and its results. Other calibration exercises based on different approaches have been carried out together with ECOS-09 and are used for consistency checks. These are: the Boxer method and the calibration applied in ECOS-02 (see Appendix E). The conclusions have been used as feedback in many aspects for the final calibration and parameterization of historical earthquakes in ECOS-09.

2 Calibration procedure

Following the strategy of ECOS-02, we have addressed the parameterization of historical earthquakes in a two-stage analysis procedure that decouples the estimation of the distance dependence of the intensity field from the estimation of magnitude. Initially different intensity attenuation relations were selected. These were then fit to a set of macroseismic calibration events (see 2.3) and those attenuation models that exhibited poor performance in describing the observed intensity fields were discarded.

Secondly, we inferred a magnitude to standardized-intensity relation for the chosen relations, in order to estimate the macroseismic magnitude. For this purpose we used a reduced calibration dataset with events that had instrumentally derived Mw available.

The ability to reproduce the instrumental magnitudes was used as an additional selection criterion for the macroseismic attenuation relationship.
Finally, we applied the best strategies to the earthquakes in the historical catalogue, whilst constraining the solution with historical knowledge.
The calibration procedure also consists of other aspects related to IDP processing, which are crucial for an adequate performance. As such, we carefully investigated issues such as 1) the removal of outlier events and IDPs from the calibration dataset for an optimum statistical performance, 2) the weighting scheme applied to the macroseismic field to assess the calibrated coefficients of the attenuation model, 3) the ability to infer a curve to derive a macroseismic magnitude from a reference intensity, and 4) the definition of the cutoff distances used in order to avoid effects of incompleteness and sampling bias in the macroseismic far-field. We also investigated the importance of site conditions. These different phases of the study are summarized in Figure 1, and are further discussed in the following sections.

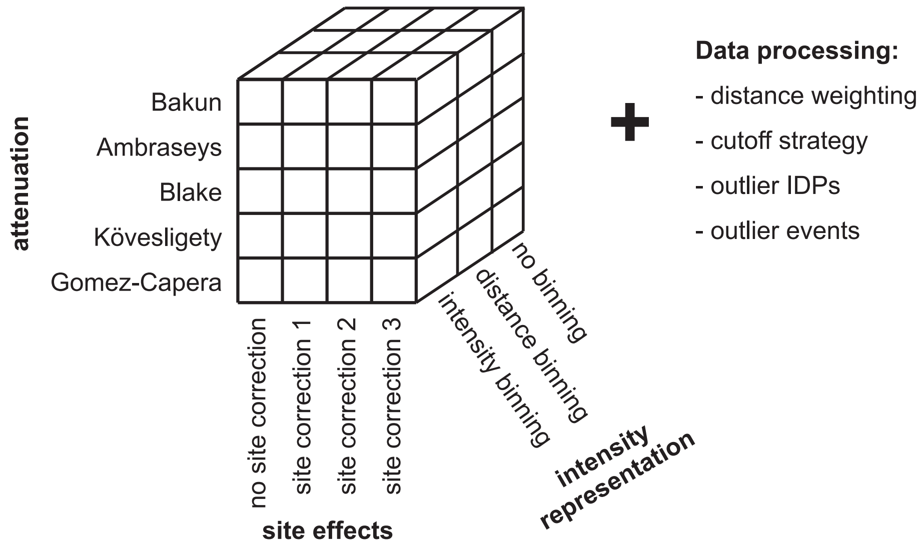

Figure 1. Representation of the phases that constitute the different strategies involved in the calibration procedure.

2.1 Attenuation estimation

For the estimation of location, we selected an intensity attenuation model by testing several models that relate the decay of intensity to distance and, in some cases, focal depth. The calibration of the coefficients of the models is performed through the following iterative process.
In general, attenuation is assessed by describing the decay of intensity with reference to a scaling intensity:

$$I_{obs} - I_{sc} = f\left(d, h\right) \tag{2}$$

where I_{obs} are the observed intensity data points, IDPs; I_{sc} is the event-individual scaling intensity derived from the iteration process detailed below; *d* stands for distance (epicentral, *D*, or hypocentral, *R*) and *h* is the focal depth.
We assessed the general attenuation coefficients *a*, *b*, etc., of equation 2 as well as the event-individual parameters I_{sc} and *h*, using the following iterative procedure:

1. $I_{\max}$ is used as a proxy of I_{sc}, whilst *h* is fixed at 10km. A set of coefficients *a*, *b*, … is derived for the attenuation description *f(d, h)* from all calibration events.
2. For each event, a new I_{sc} and *h* are derived that minimize the RMS of *f(d, h, a, b,…)*.
3. Given the new event-individual I_{sc} and *h*, a new set of *a*, *b*, … are derived, minimizing the RMS of the attenuation over all calibration events.
4. As step 2.

This procedure is repeated until I_{sc} becomes stable (changes less than by 0.02 in an iteration) for all events. For attenuation relationships that are not dependent on *h* (*fixed-depth strategy*), the same procedure was used without fitting *h* for each event.
For the *variable depth strategy*, we allowed *h* to vary between 3 and 25 km. By comparing the fixed and variable depth strategies, we were able to estimate the influence of depth on the event scaling intensity I_{sc}, and the contribution of depth to the explanation of the intensity fields.
In a third strategy ("*mixed*"), used as a performance test, we fixed the depth for those calibration events where depth is known from instrumental assessment or using known seismological constraints (for example, the fact that no events occur below 15km in the Alps), while for the other events, we used depth as a fitting parameter.

2.2 Magnitude calibration

The calibration of the macroseismic magnitude is assessed independent of the calibration of the attenuation of the intensity with distance and depth. For each attenuation model we infer the event-individual scaling intensity at a standard hypocentral distance I_{st}. Then we estimate the macroseismic magnitude as a linear fit to that standardized intensity:

$$M = \alpha I_{st} + \beta . \tag{3}$$

To formalize the intensity decay and therefore the calibration of magnitude we have tested different models. In the following section we present a summary of all these models and their characteristics.

2.3 Intensity attenuation models

The literature provides a number of empirical models that define the attenuation of the intensity assignments with distance (e.g. Gómez Capera, 2006; Musson et al., 2008). The intensity increases with the magnitude and decreases with the distance, but there are other factors that contribute to the variations of the intensity field: for instance, azimuthal variations, path effects, and site effects. We have tested different intensity attenuation relations in terms of: the variables involved (epicentral and hypocentral distances, and depth), and the functional form (linear, logarithmic or cubic). Table 1 lists the different models tested during the calibration initiative.

Based on	Intensity attenuation models
Kôveslighety (1906)	$I - I_0 = aLog\left(D/h\right) + b\left(D - h\right)$
Ambraseys (1985)	$I - I_0 = aLog\left(R/h\right) + b\left(R - h\right)$
Blake (1941)	$I - I_0 = aLog(R) + b$
Bakun and Wentworth (1997)	$I - I_0 = aD + b$
Gómez Capera (2006)	$I - I_0 = a\sqrt[3]{R} + b$

Table 1. Different intensity attenuation models tested in the ECOS-09 calibration initiative. I=intensity assignment, Io= intercept intensity, R = hypocentral distance (km), D = epicentral distance (km); h = focal depth (km), and a and b are constants.

2.4 Calibration datasets

To perform the calibration of the intensity attenuation relationship, we assembled *calibration dataset 1*. This consists of events located in Switzerland and border regions. The incorporation of macroseismic data from adjoining foreign regions benefits the calibration and allows for a better regional intensity attenuation model that will better estimate location and magnitude for critical historical earthquakes. Therefore, intensity data from Sisfrance (www.sisfrance.net, last accessed November 5, 2008) and for selected events from INGV (DBMI04, http://emidius.mi.ingv.it/DBMI04/) are included in the calibration dataset.
The events within calibration dataset 1 have a known location and good intensity fields. They are mainly the instrumentally located events of the 20th century with Ml > 3.2. However, older events from the 19th and 20th centuries are added to the datasets if their known macroseismic field contains at least 10 intensity data points (IDPs) with intensity greater than or equal to 3. Calibration dataset 1 includes, for example, the events occurring on 29/10/1835, 17/08/1846, the 1855 mainshock 25/07/1855, 27/01/1881, 18/11/1881, 13/04/1885, 22/02/1898, 06/05/1898, and 26/05/1910. *Figure 2* shows the number of IDPs contained in the calibration dataset for the different magnitude ranges.

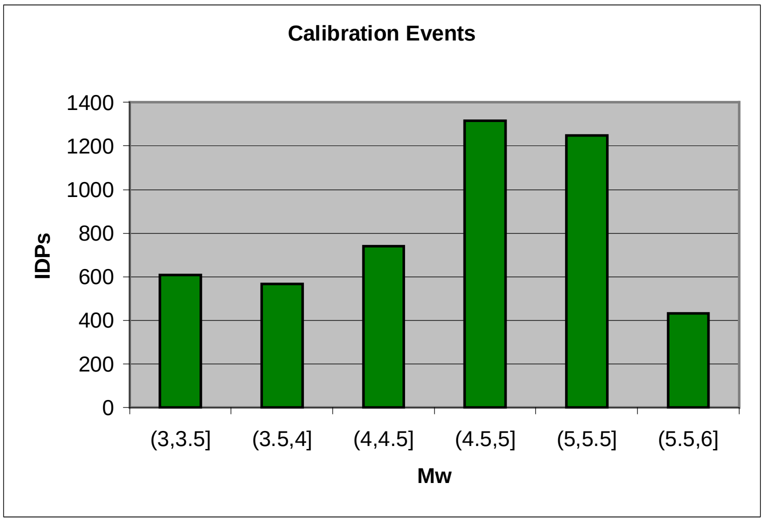

Figure 2 Number of IDPs of the calibration events for different magnitude ranges.

Calibration dataset 1 has been reduced in three steps resulting in three new calibration datasets that have been used in the calibration procedure:

Calibration dataset 2: Events with one or more of the following features in the intensity field were removed:
- events with the near-source part of the intensity field missing (e.g., foreign events);
- events where the range of reported intensities is in only one or two intensity classes;
- events with IDP fields that are probably mislocated: for instance, where all of the highest intensities are reported at distances of greater than around 20 km from the epicenter, whereas for the given epicenter, only smaller intensities are reported;
- aftershocks shortly after the main event (where intensity assessments could be biased).

  The total number of events in dataset 2 is 111.

Calibration dataset 3: the same restrictions as above were applied. Furthermore, events with the following properties were removed:
- Those with few IDPs (< ~10-15), including events in the 20th century;
- Events where IDPs are distributed over a small range of epicentral distances with a large range of reported intensities, for which we can assume that the macroseismic field is incomplete. In such cases, the missing medium- or far-field observations may be mistaken as an effect of very strong intensity decay.

Calibration dataset 4: The following events were removed from dataset 3:
- Non-damaging events;
- Events with a density of the macroseismic field which strongly varies with distance;
- Events where the best-fitting attenuation relationship still does not describe the general trend of the observed attenuation, or features many outliers (> ~10%) with more than two intensity units deviation from the general attenuation trend.

For the assessment of potential regional variation, we defined alpine and foreland events based on the following rule:

Alpine: $Y_{CH} \le \left(150000 + \left(X_{CH} - 540000\right)/2.1\right)$,

with $\left(X_{CH}, Y_{CH}\right)$ being the epicenter location using the Swiss national grid coordinate system in meters. This definition roughly describes a straight line from Lausanne to St. Gallen. For the small datasets (calibration datasets 3 and 4), we made an exception to the definition above, and referred to events 10500 and 10600 in the St. Galler Rhine valley as foreland events. This was due to the fact that the local geology in the epicentral area of these events is a deep sedimentary basin, which is more similar to Swiss foreland conditions.

For the standardized intensity to moment magnitude calibration, a decision was made to use the subset of events with an instrumentally derived Mw (either direct Mw calculations or the values published by Bernardi et. al. (2005) that are based on Ms) These Mw are hereafter called *Mw(bestmag)*, which at present are considered the most reliable values. These magnitudes were selected with the following criteria and order:

- For pre-2003 events the Mw value estimates in Bernardi et al. (2005) are used.
- For recent events, the magnitude of the Swiss local moment tensor catalog (http://www.seismo.ethz.ch/mt/RTMT/RTMT_SWISS.php) was used as long as the moment tensor model had a variability reduction of greater than or equal to 50%. This corresponds to moment tensors rated as quality ‘A’.
- When the above two Mw values were not available (independent of the quality reduction), Mw values from the online regional moment tensor catalog ("Braunmiller catalog", http://www.seismo.ethz.ch/mt/) were used.
- Magnitudes not reported above, but published in Braunmiller et al. (2005) for events before the 2001.

This defines a set of 50 events, of which 38 overlap with dataset 2, 20 with dataset 3, and 14 with dataset 4 (see Tables in chapter 4 of this report).

2.5 Data processing: weighting scheme, binning-intensity strategies, and removal of event outliers

In order to reduce the bias in the macroseismic intensity field due to reasons such as: heterogeneous distributions, incompleteness of certain intensity classes, poor data quality, significant variability of effects observed close to the epicenter, anomalously high intensity levels reported far from the epicenter, we have processed the calibration dataset applying different strategies. The attenuation relationships have been calibrated using the following weighting schemes:

- *No binning* of the IDPs. This procedure offers full error control and is the most consistent approach with the Bakun-Wentworth technique. Usually assessments based on individual IDPs are combined with a distance weighting, in order to correct for the geometrical skew in the number of IDPs (the area and hence, to an extent, the number of IDPs within the radius d from the epicentre increases proportional to d^2).
- *Distance-binning* (Gasperini, 2001; Fäh et al., 2003). This is applied in conformal bin sizes, attributing them with the mean or median distance, and observed intensity. This approach removes outliers, however, error control is reduced.

- *Intensity-binning* (Bakun and Wentworth, 1997, Hinzen and Oemisch, 2001; Bakun and Scotti, 2006). Each intensity class is attributed with the mean or median distance of the corresponding IDPs. This removes outliers, however the error control is reduced. There might be a geometric skew. Intensity-binning can be applied only to non-site corrected data.

Both binning methods remove outliers and reduce data scatter. What appears to be a clearer conformation with an attenuation law comes at the cost of a loss of error control (standard deviation introduced by the single intensity observations), as well as information on non-symmetric intensity or distance distributions within the bins. Therefore, attenuation relationships parameterized from binned data are not necessarily consistent with an application in the style of the Bakun and Wentworth (single IDP based) application context. Both binning strategies also introduce an implicit distance weighting and, in addition, possibly an overweighting of IDPs from sparsely sampled distance ranges or intensity classes. In addition intensity binning cannot be applied with site-corrected data (which would lead to floating point, rather than ordinal, intensity values).

We mostly worked with individual IDPs and to some extent with distance-binning. Only a small amount of testing was done with intensity binning, taking into account the possible limitations given above.

For the model parameter estimation, weighting schemes have been used to account for the increase in area with distance, and to avoid the influence of the incompleteness within certain intensity classes. We have implemented:

1. no weighting, with varying cutoff distances;
2. quadratic weight decay within 200 km:

$$w = \left(200 - d \big/ 200\right)^2 \tag{4}$$

3. area – conformal weighting:

$$w = 10 \Big/ \sqrt{10 + (d)^2} \tag{5}$$

Without weighting the resulting event-individual scaling intensities strongly depend on the cutoff distance. This was due to the fact that at cutoff distances close to the radius of the felt area of an event, the intensity decay is controlled by the absolute size of the event rather than by distance. With distance weighting the difference between weighting methods 2 and 3 was minimal. The two weighting schemes applied along with the same attenuation relationship resulted in a difference in the scaling intensity of ≤ 0.05 intensity units for the calibration events. In the further procedures, we therefore applied weighting scheme 2.

For calibration with events with known epicenters, a strong decay of weighting in the near-field allows the adequate representation of the attenuation behavior close to the epicenter, where the highest intensities are usually represented with only a few IDPs. In contrast, in the application of the Bakun algorithm, where the epicenter is unknown, a strong decay of weighting in the near field could lead to unstable results. To avoid this, we applied the Bakun search algorithm with a cosine-based weighting scheme (Swiss Seismological Service, 2002). This weighting function shows a similar functional form to weighting scheme 2 used for calibration, but it is less sensitive to mislocation.

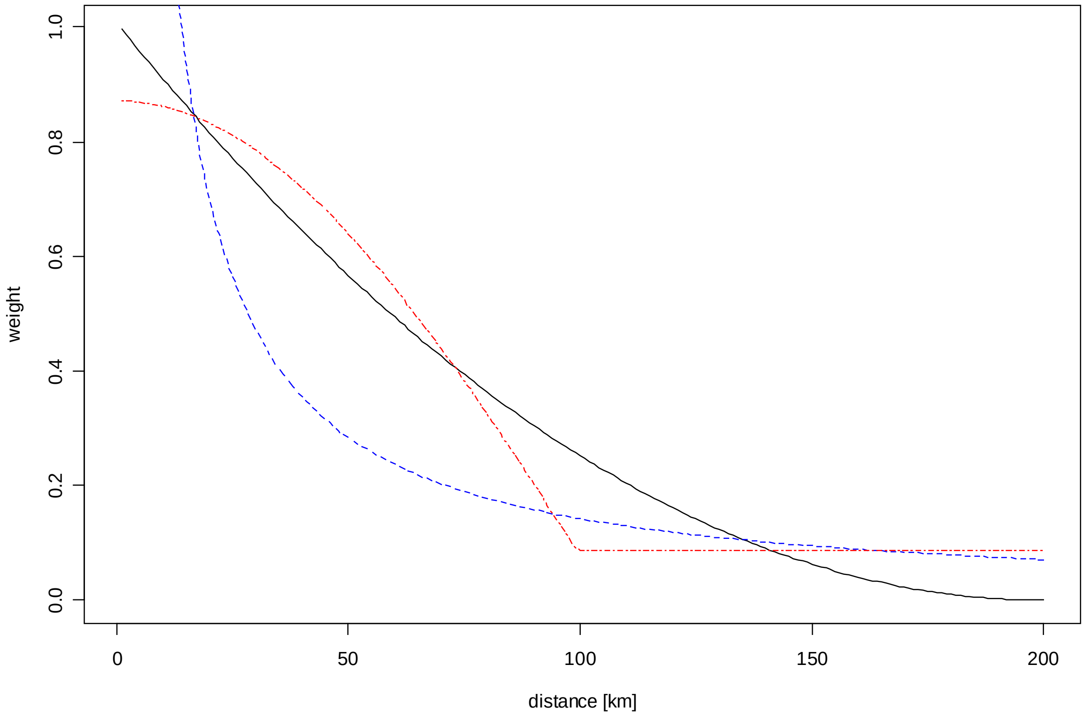

Figure 3. Different IDP weighting schemes used: Black line: quadratic decay used for calibration; Blue dashed line: area-conformal weighting tested for calibration with similar results to that of the quadratic decay; Red dot-dashed line: The cosine-conformal weighting applied with the Bakun search algorithms (here with cutoff distance 100 km). This weighting scheme mimics the quadratic decay without the sensitivity for small mis-fits of the epicenter.

The strategy to derive the intensity attenuation independently from the I_{st}-Magnitude relation requires two assumptions:

A. Intensity decay follows the same law, or functional form, over the entire intensity scale;
B. All intensity data used has a comparable relevance to describe intensity decay, independently of whether they are from a large or a small event.

Assumption A is not necessarily true, as intensity is an ordinal scale, which does not imply, nor is designed for the fact, that the same change in intensity represents the same change of any physical ground motion parameter.
Assumption B may also be problematic: firstly, intensity data from small events only describe a small range of intensity decay, while large events contribute to the description of a larger range of decay over several intensity classes.
We have developed 5 strategies to explore and handle these problems:

1. Applying a general distance cutoff for all events;
2. Applying an event-individual distance cutoff, depending on event size;
3. Include only the highest (e.g., top 3) intensity levels;
4. Include all intensities from a certain level upwards (e.g., Intensity >= III);

5. Include a uniform range of intensities for all events, e.g., at intensities IV to VI only.

The cutoff distance has a large impact on the attenuation parameters. However, there is no clear method of selecting the "ideal" general cutoff distance. Changing the distance just changes the mix of the near-source and far-field intensity fields. We therefore discarded this strategy.

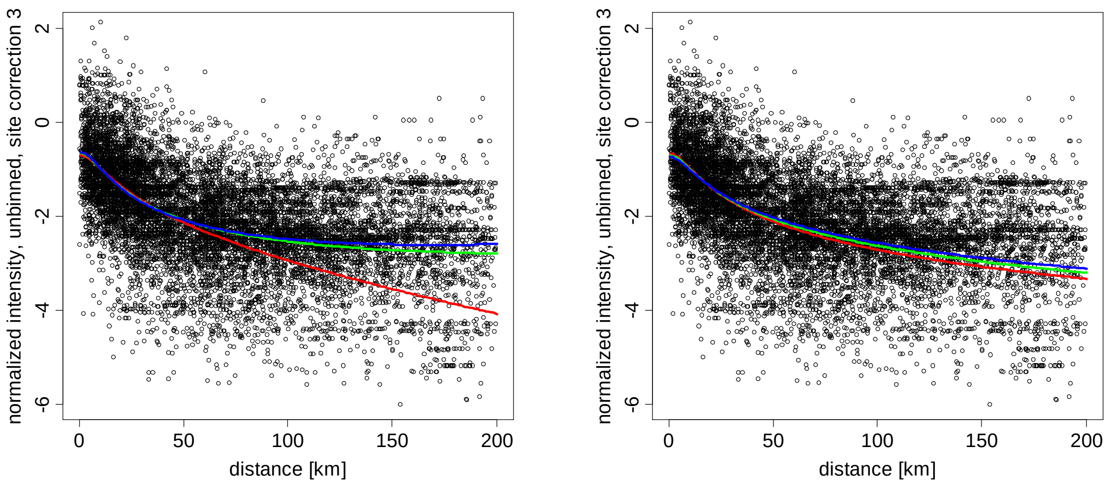

Figure 4. Intensity models derived from the first 60km (red), 100km (green) and 150km (blue) of intensity data. While the resulting model with a logarithmic and linear term strongly depends on the cutoff distance, the logarithmic model is unable to describe the far field due a lack of degrees of freedom. (a) model with a logarithmic and linear term; (b) logarithmic model.

With strategy 2, the cutoff distance depends on event-size, and is defined by the distance at which the expected intensity drops under a certain value. Because we separated intensity attenuation from magnitude determination, this strategy is impractical. Strategies 3 to 5 avoid the problem of cutoff distance by using a cutoff intensity. Strategy 3 is based on the assumption that the area with the highest intensity is sampled best and uses this for event-individual intensity cutoff. While this assumption is well founded (especially for historic catalogues where the level of completeness in event size increases with decreasing age along with the level of minimum intensity in the available reports), it is vulnerable to deviations from assumption A of a homogeneous intensity attenuation law. Strategy 5 avoids the problems of assumption A by working with a relatively small range of intensity levels (IV to VI) that are available for many events, however, it is not applicable to medieval events where intensity levels <= VI are rarely reported. Strategy 4 provides a compromise between the advantages and disadvantages of strategies 3 and 5.

As shown later in the results section, strategies 3 to 5 perform similarly in describing the intensity fields as well as in producing scaling intensities that fit the Mw of the magnitude calibration dataset. However, because of the lack of applicability of strategy 5 for some events, only strategy 3 and 4 were used in event parameter assessment.

Intensity outlier removal is a non-trivial task. This is due to the presence of three different types of outliers, of which only type 2 and 3 should really be removed:

1. Outstanding intensity points that may be real, e.g., due to site amplification effects;

2. Erroneous interpretation of incomplete information (e.g., assumptions of building types in cases where only coarse damage descriptions are available, or assumptions related to effects reported only by a single person, or for one building);
3. They may be completely wrong, due to incorrect reporting, mis-location of the site the report refers to, or the incorrect identification of the described event.

We tested the removal of outliers based on their deviation from the best-fitting attenuation law. This removes some outliers of all types, but it leads to an underestimation of parameter uncertainty, as type 1 outliers are also affected. To avoid this, we abandoned the idea of specific outlier removal. We applied then only the before mentioned distance weighting, which might remove some of the erroneous macroseismic information described above in 2 and 3.

3 Results of the calibration

3.1 Intensity attenuation model

All attenuation models listed in Table 1 were calibrated using the four calibration datasets defined in 2.4: datasets 2, 3, 4, and the regionalized datasets ‘alpine’ and ‘foreland’. The different phases of the procedure are as follows: the decisions made on the processing of the data; such as the weighting schemes, cutoff distances, and removal of outliers (see section 2.5) were followed. The results for the different functional forms in Table 1 were analyzed and the most suitable intensity attenuation models were chosen. For these models the coefficients were calibrated according to the macroseismic information used: all IDPs available (intensity three and above) for each event (*allint*); only the three highest intensity levels (*top3*); and using the intermediate intensity levels (*int4_6*). The calibration coefficients of the intensity attenuation models were obtained through the iteration process described in section 2.1, and following the three strategies established in terms of the treatment of the focal depth: *fixed depth, variable depth* and *mixed strategy*.

Each calibration exercise can be defined in terms of: the attenuation model, the region where it is applied, the calibration dataset, the intensity field used within the calibration dataset and the depth strategy. For the calibration of the macroseismic magnitude, we developed for each attenuation model a specific scaling intensity to magnitude relation, and applied different weighting schemes to the calibration events used.

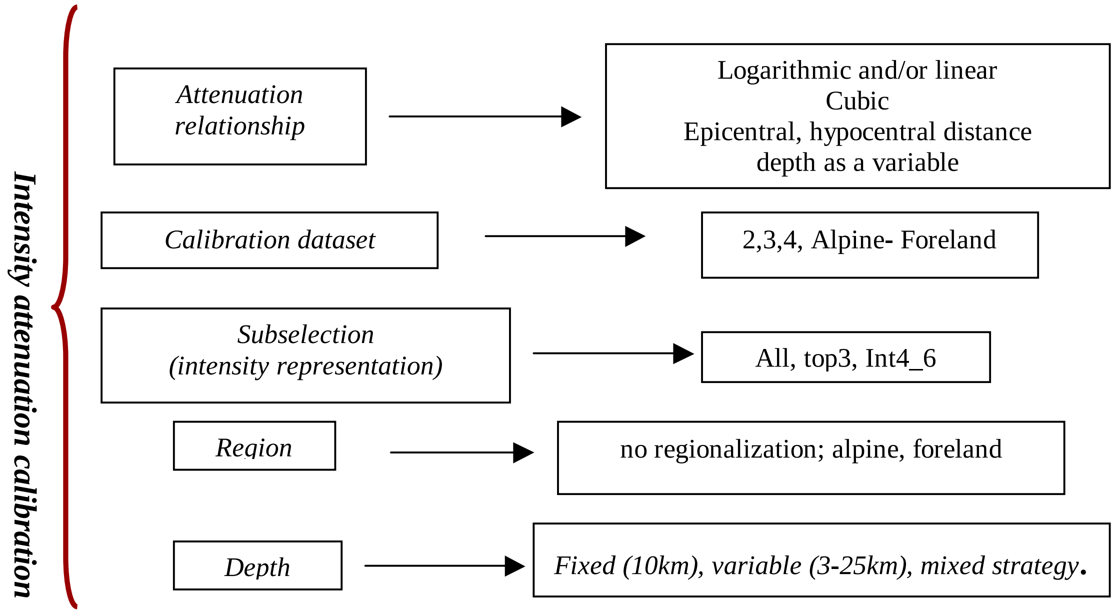

Figure 5. The different calibration strategies for intensity attenuation models and their characteristics.

One of the first results of this calibration is that those models established in terms of the epicentral distance were discarded as they were unable to resolve focal depth. Therefore our set of models is reduced to the types in Table 2.

Definition	Intensity attenuation model formulation
Logarithmic and linear model	$I - I_{sc} = aLn\left(R/h\right) + b\left(R - h\right)$
Logarithmic model	$I - I_{sc} = aLn(R) + b$
Cubic model	$I - I_{sc} = a\sqrt[3]{R}$

Table 2. Remaining intensity attenuation models that have been investigated in the final phase of ECOS-09. (R: hypocentral distance; h: focal depth; a and b: coefficients of the model).

The results of the fit of the models in Table 2 for fixed depth, taking depth as *10km* in all cases, were initially analyzed. As shown in Figure 6 the model with a *logarithmic and linear* term gives consistently better results over different strategies. Therefore this functional form was selected, and from now on it will be referred to as the *ECOS-09 intensity attenuation model*.
In the calibration exercise carried out with the Boxer method (see Appendix E) it was observed that, due to completeness problems in certain intensity classes, the estimation of macroseismic parameters can be improved when assessing only the three highest intensity levels (*top3*). For this reason the calibration coefficients of the chosen functional forms are derived with two intensity representations: *allint* and *top3*.
The attenuation model derived from dataset 2 can describe attenuation equally well as that from dataset 3. Only the attenuation in dataset 4 is better described, however this

may be expected, as the fitting quality of the attenuation relation was used for event selection in dataset 4.

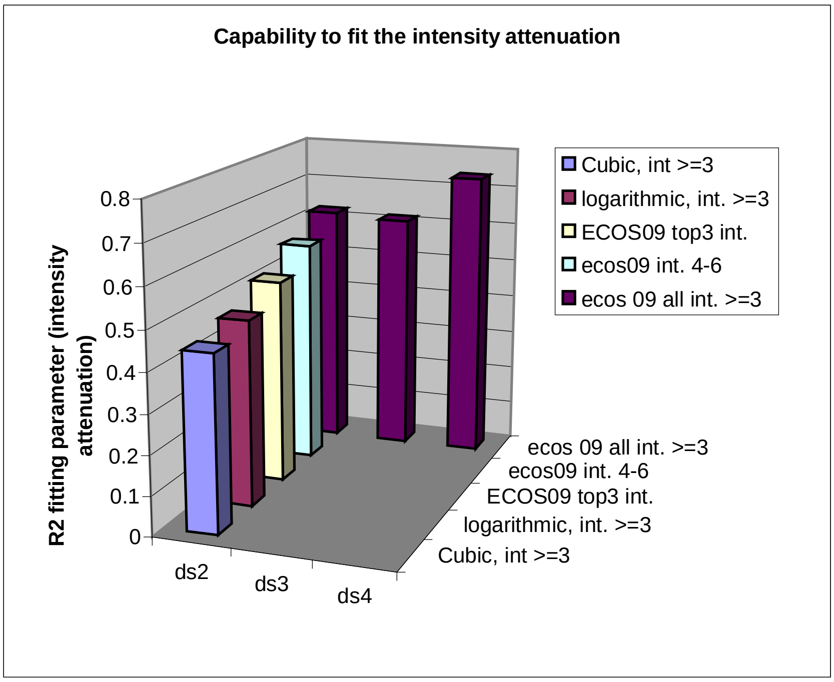

Figure 6. Capability of describing the intensity attenuation, measured by the coefficient of determination R2 fitting parameter for different functional forms (cubic, logarithmic, ECOS-09 with a logarithmic and a linear term) using calibration datasets 2, 3, and 4 (ds2, ds3, ds4 respectively), and different intensity classes (intensity >=3, intensities in the classes 4-6, and top 3 intensity classes).

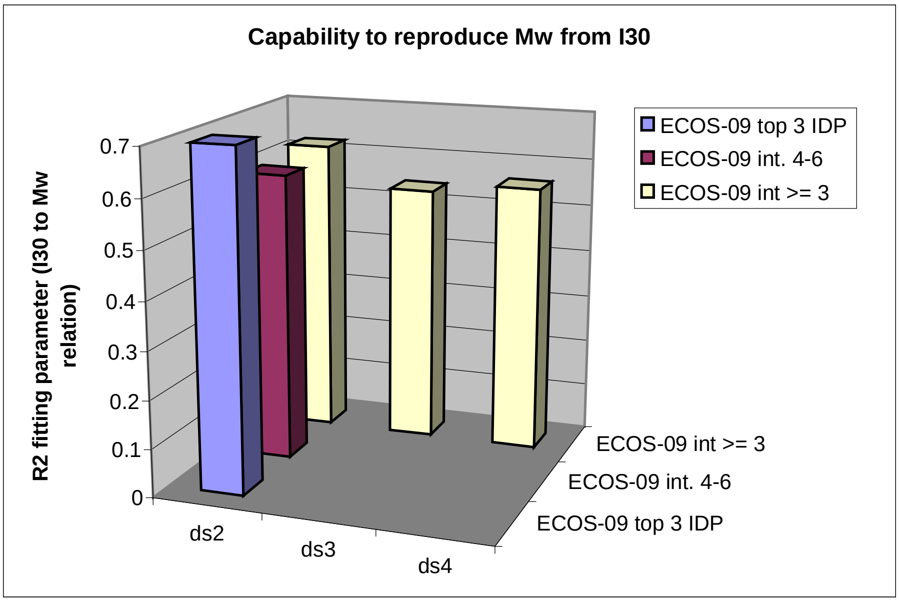

Figure 7. Fitting quality of different I_{30} (standardized intensity as intercept at 30km hypocentral distance) to magnitude relationships, measured by the coefficient of determination R2.

The standardized intensity to magnitude relation from dataset 2 is better confined than those from dataset 3 or 4 (see Figure 7). For this reason we use relations mainly based on this dataset for our further work. The standardized intensity to magnitude relationship based on the attenuation of "top3" intensities shows the best fit. We have addressed the estimation of focal depth, with the variable depth strategy, which allows depths ranging from 3 to 25 km. A series of sensitivity analyses was performed, where the quality of the macroseismic field used was improved by starting with dataset 2, then dataset 3 and finally dataset 4. The reduction of the number of events from one dataset to another means that a particular event can be better fitted with an event-individual scaling intensity and focal depth. In Figure 8, a sample of ECOS-09 intensity attenuation models are depicted for three different depths. Table 3 provides the different calibration coefficients.

ECOS-09 intensity attenuation model Strategy				Calibrated coefficients	
Calibration dataset	Intensity representation	Regionalization	depth	Logarithmic coefficient (a)	Linear coefficient (b)
2	All intensity levels$^{(*)}$	-	Fixed depth (h=10Km)	-0.67755	-0.00174
2	Three highest intensity levels	-	Fixed depth (h=10Km)	-0.4834	-0.00179
2	Intermediate intensity levels 4-6	-	Variable depth (h=3-25Km)	-0.71377	-0.00125
2	All intensity levels$^{(*)}$	-	Variable depth (h=3-25Km)	-0.69182	-0.00084
2	Three highest intensity levels	-	Variable depth (h=3-25Km)	-0.50945	-0.00192
3	All intensity levels$^{(*)}$	-	Variable depth (h=3-25Km)	-0.79156	-0.0002
3	All intensity levels$^{(*))}$	-	mixed strategy	-0.81028	0.00028
3	All intensity levels$^{(*)}$	alpine	Variable depth (h=3-25Km)	-1.07853	0.00414
3	All intensity levels$^{(*)}$	foreland	Variable depth (h=3-25Km)	-0.56258	-0.00255

Table 3. Calibrated coefficients of ECOS-09 intensity attenuation models for the different strategies investigated. (*) Intensity three and larger.

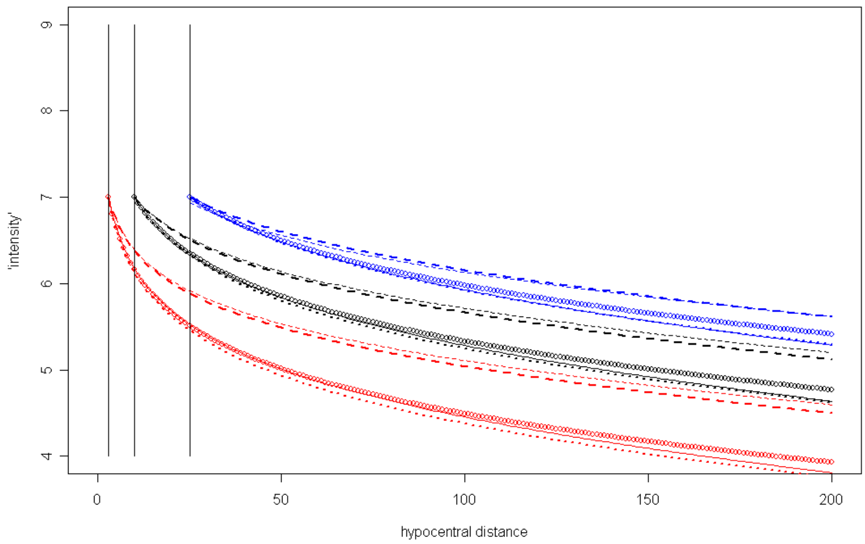

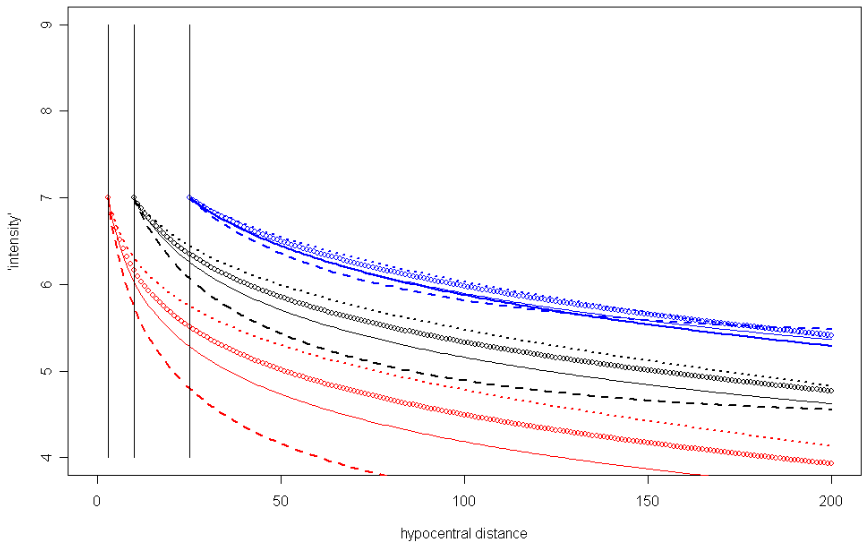

Figure 8. Attenuation models derived from dataset 2 and 3 compared to each other. Red=3km depth; black = 10 km depth; blue = 25 km depth. Hypocentral distance is given in km.

Top) Circles: dataset 2, variable depth, all intensities; Line: dataset 2, fixed depth, all intensities; Bold dashes: dataset 2, top 3 intensities, variable depth; Small dashes: dataset 2, top 3 intensities, fixed depth; Dots: dataset 2, intensities 4-6, variable depth.

Bottom) Circles: dataset 2, variable depth, all intensities; thick line: dataset 3, variable depth, all intensities; thin line: dataset 3, mixed depth strategy; dashed line: dataset 3, Alpine events, variable depth; dotted line: dataset 3, foreland events, variable depth.

The results in Figure 8 show that the derived intensity attenuations are different when using all intensities or only the three highest intensity classes. Intensity attenuation is similar for dataset 2 and dataset 3. For dataset 3 - alpine events the results are however rather different. The results of dataset 4 are not shown here, because the restricted magnitude range of the calibration events does not allow the development a reliable standardized intensity to magnitude relation. The same problem occurs with the models using foreland events only.

It was always the case that the largest dataset, *dataset 2*, allowed us to derive a meaningful magnitude to standardized intensity relation. Therefore the estimation of the macroseismic parameters for the application of the *BW* grid search technique will be achieved by implementing the *ECOS-09* attenuation models calibrated with strategies based mostly on dataset 2. Dataset 3 - alpine events is an interesting case that was also implemented in order to observe the effect of the regionalization on the macroseismic parameters.

Within the variable depth approach, the question: “can we determine the depth from historical events in a reliable way?” was addressed. This issue was investigated by assigning a best fitting depth to each calibration event during the iteration process of the regression analysis with the variable depth strategy. The resulting depths derived for each of the calibration events are plotted geographically for two strategies (see Figure 9). A trend can be recognized where more shallow events are in the Alpine area and more deep events are located in the foreland area. This observation is consistent with our understanding of the depth distribution of earthquakes from the instrumental period. The main question is, whether a reliable depth for a particular event can be derived, taking into consideration that our calibration dataset has no reliable depth estimate for most of the events. This means that we cannot test any procedure for depth determination. There might also be a trade-off between attenuation for Alpine/Foreland sources and the depths, which cannot be solved with our strategy.

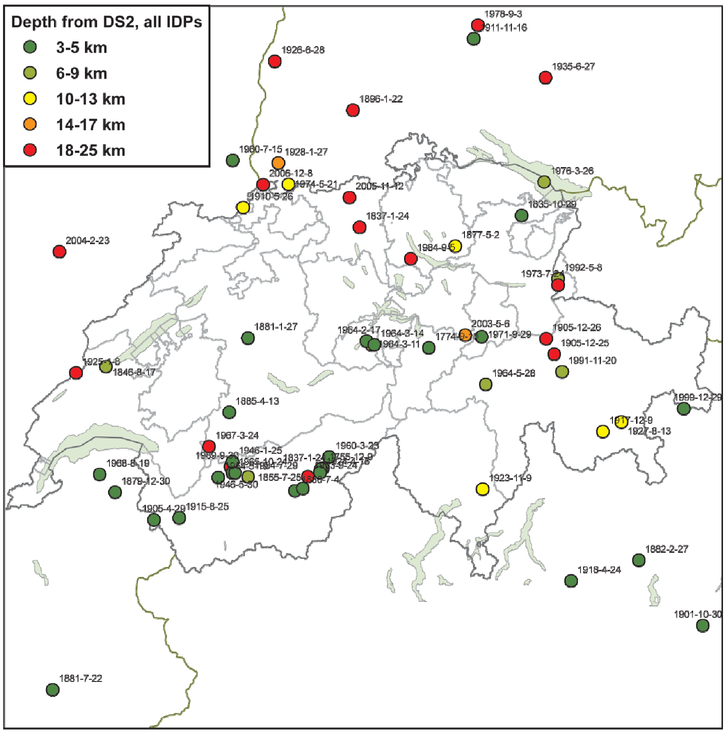

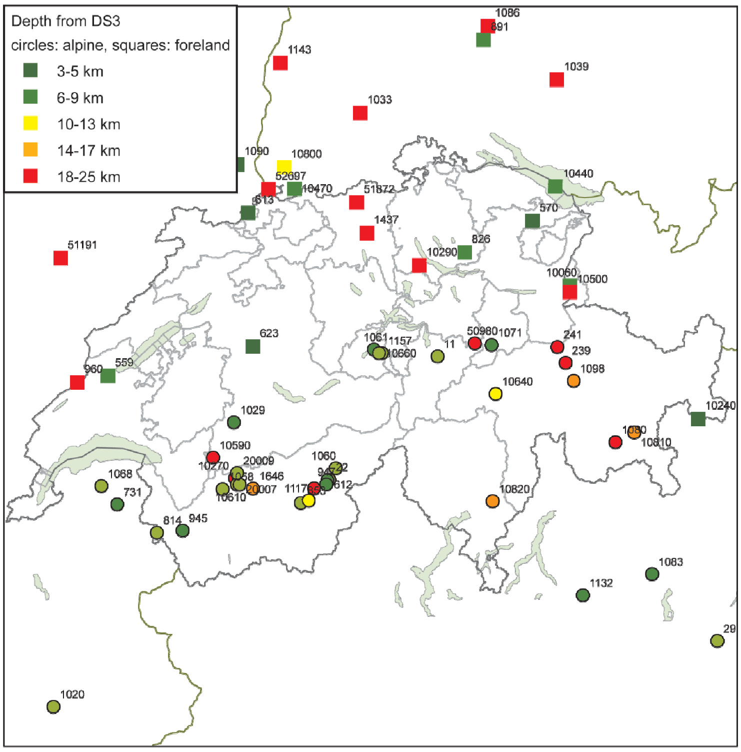

Figure 9. Depth of the events in calibration datasets 2 and 3 (DS2, DS3 respectively) obtained during the regression analysis for the intensity attenuation calibration with the variable depth strategy.

3.2 Macroseismic magnitude calibration

Macroseismic magnitude has been assessed in the second phase of the calibration procedure whilst decoupled from the intensity attenuation calibration. As was briefly presented in 2.4, we have used the subset of events with instrumentally derived Mw to derive a macroseismic magnitude to standardized intensity (I_{st}) relation. After several tests, we have defined this standardized intensity as the *intercept at 30km hypocentral distance* (I_{30}). In this way the influence of depth on the estimation of the magnitude is significantly reduced. With the definition of the magnitude based on I_{30}, the whole calibration procedure is formulated as follows:

1. The ECOS-09 intensity attenuation model is defined as:

$$I_{obs} - I_{sc} = aLn\left(R/h\right) + b\left(R-h\right) \tag{6}$$

   where: I_{obs} are the observed IDPs; I_{sc} is the scaling intensity; R is the hypocentral distance; h is the focal depth; and a and b are calibrated coefficients.

2. The magnitude to standardized intensity is established as:

$$\begin{gathered} M = \alpha I_{30} + \beta \\ I_{30} = aLn\left(30/h\right) + b\left(30-h\right) + I_{sc} \end{gathered} \tag{7}$$

   where: M is the macroseismic magnitude; I_{30} is the intercept intensity at 30km hypocentral distance; and α, β are calibration coefficients.

3. Location and magnitude are assessed in the *BW* method by implementing the expression:

$$M = c_1 I_{obs} + c_2 Ln\left(R/h\right) + c_3\left(R-h\right) + c_0 \tag{8}$$

where the calibration coefficients c_0, c_1, c_2, c_3 are calculated from a, b, α, β as:

$$c_0 = \alpha\left(aLn(30/h) + b(30-h)\right) + \beta;\ c_1 = \alpha;\ c_2 = -a\alpha;\ c_3 = -b\alpha \tag{9}$$

The regression of the calibration of the magnitude was performed using three weighting schemes:

a) No weighting of the IDPs.
b) Weighting by the number of IDPs.
c) Weighting by the quality of the IDPs.

In Figure 10, the magnitude to I_{30} relations are depicted for the five ECOS-09 strategies together with the data from the calibration dataset. In Tables 4, 5 and 6 the calibrated coefficients are listed.

ECOS-09 intensity attenuation model Strategy				Calibrated coefficients		Fitting quality	
Calibration Dataset	Intensity representation	Regionalization	depth	Logarithmic coefficient *(a)*	Linear coefficient *(b)*	StDev	R^2
2	All intensity levels(*)	-	Fixed depth (h=10km)	-0.67755 +- 0.02636	-0.00174 +- 0.0006007	0.4073	0.4457
2	Three highest intensity levels	-	Fixed depth (h=10km)	-0.4834 +- 02589	-0.00179 +- 0.0006097	0.36474	0.3631
2	All intensity levels(*)	-	Variable depth (h=3-25km)	-0.69182 +- 0.008803	-0.00084 +- 0.0002967	0.3897	0.6234
2	Three highest intensity levels	-	Variable depth (h=3-25km)	-0.50945 +- 0.008224	-0.00192 +- 0.0002836	0.3556	0.5183
3	All intensity levels(*)	Alpine	Variable depth (h=3-25km)	-1.07853 +- 0.01952	0.00414 +- 0.000630	0.4226	0.7383

Table 4. Calibrated coefficients of ECOS-09 intensity attenuation model for the selected strategies. (*) Intensity three and larger.

ECOS-09 intensity attenuation model Strategy				Magnitude to intensity at 30 Km distance calibration Different weighting schemes											
				No weighting				Weighting by IDP number				Weighting by IDP quality			
Calibration dataset	Intensity representation	Regiona-lization	depth	(α)	(β)	R^2	StDev	(α)	(β)	R^2	StDev	(α)	(β)	R^2	StDev
2	All intensity levels(*)	-	Fixed depth (h=10Km)	0.7725	1.0363	0.718	0.325	0.7482	1.178	0.738	0.332	0.734	1.28	0.722	0.342
2	Three highest intensity levels	-	Fixed depth (h=10Km)	0.732	1.132	0.749	0.309	0.698	1.329	0.750	0.319	0.6753	1.4617	0.720	0.327
2	All intensity levels(*)	-	Variable depth (h=3-25Km)	0.7364	1.1568	0.612	0.394	0.7561	1.0934	0.620	0.395	0.7317	1.2567	0.602	0.407
2	Three highest intensity levels	-	Variable depth (h=3-25Km)	0.7124	1.1288	0.701	0.332	0.7194	1.1075	0.700	0.331	0.6944	1.258	0.673	0.333
3	All intensity levels(*)	Alpine	Variable depth (h=3-25Km)	0.4623	2.7547	0.393	0.332	0.4817	2.758	0.470	0.333	0.4506	2.9314	0.460	0.332

Table 5. Calibrated coefficients of the relation between magnitude and intensity at 30 km hypocentral distance (ECOS-09) for the selected strategies.

ECOS-09 intensity attenuation model Strategy				Magnitude to intensity at 30 km distance calibration Different weighting schemes								
				No weighting			Weighting by IDP number			Weighting by IDP quality		
Calibration dataset	Intensity representation	Regionalization	depth	(c_1)	(c_2)	(c_3)	(c_1)	(c_2)	(c_3)	(c_1)	(c_2)	(c_3)
2	All intensity levels(*)	-	Fixed depth (h=10Km)	0.7725	0.5234	0.00135	0.7482	0.5069	0.0013	0.734	0.4973	0.0013
2	Three highest intensity levels	-	Fixed depth (h=10Km	0.732	0.3538	0.00131	0.698	0.3374	0.0012	0.6753	0.3264	0.0012
2	All intensity levels(*)	-	Variable depth (h=3-25Km)	0.7364	0.5094	0.00062	0.7561	0.5231	0.0006	0.7317	0.5062	0.0006
2	Three highest intensity levels	-	Variable depth (h=3-25Km)	0.7124	0.3629	0.00137	0.7194	0.3665	0.0014	0.6944	0.3538	0.0013
3	All intensity levels(*)	Alpine	Variable depth (h=3-25Km)	0.4623	0.4986	-0.00192	0.4817	0.5195	-0.002	0.4506	0.4859	-0.0019

Table 6. Calibrated coefficients of the magnitude to intensity relation, see equations (8) and (9). c_0 depends on focal depth

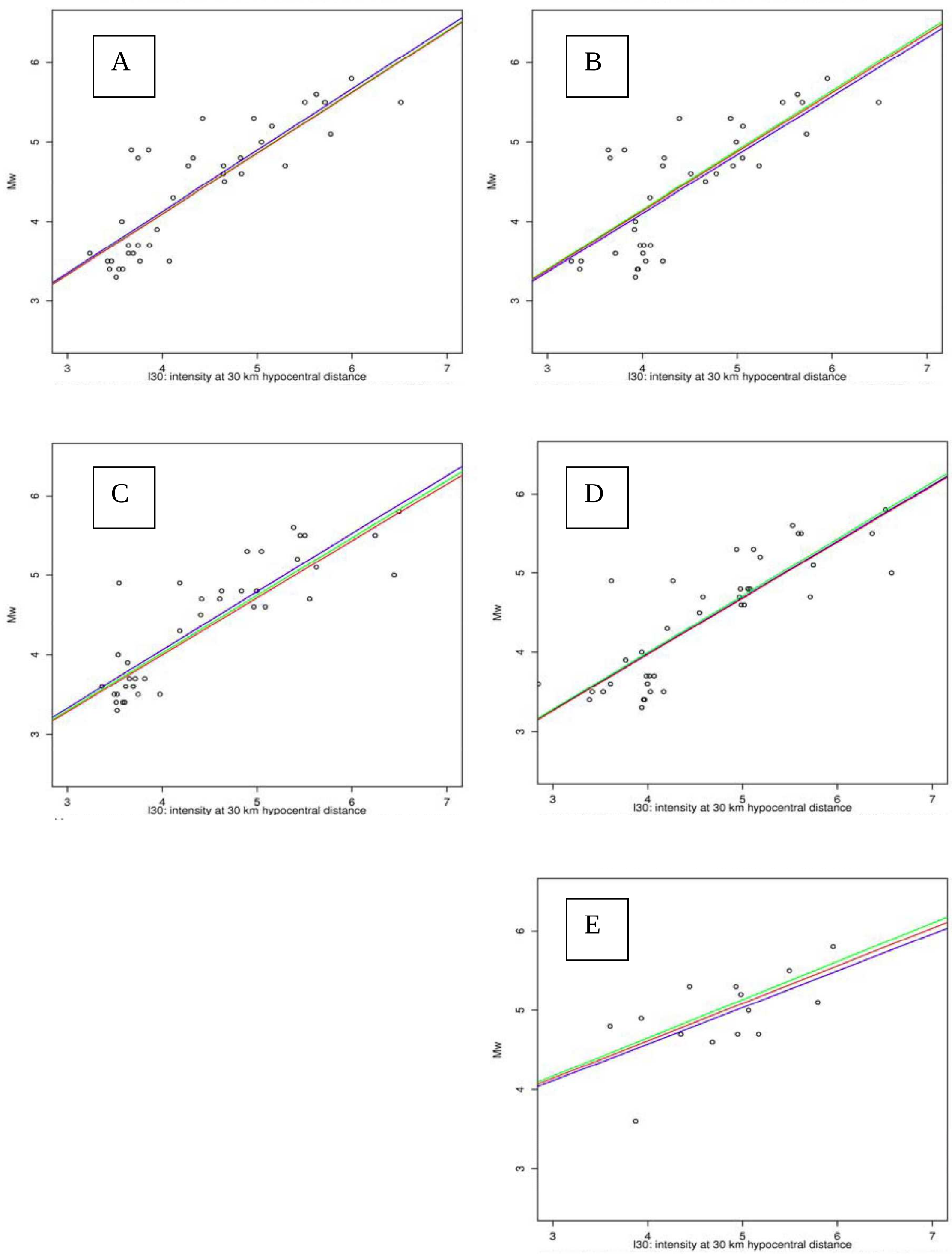

Figure 10. Magnitude to I_{30} relations for the five ECOS-09 strategies.

The three different lines in each plot correspond to the three weighting schemes tested for the relation: no weighting, number of IDP weighting and IDP quality weighting. The strategies are

A) Dataset 2, all intensities, fixed depth;

B) Dataset 2, all intensities, variable depth (depth set here to 10km);

C) Dataset 2, top 3 intensity levels, fixed depth;

D) Dataset 2, top 3 intensity levels, variable depth (depth set here to 10km);

E) Dataset 3, Alpine events, all intensities, variable depth (depth set here to 10km).

3.3 Implementation in BW and testing with the calibration dataset

With the BW technique, the assessment of the macroseismic location depends critically on the quantity and quality of the IDPs, along with their distribution relative to the earthquake source location. For this reason, and in order to avoid fake minimum residuals, special care has been taken when setting and scaling the grid search area of trial epicenters, with the dimensions of the area delimited by the macroseismic field.

Any available historical information is always used in order to constrain the epicenter location, and therefore the search area. In the cases where the catalogue location is known, the search area has been centered on this point and extended by a total width of 75 km in each direction. In the case where there is no certain catalogue location, the search area was centered at the highest values of the intensity field, and it was extended to cover the two intensity classes below the maximum intensity. Different cutoff distances (in the range of the search grid) have been implemented and tested in the BW code in order to avoid spatially biased distributions of IDPs. The macroseismic magnitude was assessed at the catalogue location (hereafter *Bk_cat*), at the minimum magnitude location (*Bk_mag*) and the minimum RMS location (*Bk_RMS*). Two examples (the 1855 Valais event and the 1356 Basel earthquake) are given in Figure 11.

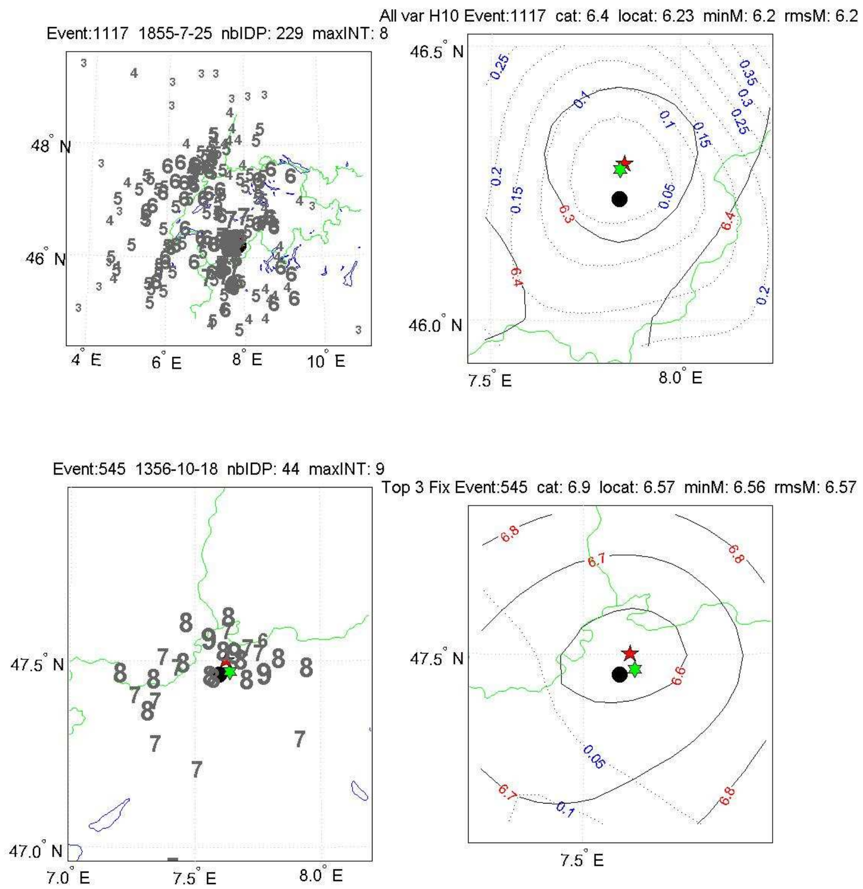

Figure 11. Examples of results obtained with the BW assessment when using calibration dataset 2: all intensities and variable depth (results for the depth of 10km are shown); three highest intensity classes, fixed depth (depth is 10km). Solid contours: magnitude values; dashed contours RMS values; black circle: catalogue location; red star: minimum magnitude location; green star: minimum RMS location.

Control tests of the different calibrations were carried out in order to select the best calibration in terms of IDP weighting, cutoff distances, and weighting in the magnitude to I_{30} relation. The different magnitude estimations provided by the BW method can be taken as a measure of the epistemic uncertainty related to the model itself, see 3.5. In Figure 12 an example of the results of the performance of the *BW* method is shown, for the subset of events in calibration dataset 2 with instrumental Mw.

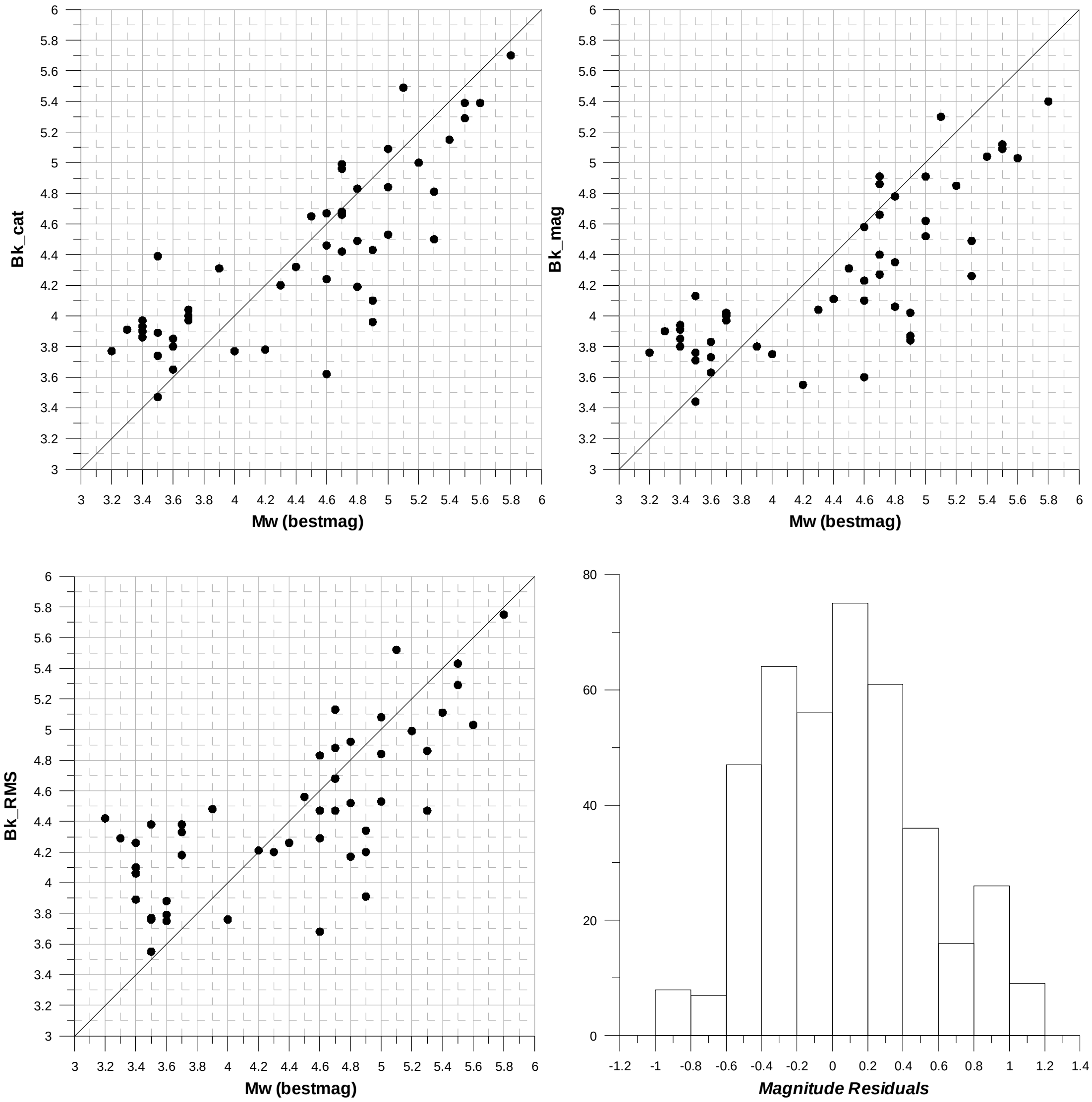

Figure 12. Example of the performance of the BW method for the ECOS-09 model for a subset of events of calibration dataset 2, using strategy allint with fixed depth. Estimated magnitudes are compared with instrumentally determined magnitudes Mw(bestmag).
Magnitudes estimated at the catalogue location (Bk_cat);
Minimum magnitudes in the search area (Bk_mag);
Magnitudes estimated at the location with the minimum RMS (Bk_RMS).
Magnitude residuals (difference between Mw(bestmag) and assessed magnitude at the catalogue location) using all three weighting procedures of the magnitude calibration and different cutoff distances in the BW software.

From the analysis of the results we have seen that the assessment of the magnitude at the epicenter location is good in almost all cases. After a series of performance tests with the BW technique using different combinations of cutoff-distances and weightings, the following five ECOS-09 intensity attenuation models were implemented in the BW technique to be applied to the historical events. These are:

1) Calibration dataset 2, using all intensities (intensity three and above), with fixed depth (10 km) and variable depth (*allint_fix; allint_var*);
2) Calibration dataset 2, using the three highest intensities (intensity three and above), fixed depth (10km) and variable depth (*top3_fix; top3_var*);
3) Calibration dataset 3, Alpine events, using all intensities (intensity three and above), variable depth (*all_alpine_var*);

Figure 13 shows the comparison between the estimated magnitudes at the epicenter location with the instrumentally determined magnitude for the calibration dataset. The performance of the BW method is good, especially for events with magnitudes larger than about magnitude 4, which is also the magnitude range of particular interest for the historical period of the catalogue.

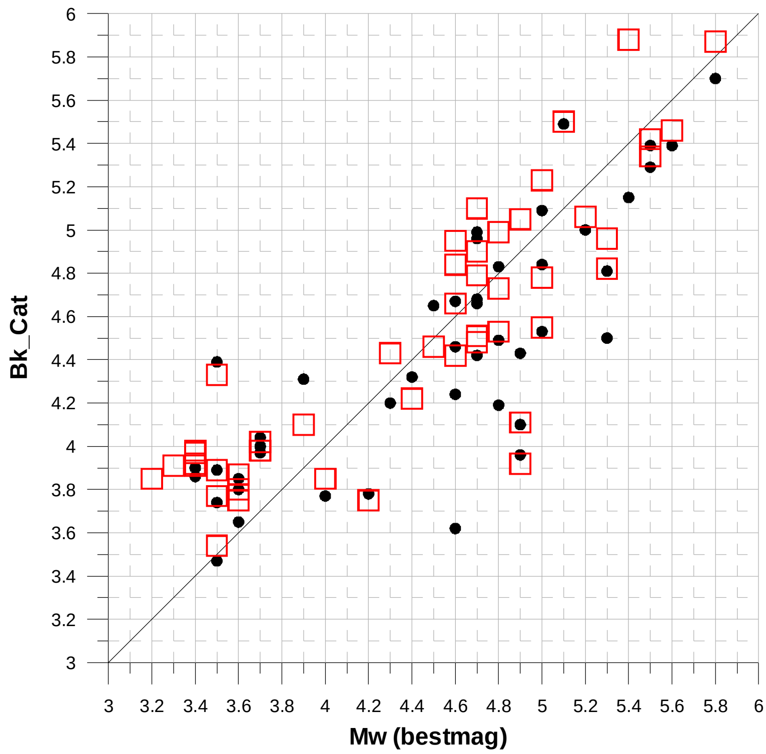

(a)

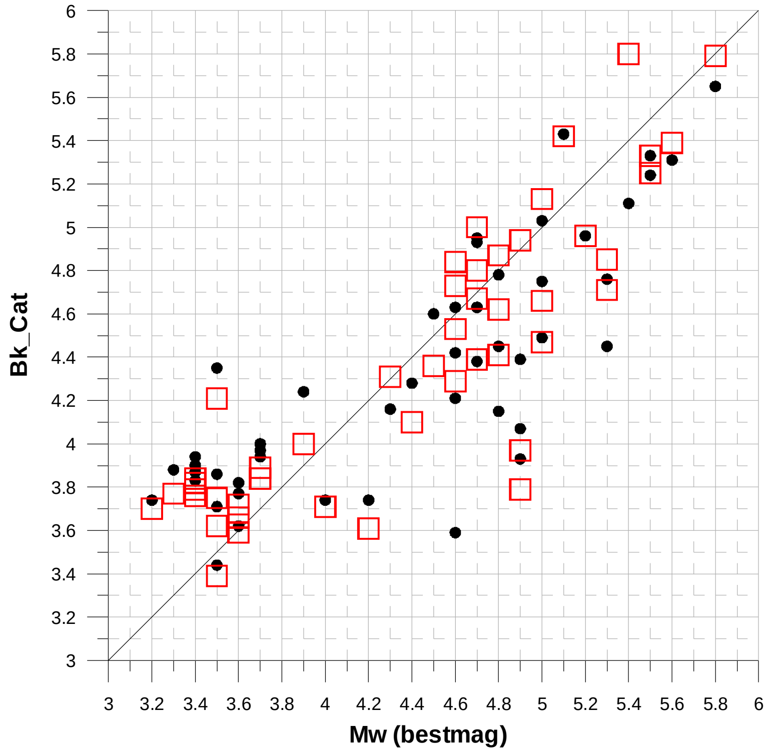

(b)

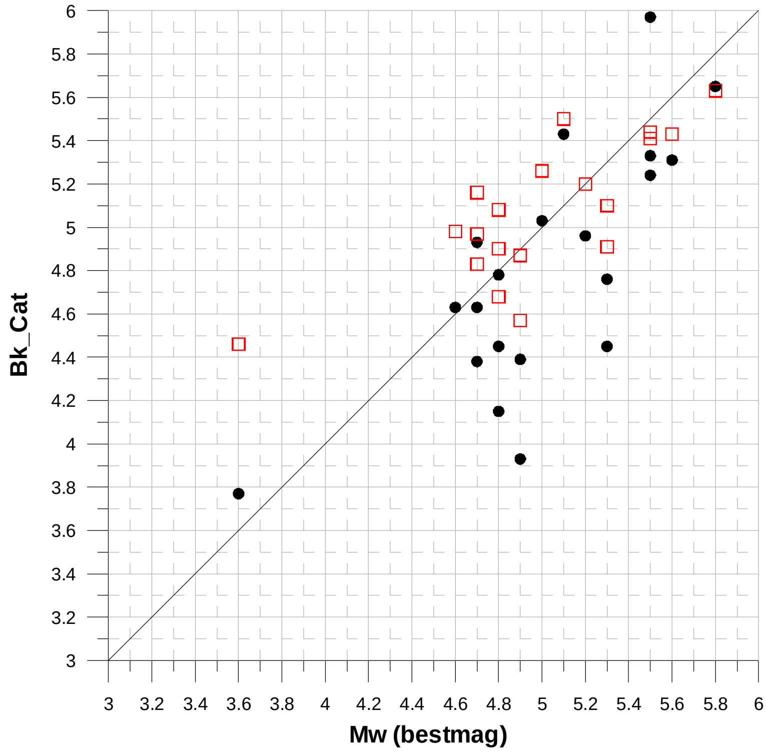

(c)

Figure 13. Estimated magnitudes at the epicenter locations for a subset of events of calibration dataset 2 with Mw(bestmag). In the magnitude calibration, IDPs are weighted by their quality.
(a): (●) allint_fix strategy; (□) top3_fix strategy.
(b): (●) allint_var strategy (h=10km); (□) top3_var strategy (h=10km).
(c): (●) allint_var strategy (h=10km); (□) all_alpine_var strategy (h=10km).

The determination of focal depth is addressed in the strategies with variable depth. We derived the RMS as a function of depth at the selected epicenter location. If the RMS curve shows a relevant minimum at a certain depth between 3 and 25 km, we selected this depth for the event and derived the corresponding magnitude at this depth. In order to better control the selection of depth, the intensity field was plotted as a function of epicentral distance, overlaying the theoretical *ECOS-09* curves at fixed depth levels and using the assessed magnitudes at the corresponding depth (see Figures 14 to 16). The final decision on magnitude and depth is made together with the RMS plots. If no clear decision can be made, the magnitude at 10km depth is proposed and no depth is assigned to the event. Some examples of the parameterization are shown in chapter 5.

3.4 Strategy of the assessment of macroseismic earthquake parameters of historical events

The following strategy has been applied for the assessment of earthquake parameters of historical events in ECOS-09 using the *BW* method:

1) Four calibrated non-regional attenuation models and one Alpine model were applied. Two models are for fixed depth at 10km, whilst three strategies are with variable depth. The four non-regional relations are derived from the largest calibration dataset (dataset 2) and the Alpine relation is derived from a smaller one (dataset 3) (the coefficients are given in Tables 4 to 6).
2) Using the *BW* method, the macroseismic magnitude was assessed at the original catalogue location, at the location of the minimum magnitude and the minimum magnitude root mean square (RMS). The epicenter location presently in the catalogue was defined taking into account the available historical information. As long as there is no historical evidence that the epicenter is incorrect, the location was not altered. The RMS as function of depth at the epicenter location was then derived. If the RMS curve shows a relevant minimum, the depth and corresponding magnitude were estimated (see an example in Figure 14 and Figure 15). For events that have new historical evidence or a new set of IDPs, a full re-assessment of the epicenter location was performed using all information.
3) In order to better control the depth selection, the IDPs as a function of epicentral distance were plotted (Figure 16). The IDPs are plotted overlaying the theoretical curves by assuming different depth levels and using the derived magnitudes at the corresponding depth. The final decision on the event’s magnitude and depth is made by including information from the RMS plots (horizontally as well as vertically) and taking into account the possibility of poor performance of one of the calibration strategies. If no clear decision of depth was possible the magnitude for a depth of 10km was taken. In this case depth is not assigned to the event. The magnitude is defined by the median of magnitudes from the strategies that perform well and are valid for this case (Alpine only for alpine events, only depth strategies in case a depth is assigned to the events). Finally each event was compared to events of similar magnitude, and magnitudes are adjusted for those cases in which the event has obviously too high or too low magnitude. Such cases are typical of events with irregular or sparse macroseismic fields.

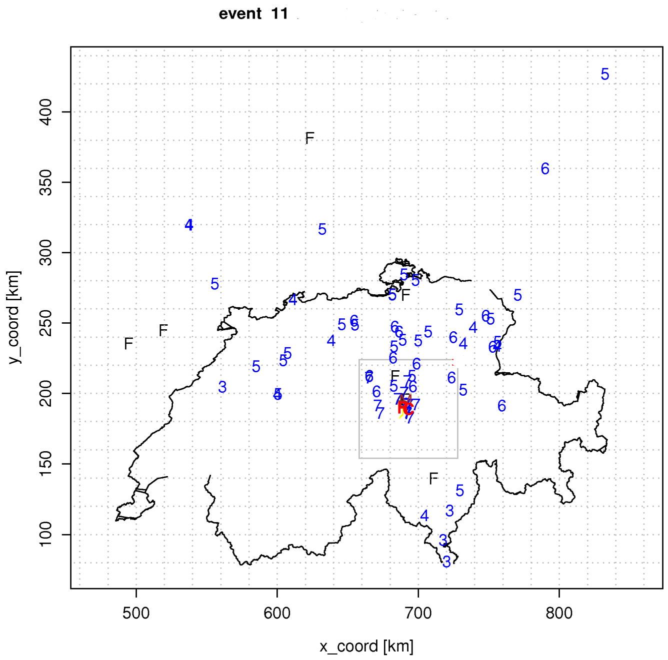

Figure 14. Intensity field of event 11 (1774.09.10)). In red the catalogue location is shown. In this example the catalogue location corresponds well to the minimum RMS location assuming shallow depth..

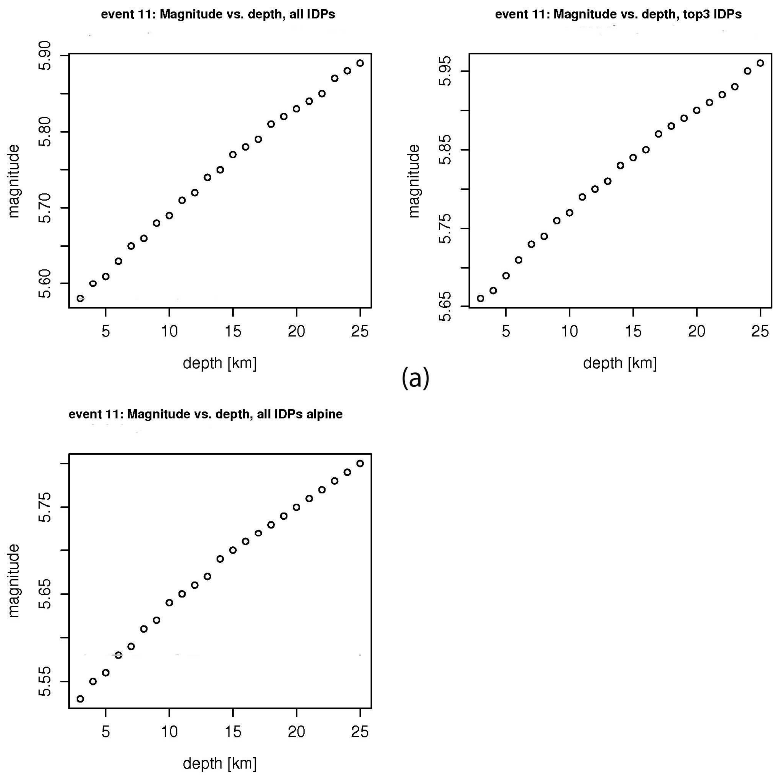

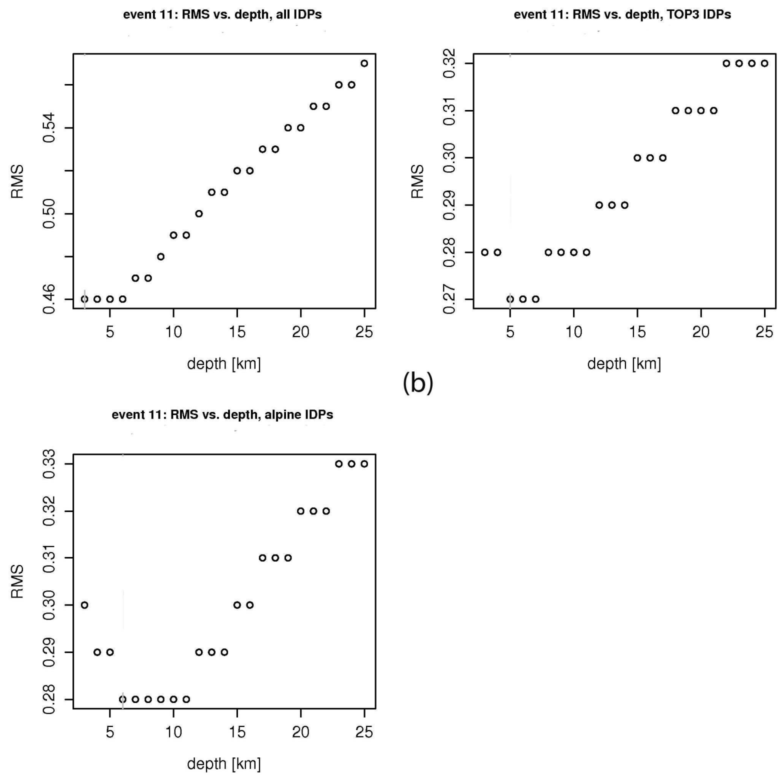

Figure 15. After the epicenter is defined, a) the magnitude as function of depth and b) the RMS as a function of depth are computed. The figures refer to event 11 (1774.09.10) and the strategies: dataset 2, all intensities and the three highest intensity levels for variable depth; dataset 3, Alpine events, all intensities for variable depth. This is one part of the information used to validate the depth of the event. For this event the assigned depth is 8 Km and the corresponding magnitude is 5.7

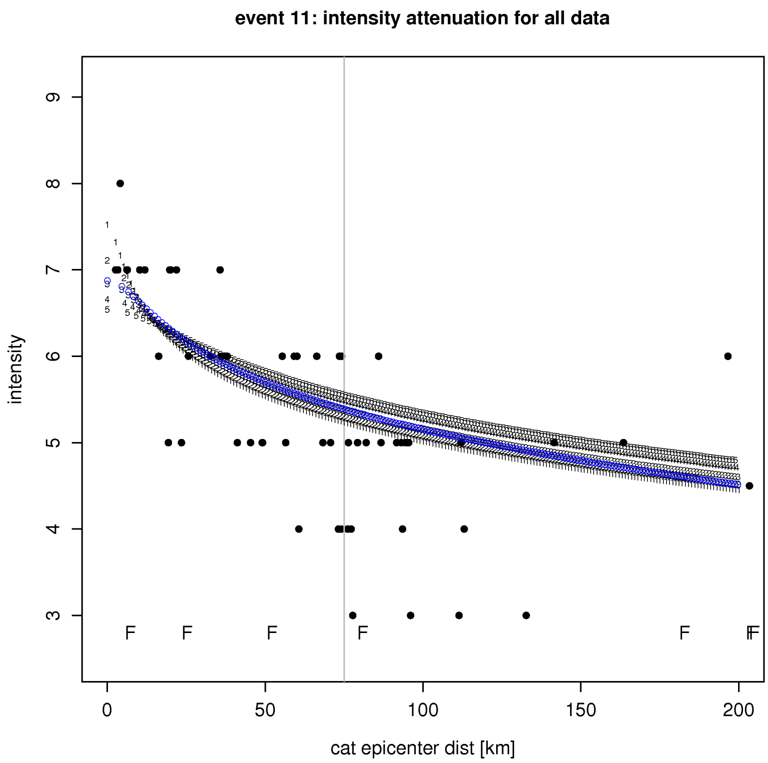

event 11: intensity attenuation for TOP3 data

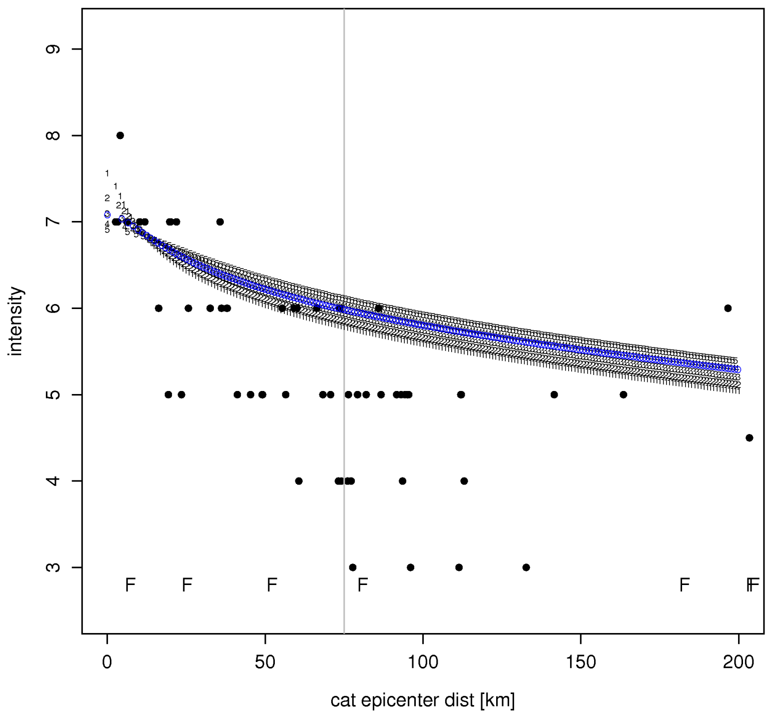

event 11: intensity attenuation for ALPINE data

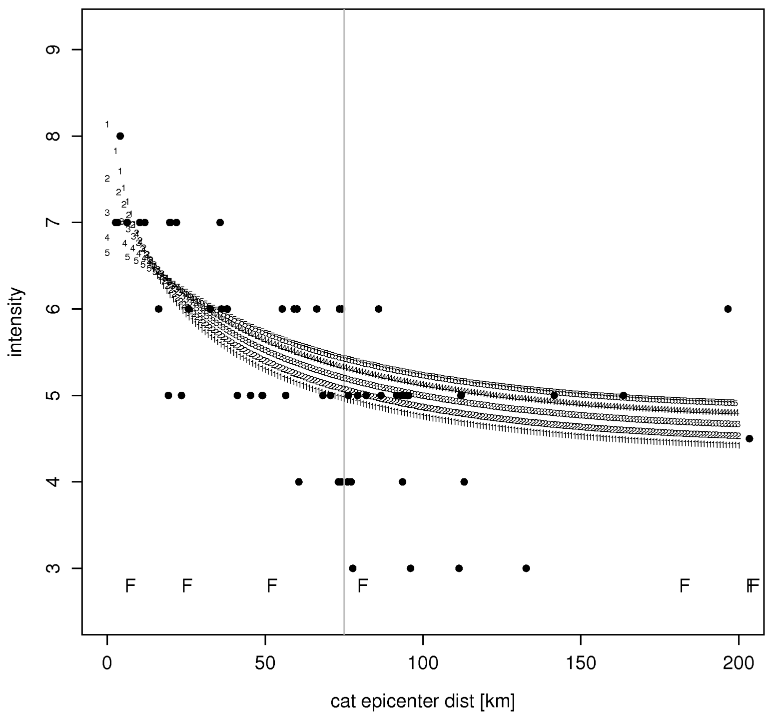

Figure 16. After the epicenter is defined, the IDPs are plotted as a function of epicentral distance, overlaying the theoretical curves by assuming different depth levels (at 3km, 6km, 10km, 15km and 20km), and using the derived magnitudes at the corresponding depth. The figures refer to event 11 (1774.09.10) and the strategies: dataset 2, all intensities (top figure) and the three highest intensity levels (figure in the middle),; dataset 3, Alpine events, all intensities (figure on the bottom). This is another part of the information used to validate the depth of the event. The assigned depth is 8 Km and the corresponding magnitude is 5.7. The blue curves correspond to the attenuation model assuming fixed depth.

3.5 Uncertainties in the assessment of location and magnitude

The calibration procedure is a complex process in terms of components such as models, macroseismic information and data processing. The final five calibration strategies were accomplished stepwise through a continuous selection process based on intermediate tests and results. The selection of the final calibration strategies can be represented by a logic tree structure, summarized in Figure 17, which depicts the workflow and decisions during the calibration exercise.

The final assessment of the macroseismic earthquake parameters of historical events, presented in ECOS-09, is based on an expert judgement by consideration of the BW results and the performance of the different calibration strategies on one hand, and of our historical knowledge on the other. Each stage of the assessment has an inherent random and model uncertainty, which propagates through the process and determines the total uncertainty in the estimated earthquake parameters. The nature of the sources that determine the total uncertainty in the earthquake parameter estimation are represented schematically in Figure 17. In the following we will argue that an exact statistical evaluation of errors is not achievable, due to a lack of information. Nevertheless we are able to quantitatively assess bounds of the uncertainties for magnitudes and locations.

Two of the main sources of uncertainty are related to the macroseismic field. The first stems from the intensity range assigned to a single IDP. Each IDP has a most probable intensity *Iw*, and a minimum intensity *Imin* and maximum intensity *Imax*. Imin and Imax define the possible intensity range. The second source of errors is the distribution of IDPs in the macroseismic field. Problems might arise from irregular azimuthal coverage due to national borders, gaps in historical information, and variability of the number of IDPs due to factors such as population density. A further source of uncertainty has a methodological origin. Calibration models, both the attenuation model and the standardized intensity to magnitude relation, also introduce uncertainties. They rely on calibration datasets with more or less reliable moment magnitudes, and irregular macroseismic fields. An uncertainty range is provided for most of the Mw(bestmag), but not all. Furthermore, these values do not cover the full uncertainty related to the methods applied by Bernardi et al. (2005) and Braunmiller et al. (2005). Some of the calibration events have an inhomogeneous geographical distribution of IDPs; depth is unknown for most of the calibration events, and epicenter location uncertainty of the calibration events cannot be assessed. We have limited control on the contribution of these uncertainties to the overall uncertainty. Nevertheless we have studied some of aspects of this problem.

The bootstrap statistical method is a procedure that deals with the problems arising from the incompleteness of the intensity field. The sampling with replacement can provide a set of different resampled IDP fields, such that the uncertainty of the magnitude and location is represented by the distribution of the locations and magnitudes obtained from the resampled IDPs (see Bakun and Scotti, 2006). We applied bootstrap to a selection of events with dense and sparse intensity fields. In a first step, for each event 1000 intensity sets were prepared in a standard bootstrap with replacement process, providing in each sample and for strategies “dataset2 allint”, “dataset2 top3_fix” and “dataset3 all_alpine”, the same number of intensity points as in the original IDP field. In a second step, we resampled each individual intensity assessment in order to reflect its uncertainty. We assigned one of the three intensity values Iw, Imin or Imax, assuming a probability model with the following rule set:

Assigned Intensity	Probability
If Imin= Iw-1 and Imax= Iw+1	Imin ->25% Iw->50% Imax->25%
If Imin= Iw-2 and Imax= Iw+2	Imin ->7% Iw-1->18% Iw->50% Iw+1->18% Imax ->7%
If Imin= Iw and Imax = Iw+1	Iw->75% Imax ->25%
If Imax= Iw and Imin = Iw-1	Imin->25% Iw->75%
Etc.	

If Iw was not given, then each intensity between Imin and Imax was equally weighted. If Imin or Imax was not given, it was assumed to be Iw-1, or Iw+1 respectively. If Iw was half a unit (in some cases with data from other agencies than SED), it was in a first step randomly changed into either the next upper or the next lower integer intensity. Imin and Imax were adapted, if necessary, in order to be <= Iw, or >= Iw, respectively. Based on this probability model, the intensity of each data point was randomly assigned. We then applied the BW method to all the resampled datasets to assess location and magnitude for the above mentioned strategies (alpine strategy only in case of alpine event), resulting in a distribution of locations and magnitudes for the event, that allows the analysis of the parameter uncertainty. We computed distribution of locations and magnitudes for the events listed in Table 7, without taking into account our historical knowledge.

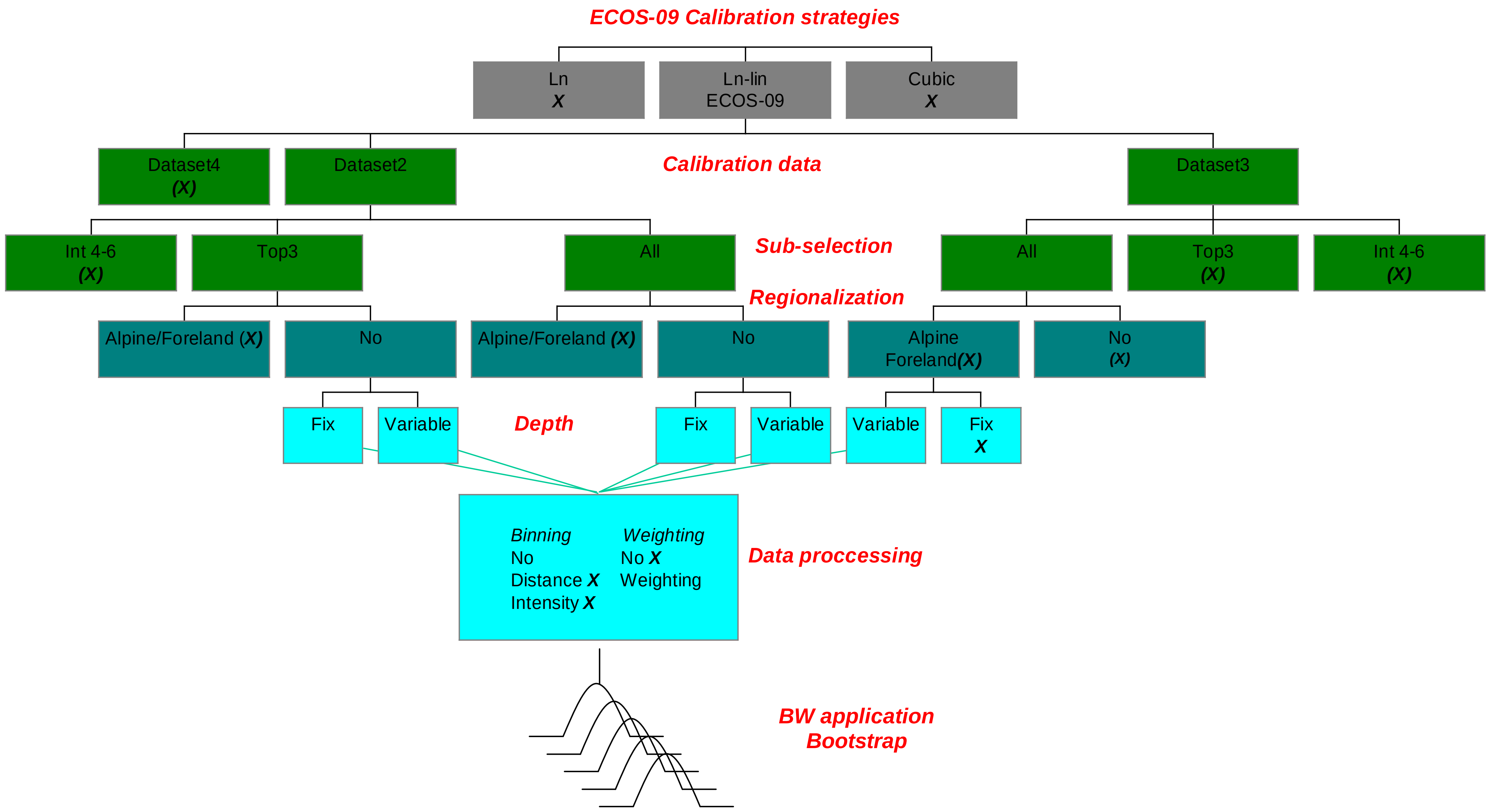

Figure 17. Definition of the final five calibration strategies through a continuous selection process based on intermediate tests and results. Crosses indicate branches that were not used for the calibration of the historical earthquake

Year	Month	Day	Hour	Event Name in ECOS-02	Number IDPs	Mw (bestmag) (1)	Mw ECOS-02 (2)	Mean Mw Bootstrap	Stdv Bootstrap	Mw from BW method (3)	Mw ECOS-09 (4)
1295	09	03	00	Churwalden	9	-	6.5	6.4	0.33	6.2	6.2
1356	10	18	21	Basel	47	-	6.9	6.6	0.12	6.6	6.6
1584	3	11	11	Aigle	27	-	6.4	5.9	0.17	5.9	5.9
1601	9	18	1	Unterwalden	67	-	6.2	5.9	0.15	5.9	5.9
1685	3	8	19	Mittelwallis	9	-	6.1	5.6	0.17	5.3	5.3
1755	12	9	13	Brig-Naters	128	-	6.1	5.7	0.19	5.7	5.7
1770	3	20	15	Château-d'Oex	8	-	5.7	5.2	0.21	5.2	5.2
1855	7	25	11	Törbel	265	-	6.4	6.2	0.16	6.2	6.2
1905	12	25	17	Domat-Ems	99	4.7	4.8	4.79	0.16	4.8	4.7
1905	12	26	0	Tamins	96	-	5.1	4.77	0.17	4.7	4.7
1913	7	20	12	Ebingen	880	-	5.2	5.0	0.13	5.0	5.2*
1929	3	1	10	Bioley-Magnoux	64	5.0	5.3	4.74	0.23	4.7	5.0
1946	1	25	17	Ayent	602	5.8	6.1	5.73	0.12	5.7	5.8
1946	5	30	3	Ayent	404	5.5	6.0	5.42	0.06	5.4	5.5
1978	9	3	5	Ebingen	1120	5.5	5.15	5.47	0.23	5.3	5.5
1991	11	20	1	Vaz/GR	322	4.7	4.6	4.65	0.18	4.6	4.7

Table 7. Mean and standard deviation of the magnitude distributions (at catalogue location and minimum RMS locations) applied to resampled IDP fields using the bootstrap technique (Stdv: standard deviation).

1. *Mw (bestmag): Mw derived from instrumental recordings by Bernardi et al. (2005).*
2. *Mw in the ECOS-02 catalogue.*
3. *Mw estimated with the BW method for ECOS-09.*
4. *Mw in the ECOS-09 catalogue.*

   The event names refer to the names in the 2002 catalogue. They changed in ECOS-09.

   ** Magnitude from foreign catalogue.*

The uncertainty in location is assessed through the analysis of the distributions of epicenter locations defined by the position of the minimum RMS in the BW approach. The catalogue location, in most of the cases, corresponds to the center of the grid search area. A high percentage of the RMS locations of the resampled datasets, are within a distance less than 20km from the catalogue epicenter. Figure 18 provides two examples of the distributions of epicenter locations. These two cases represent a good macroseismic field (event 545) and a poor one (event 49). We propose that the uncertainty in location in the ECOS-09 catalogue is equivalent to two standard deviations. For most of the events that were assessed with the BW method, this uncertainty corresponds to either 20km radius (error class 3) or 50 km (error class 4) (equal to 2 standard deviations) around the epicenter location. The smaller error was assigned when the intensity field is considered to be sufficiently complete in terms of azimuth coverage, absence of gaps in historical information, and the number of IDPs with a large intensity range. For events that had an insufficient number of IDPs to apply the BW technique, the error class was chosen according to the available macroseismic and historical information.

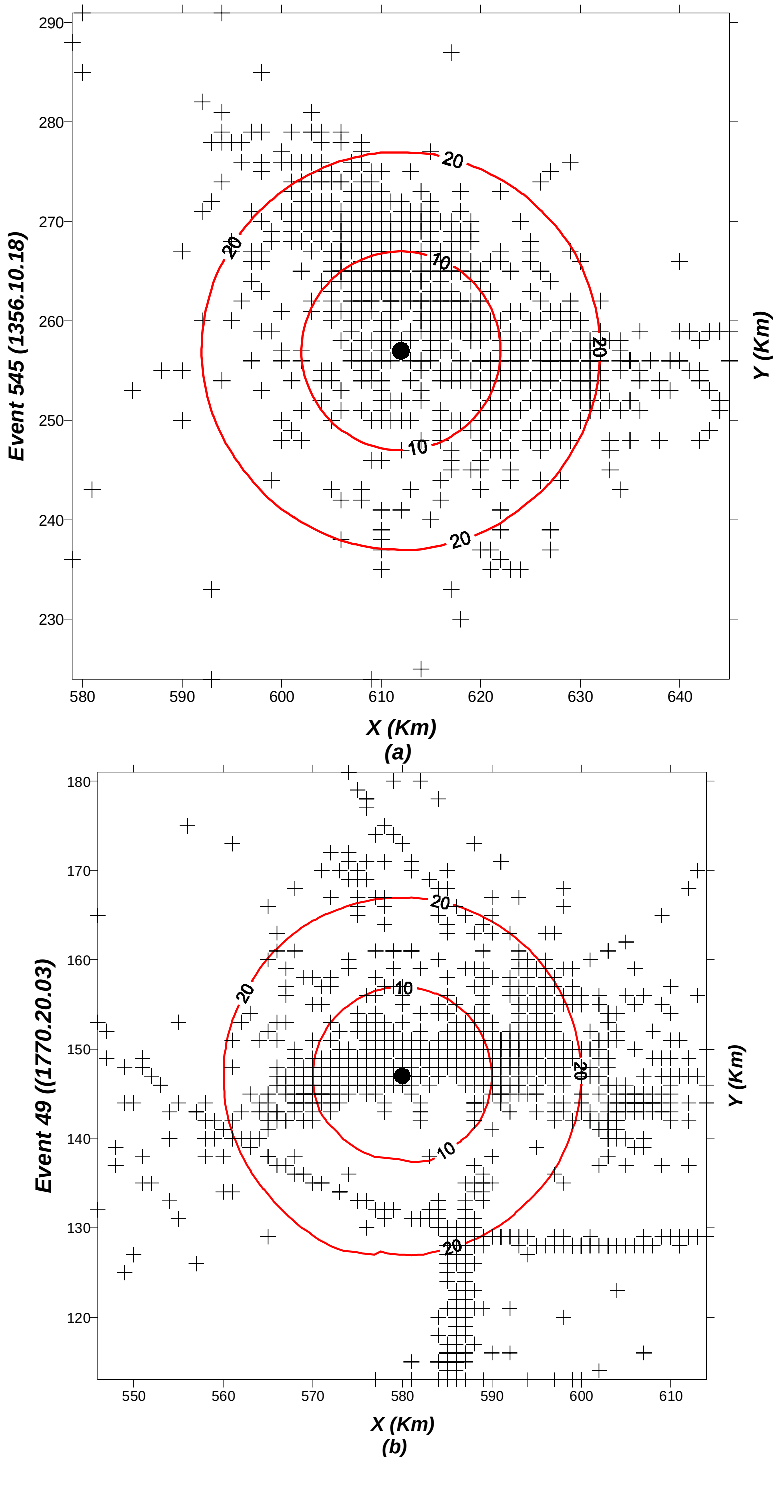

Figure 18. Distribution of possible epicenter locations from the bootstrap technique for the strategies: "dataset 2 allint_fix"; "dataset2 top3_fix", "dataset3_alpine_var_h=10",(this last only for event 49). The black dot corresponds to the catalogue location. Contour lines represent the distance to the catalogue location (10 and 20km). The percentage of locations within the 20km distance from the catalogue location is: (a) 95%, (b) 80%.

We have computed the distribution of the magnitudes at the catalogue location (Bk_cat) and at the minimum RMS location (Bk_RMS) for all strategies and the 1000 resampled datasets.

We then analyzed the distributions, and estimated the mean and standard deviation for the selected events (see Table 7). The uncertainty of the magnitude is given in terms of one standard deviation. The standard deviations can be reduced if we only consider the distribution of magnitude at the catalogue location, which is equivalent to the use of historical information. In Figure 19 the distributions of magnitudes are shown for two different events. These distributions include the magnitude estimates obtained for the strategy “dataset2 - fixed depth - all intensities”, “dataset2 - fixed depth - top3”, and “dataset3 –alpine - variable depth with depth 10 km” (this last strategy only applied to event 49). The contribution of varying the depth to the distribution is within the range of the overall distributions. We interpret the uncertainty of magnitude from bootstrap resampling as a lower bound of the uncertainty. This however does not account for the information missing in the macroseismic field. Finally, we have visually tested the fit to a normal distribution by using the Quantile/Quantile Plot. If the distributions follow a normal distribution, the points fall along the line. In both cases shown in Figure 19, the distributions follow approximately a normal distribution.
In chapter 3.3, we addressed the uncertainty related to the calibration methods by testing the performance of the BW technique for the different ECOS-09 strategies. Figure 12d shows the magnitude residuals, that is the difference between the magnitude assessed by BW and the Mw(bestmag) of the calibration dataset. These residuals are depicted for the magnitude at the given epicenter location, for the three different weighting schemes tested during the macroseismic magnitude calibration, as well as for the different cutoff distances applied in BW. Because we selected the best-performing weighting scheme and cut-off distance for the final calibration strategies, we expect that the magnitude residuals provided in Figure 12d then correspond to an upper bound.
We have computed such magnitude residual distributions for all five ECOS-09 strategies (depth is fixed to 10km for variable depth strategies) and all events of the calibration dataset. We consider the distribution of the magnitude residuals related to computed magnitudes at the catalogue and minimum RMS location of each event in the calibration dataset having a reliable Mw(bestmag) (Figure 20).
We propose that the residual distribution defines an upper bound of the overall uncertainty, because the Mw(bestmag) have an unknown error that cannot be assessed. Figure 20 shows the distributions of residuals and the normal probability density function fitted to the data. In Figure 20 one standard deviation corresponds to 0.45 magnitude units. This standard deviation relates to the fact that it has taken into account all minimum RMS locations and therefore excludes any historical information. Events with Mw(bestmag) smaller that 4.0 are also included, although they do not play an important role in the historical assessment, but significantly contribute to the tail of the distribution (see Figure 13).
The residuals between the BW magnitude assessed for all strategies and the Mw(bestmag) of the calibration dataset are considered to be a measure of the epistemic uncertainty derived from modelling, if the Mw(bestmag) would be without error. This error in the magnitudes Mw(bestmag) makes the distribution broader. We therefore consider the distribution of these residuals to reflect an expected upper bound of overall uncertainty. In summary and taking into consideration the different estimations of uncertainty discussed here, an estimate of magnitude uncertainty in terms of a standard deviation ($\pm\sigma$) would be in the range 0.1 to 0.45 magnitude units.
In the catalogue uncertainties are given as 2 standard deviations. For most of the events that were assessed with the BW method, the chosen magnitude uncertainty in the catalogue corresponds to 0.5 magnitude units (error class 2) or 1.0 magnitude unit (error class 3) (equal to 2 standard deviations). For events with only few IDPs and for which an assessment with BW method was not possible, we assigned the error class 3 or larger, or class 0 (unknown).

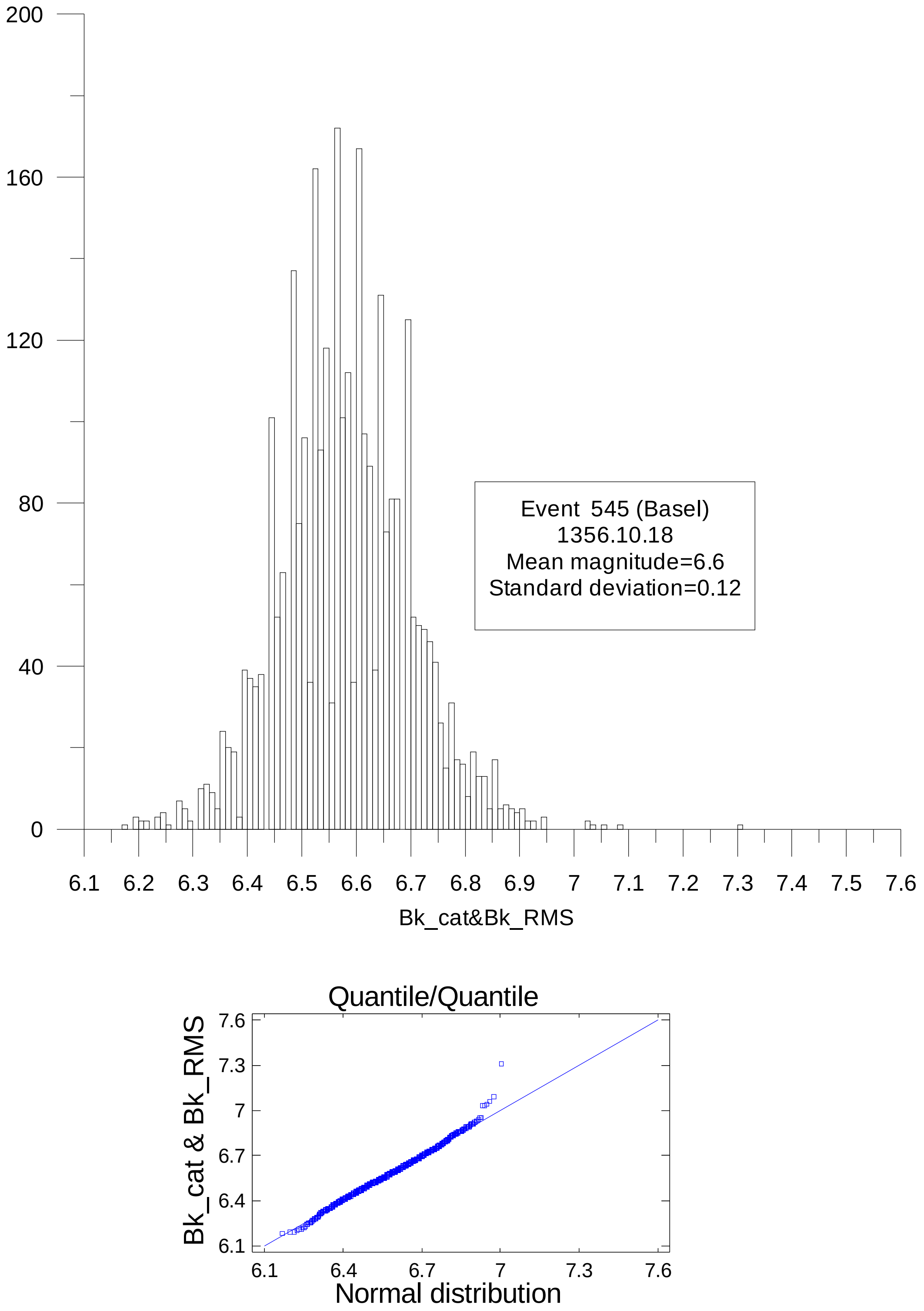
200
160
120
80
40
0
6.1
6.2
6.3
6.4
6.5
6.6
6.7
6.8
6.9
7
7.1
7.2
7.3
7.4
7.5
7.6
Bk_cat&Bk_RMS
Event 545 (Basel)
1356.10.18
Mean magnitude=6.6
Standard deviation=0.12
Quantile/Quantile
Bk_cat & Bk_RMS
7.6
7.3
7
6.7
6.4
6.1
Normal distribution

(a)

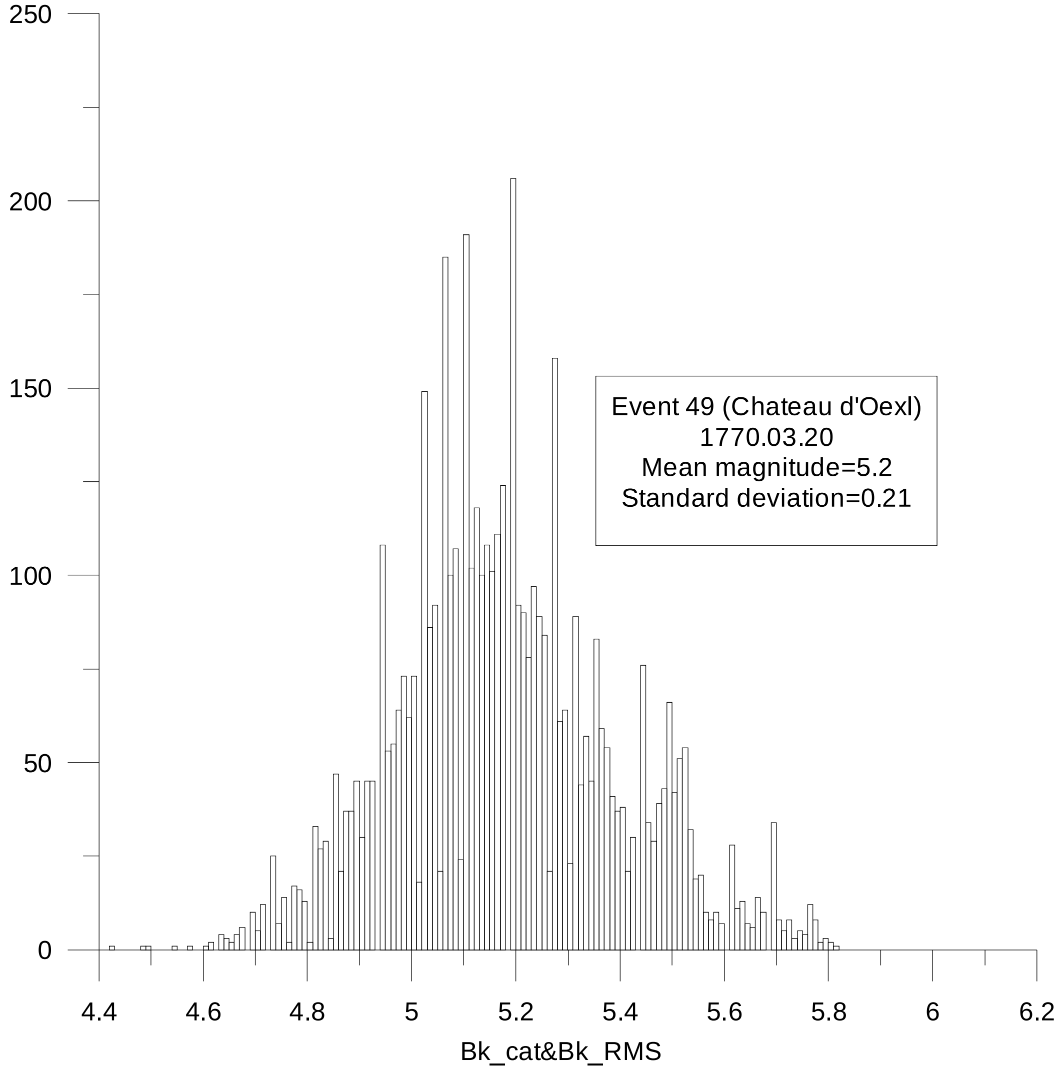

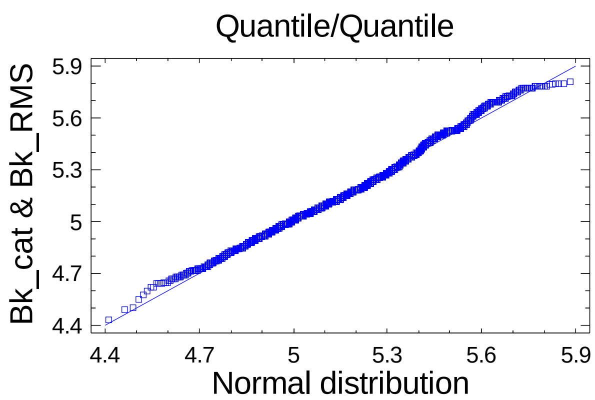

(b)

Figure 19. Distributions of magnitudes at the catalogue location and minimum RMS locations for the 1000 resampled datasets of (a) the 1356 Basel event and (b) the 1770 Chateau d'Oex event (see Table 7). The Quantile/Quantile Plot allows testing for normal distribution.

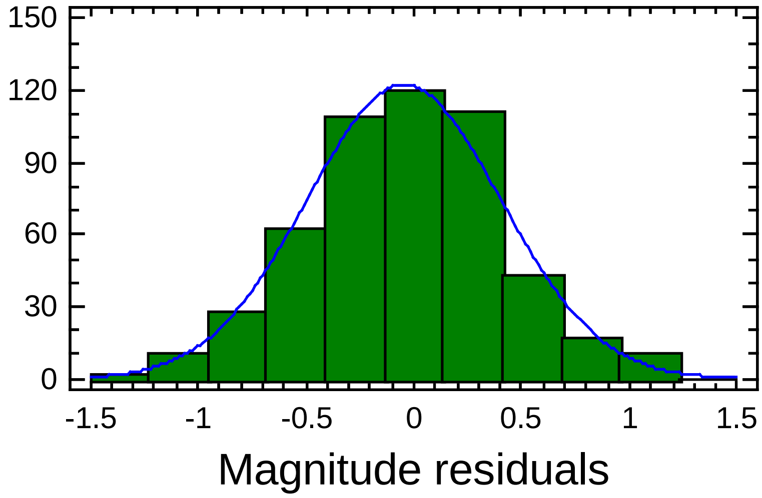

Figure 20. Histogram and fitted normal probability density function of the magnitude residuals obtained with the five ECOS-09 strategies at the catalogue and minimum RMS locations for all events of the calibration dataset with Mw(bestmag). Depth is fixed for the variable depth strategies.

3.6 Influence of site effects

Local soil conditions can notably affect earthquake ground motion. This is often observed in macroseismic intensity fields where sites located on soft sediments show higher intensities than those located in neighboring locations on rock. We statistically analyzed differences between observed macroseismic intensity and intensity estimates based on the derived Swiss attenuation relations, using the macroseismic data from the calibration dataset. The goal of the analysis is two-fold:

1) to define the reference soil condition for the derived attenuation models, and
2) to provide an estimate of the influence of the soil conditions on the magnitude determination of historical events.

The starting position of our assessment is an as yet unpublished study that is attached in Appendix D-1 of this report. In this study the two regional attenuation relations of ECOS-02 were used (Alps and Foreland), each of them with the two parameter sets for deep and shallow sources. The subsoil conditions of the localities were described by a combination of geological and tectonic characteristics. The site conditions were categorized using a standardized size for the area around the centre of each settlement. Typical intensity amplifications of the site classes were calculated from the median intensity residuals between observed and calculated intensities. Median observed amplifications relative to well-compacted sediments vary between about +0.7 intensity units for some eroded maritime sedimentary rocks and organic soils, and about –0.3 intensity units for Alpine Flysch. Many crystalline rock classes could not be characterized, since there are too few settlements located on them. We found an influence of the sediment grain size, the compaction and cementation

of deposits, the grade of sorting in loose sediments, the share of marl in mixed rocks and the related state of weathering. Thick layers of Holocene sediments are not well covered by the analyzed dataset.
Variability within one site class is large, and reached values in the range of about one intensity unit. Some investigated villages also show remarkable intensity anomalies for all analyzed earthquakes. Such an analysis has some limitations where settlements are not regularly distributed within one soil class. A good example occurs in alluvial plains, where most settlements are located at the edges of sedimentary basins. Moreover, regional attenuation relations intrinsically account for some site effects.
In order to analyze site effects in relation to the newly developed attenuation relations, two strategies are applied:

1. Site amplification based on the differences between observed macroseismic intensity and intensity estimates computed from the new Swiss macroseismic attenuation relation. The attenuation relation developed with calibration dataset 2 was used, including all intensity data points (IDPs) with intensity greater than or equal to 3.
2. Site amplification based on comparison of intensity observations on different soil classes to observations on a standard soil class (moraines on midland molasses which is the soil class with the largest number of IDPs) within defined magnitude-distance bins. Site-specific amplification is defined as the weighted mean of the difference between intensities at that specific soil class and the mean of intensity observations on moraines. Weighting factors were used to weight the quality of each IDP (very poor = 1, very good = 5) as well as the data quantity for the assessed soil class and the reference soil class. Bin size in magnitude is 0.1 magnitude units. The distance bin size is dependent on epicentral distance and increases with epicentral distance. We assume that the amplification term is independent of magnitude and distance.

We use the same site classes as defined in Appendix D-1. The macroseismic data are the IDPs from calibration dataset 2 (all IDPs with intensity ≥ III). While method 1 was successful, method 2 provided no useful results, most probably due to an insufficient number of IDPs. Table 8 summarizes the residuals derived using method 1 (the difference between observed and computed intensities) for the geologic and geotechnical soil classes for which sufficient data are available. These residuals are additive to the expected intensity from the attenuation model. Since residuals are differences between values on an ordinal scale (observed intensities are given in integers) and a continuous regression function, we do not expect them to follow a normal distribution. We describe their distribution with non-parametric statistics as far as possible. In this context, the standard deviation of the mean residual is more an indication of the computed median's significance than a quantitative measure.
From Table 8 we can conclude that the ECOS-09 macroseismic attenuation functions are valid for sites with well-consolidated sediments or soft rock. The soil classes with the most IDPs are moraines on midland Molasses and fluvio-glacial gravels with amplifications in the range +0.25 to +0.35. Many of the amplification values are similar to those derived for the ECOS-02 attenuation models, others differ considerably. The main reason for the differences is probably that we were less restrictive in the assignment of the soil class for ECOS-09 (homogeneous soil conditions within a minimum of 2/3 of the area within a circle of 500 m around the settlement center).
Considering all IDPs together, we would expect a median site amplification of ~ 0. The apparent overall amplification of the IDPs however is + 0.17 intensity units. There might be different reasons for that. These are:

1) Site amplification is derived from 7082 IDPs which have homogeneous soil conditions within a minimum of 2/3 of the area defined by a circle of 500 m around the

settlement center, while the attenuation relationship was derived from all IDPs, including about one third of all IPDs with no assignment of a soil class.

2) For site amplification assessment, the intensity residuals were used independently of their source distance (no distance weighting), assuming that amplification effects measured in intensity are independent of magnitude and source distance. Actually the mean site amplification over all IDPs used for site assessment is reduced to 0.003 if the same distance weighting scheme is applied to the residuals as for the assessment of the attenuation parameter. However, further investigation is required to check whether this is a result of distance dependency or magnitude dependency of macroseismic site effects, or an effect of spatial correlations to seismic activity and to the distribution of geological site classes in Switzerland.

Some trends in the site amplification factors are observable as in the earlier study: we recognize an influence of the sediment grain size (fine-grain sediments tend to have higher amplification), the grade of sorting in loose sediments (sorted sediments tend to have higher amplification), and the compaction and cementation of deposits. Rock sites tend to de-amplify when compared to the mean amplification.

These results must be used with care, because we may underestimate site amplification on some specific soil classes (e.g. organic soils, big alluvial plains), as the IDPs that contribute the most to the datasets are from the 19^{th} and early 20th centuries with a tendency of the sites to be at the edges of these soil types rather than on their typical formations.

The overall influence of site effects is small compared to the mean standard deviation of observed intensities from the attenuation relation (0.68). Thus, we expect that site corrections to the IDPS have a small influence on the determination of the magnitude. This, however, would need further testing.

(geological unit)	Geotectonic/regional restriction	Additional explanation	This study, using ECOS-09 attenuation: # of IDPs	50% percentile	StDev (mean)		Comparative study using ECOS-02 attenuation: # of IDPs	50% percentile	StDev (mean)
a) Crystalline									
Gneis and micaceous schists			65	-0.07	0.10		69	0.48	0.14
b) Paleozoic									
Perm, Verrucano	Sediment cover	Remaining sediment covers of the central alpine syncline	16	-0.55	0.27		18	0.72	0.24
c) Mesozoic									
c.1 Jura and northern Switzerland									
Lacustrine Limestones	Jura, Mesozoic and Epivariszic platforms	Limestone and Dolomite, medium phase also with thicker layers of marl	73	0.42	0.08		49	0.74	0.09
Keuper		Deposits of coastal areas and lagunes: heterogeneous layers of limestone, gypsum, marl	26	0.32	0.14		15	0.75	0.19
Dogger	Jura, mesozoic and epivariszic platform	sandstone	141	0.12	0.06		49	0.47	0.14
Malm, Jura	Mesozoic and epivariszic platform		275	-0.01	0.05		83	0.49	0.1
Malm, Jura	Alpine nappes		35	0.02	0.10		38	-0.05	0.15
Lower Cretaceous	Inner jura	Marls and mudstones	71	-0.09	0.12		33	0.64	0.22
	Other facies of inner jura		25	0.15	0.15		27	0.9	0.21
c.2 Northern Pre-alps									
Malm & lower Cretaceous	Alpine nappes	Malm: High share of compact, nearly pure (“white”) calcium carbonate rocks	71	-0.09	0.12		39	-0.03	0.14
d) Tertiary									
d.1 Tertiary of Swiss midland and northern									

Switzerland									
Ruppelien, lower saltwater molasse	Tertiary grabens	Fine-grain sandstones, marls and clay	47	0.25	0.09		26	0.47	0.11
Aquitanien, lower freshwater molasses	Midland molasse		202	0.43	0.05		132	0.52	0.1
Chattien/lower freshwater molasse	Jura and midland molasse	sandstones, marls and clay (grain size decreases from the northern Pre-alps towards the Jura)	96	0.51	0.09		63	0.58	0.12
Burdigalien, Helvetien of the Allgäu region. Upper saltwater molasse	Midland molasse	sandstones, marls and clay (grain size decreases from the northern Pre-alps towards the Jura)	135	0.14	0.06		95	0.56	0.13
Upper feshwater molasse		sandstone interbedded with marl and siltstone. Grey marl is the dominant lithology	238	0.43	0.05		257	0.6	0.07
	Other facies of midland molasse		82	0.45	0.08		65	0.47	0.12
d.2 Tertiary of the Northern Prealps									
Flysch	Alpine and prealpine area		71	-0.53	0.09		49	-0.31	0.14
Chattien, lower freshwater molasse	Subalpine molasse	Dominant conglomerates, intersected with sandstones	35	-0.14	0.16		52	0.06	0.17
e) Pleistocene									
e.1 moraines									
Moraine on flysch		Alps and Pre-alps	57	-0.37	0.13		33	0.14	0.22
Moraine on subalpine molasse		Alps and Pre-alps	77	-0.80	0.11		28	0.1	0.25
Moraines, incl. recent moraines	Alpine nappes	Alps and Pre-alps	119	-0.06	0.08		137	0.14	0.10
Moraines, including recent moraines	Midland molasses and Jura	Foreland	1077	0.35	0.03		846	0.39	0.04
e.2 non-glacial deposits									
Older fluvioglacial gravel terrasses			25	0.38	0.10		21	0.73	0.22
Loess, loess loam and weathered loams			303	0.29	0.05		58	0.72	0.11
Fluvioglacial and glaciolakustric gravels			1111	0.25	0.02		931	0.47	0.03

(terraces)									
Late pleistocene landslide deposits	Thick late Pleistocene landslide deposits		31	-0.01	0.11		19	-0.02	0.24
f) Holocene									
Alluvials	Jura, Mesozoic/Epivariszic Platform, Midland molasses		341	0.23	0.05		249	0.41	0.07
Alluvials	Big alluvial plains		496	-0.01	0.11		419	0.33	0.05
Alluvials	Wildhorn nappes	Area of Stans, valleys of Sarner and Engelberger Aa; with high share of lake sediments	20	0.19	0.19		52	0.32	0.14
Alluvials	Buendnerschiefer nappes	Hinterrheintal and other small areas of Graubünden	22	0.34	0.19		15	-0.02	0.21
Alluvials	Other alpine nappes	Small areas along steep alpine river, throughout the alps	84	-0.39	0.11		78	0.00	0.15
Hill foot debris			54	-0.05	0.10		51	0.46	0.17
Postglacial landslides							53	0.23	0.15
Debris cones of rivers		Mostly cones of steep contributory rivers and ravine grabens in the alpine and pre-alpine main valleys	312	0.02	0.05		369	0.09	0.06
organic soils			26	0.50	0.12		62	0.72	0.15
	Thick quarternary deposits in general		4	0.43	0.30		10	0.48	0.17
Median overall offset				0.17				0.25	

Table 8. Intensity residuals for different geologic and geotechnical soil classes (in EMS98 intensity units).

4 List of calibration events

Event Number	Year	Month	Day	Hour	Minute	Second	Mw(bestmag)	Catalogue-02 Magnitude
11	1774	9	10	15	30	0		5.9
14	1901	5	22	7	57	0		4.7
22	1755	12	9	13	45	0		6.1
29	1901	10	30	14	49	0		5.3
52	1771	8	11	7	20	0		5.4
239	1905	12	25	17	5	0	4.7	4.8
241	1905	12	26	0	25	0		5.1
311	2001	2	23	22	19	41.4	3.4	3.55
559	1846	8	17	6	15	0		5.5
570	1835	10	29	2	45	0		4.6
612	1837	1	24	1	0	0		5.7
613	1910	5	26	6	12	0		4.8
623	1881	1	27	13	20	0		5
680	1881	3	3	2	30	0		4.3
731	1879	12	30	11	27	0		5.5
754	1897	9	18	9	15	0		4.3
778	1894	11	27	0	0	0		4.5
790	1881	11	18	4	0	0		5
814	1905	4	29	1	59	0	5.1	5.7
826	1877	5	2	19	40	0		4.4
853	1880	7	4	8	20	0		5.2
866	1898	2	22	10	45	0		4.6
891	1911	11	16	21	25	48	5.5	5.8
945	1915	8	25	2	15	0	4.6	4.9
947	1924	4	15	12	50	0	5.2	5.5
960	1925	1	8	2	45	0	4.8	5
1020	1881	7	22	2	45	0		5.8
1029	1885	4	13	10	25	0		5
1033	1896	1	22	0	47	0		4.5
1039	1935	6	27	17	19	30	5.6	5.7
1058	1954	5	19	9	35	0	5.3	5.4
1060	1960	3	23	23	10	0	5	5.3
1061	1964	2	17	12	20	0	4.8	5
1068	1968	8	19	0	36	40.6	4.7	5.2
1071	1971	9	29	7	18	52	4.9	5.1
1080	1917	12	9	21	40	0		5
1083	1882	2	27	6	30	0		4.5
1086	1978	9	3	5	8	32	5.5	5.15
1090	1980	7	15	12	17	22.1	4.8	4.9
1098	1991	11	20	1	54	18.6	4.7	4.6
1102	1996	7	15	0	13	31	4.6	4.59
1108	1994	12	14	8	56	0.1	4.3	4.26
1117	1855	7	25	11	50	0		6.4

1132	1918	4	24	14	21	0		4.5
1141	1925	7	21	12	2	0		4.2
1143	1926	6	28	22	0	40		4.4
1150	1930	10	7	23	27	0		5.3
1157	1964	3	14	2	39	0	5.3	5.7
1437	1837	1	24	1	30	0		5.2
1646	1954	7	29	4	40	27		4.3
1782	2002	4	29	15	14	9.3	3.5	3.5
10060	1992	5	8	6	44	40.2		4.34
10110	1995	6	25	18	53	7.1		3.4
10130	1995	11	16	5	57	21.5		3.8
10160	1996	8	24	2	38	22.4		3.8
10180	1997	11	22	4	56	10.6	3.6	3.62
10220	1999	2	14	5	57	54	4	4
10240	1999	12	29	20	42	34	4.9	4.9
10270	1989	9	30	4	41	2.1		3.9
10280	1989	1	7	2	29	41.5		3.4
10290	1984	9	5	5	16	49.3		3.8
10300	1983	8	31	0	18	27.8		3.8
10310	1983	7	31	20	52	56		4.1
10320	1981	9	26	13	54	44.6		2.9
10370	1978	8	28	14	44	39.9		2.9
10390	1978	2	23	9	49	20.4		3.5
10420	1976	7	17	9	13	34.5		4
10440	1976	3	26	22	28	31.3		3.5
10450	1975	11	25	6	17	35		3.4
10470	1974	5	21	7	42	38		3.9
10500	1973	7	24	0	48	38		3.9
10510	1973	7	9	0	27	4		3.9
10590	1967	3	24	17	38	38		3.5
10600	1966	3	16	11	23	46		3.5
10610	1965	10	24	12	16	57		4.3
10630	1965	2	10	4	43	47		3.5
10640	1964	5	28	20	52	3		3.9
10660	1964	3	11	19	19	8		4.3
10690	1955	12	24	23	40	29		3.5
10760	1933	9	24	23	55	5		4.3
10780	1933	1	24	1	43	0		3.9
10800	1928	1	27	3	13	0		4
10810	1927	8	13	1	0	51		3.5
10820	1923	11	9	13	22	0		3.9
20007	1946	5	30	3	41	0	5.5	6
20009	1946	1	25	17	32	0	5.8	6.1
40019	1931	4	14	22	13	0		4.2
40022	1960	2	19	2	30	0		4.2
50022	1955	11	23	5	39	0		4.2
50024	1958	3	30	16	10	0		4.4
50952	2003	2	22	20	41	4		4.8

50973	2003	3	22	13	36	16	3.9	3.8
50977	2003	4	29	4	55	9	3.4	3.5
50980	2003	5	6	21	59	43	3.6	3.7
51030	2003	7	17	2	27	16	3.5	3.6
51039	2003	7	18	11	1	35	3.5	3.6
51051	2003	8	1	3	20	23	3.7	3.7
51075	2003	8	22	9	21	32	3.6	3.7
51077	2003	8	22	9	30	9	3.5	3.5
51191	2004	2	23	17	31	20		4.6
51260	2004	6	21	23	10	2	3.3	3.6
51278	2004	6	28	23	42	29	3.4	3.8
51355	2004	12	5	1	52	39	4.5	4.9
51437	2005	5	12	1	38	0	3.7	3.9
51872	2005	11	12	19	31	16		3.9
52697	2006	12	8	16	48	39		3.2
52825	2007	1	6	7	19	52		2.9
52837	2007	1	16	0	9	7		3
54174	2007	8	23	21	35	0		2.6
54351	2008	1	21	16	40	35	3.7	3.8

Table 9. Calibration dataset 2.

Event Number	Year	Month	Day	Hour	Minute	Second	Mw(bestmag)	Catalogue-02 Magnitude
11	1774	9	10	15	30	0		5.9
22	1755	12	9	13	45	0		6.1
29	1901	10	30	14	49	0		5.3
239	1905	12	25	17	5	0	4.7	4.8
241	1905	12	26	0	25	0		5.1
559	1846	8	17	6	15	0		5.5
570	1835	10	29	2	45	0		4.6
612	1837	1	24	1	0	0		5.7
613	1910	5	26	6	12	0		4.8
623	1881	1	27	13	20	0		5
731	1879	12	30	11	27	0		5.5
814	1905	4	29	1	59	0	5.1	5.7
826	1877	5	2	19	40	0		4.4
853	1880	7	4	8	20	0		5.2
891	1911	11	16	21	25	48	5.5	5.8
945	1915	8	25	2	15	0	4.6	4.9
947	1924	4	15	12	50	0	5.2	5.5
960	1925	1	8	2	45	0	4.8	5
1020	1881	7	22	2	45	0		5.8
1029	1885	4	13	10	25	0		5
1033	1896	1	22	0	47	0		4.5
1039	1935	6	27	17	19	30	5.6	5.7
1058	1954	5	19	9	35	0	5.3	5.4
1060	1960	3	23	23	10	0	5	5.3

Event Number	Year	Month	Day	Hour	Minute	Second	Mw(bestmag)	Catalogue-02 Magnitude
1061	1964	2	17	12	20	0	4.8	5
1068	1968	8	19	0	36	40.6	4.7	5.2
1071	1971	9	29	7	18	52	4.9	5.1
1080	1917	12	9	21	40	0		5
1083	1882	2	27	6	30	0		4.5
1086	1978	9	3	5	8	32	5.5	5.15
1090	1980	7	15	12	17	22.1	4.8	4.9
1098	1991	11	20	1	54	18.6	4.7	4.6
1117	1855	7	25	11	50	0		6.4
1132	1918	4	24	14	21	0		4.5
1143	1926	6	28	22	0	40		4.4
1157	1964	3	14	2	39	0	5.3	5.7
1437	1837	1	24	1	30	0		5.2
1646	1954	7	29	4	40	27		4.3
10060	1992	5	8	6	44	40.2		4.34
10240	1999	12	29	20	42	34	4.9	4.9
10270	1989	9	30	4	41	2.1		3.9
10290	1984	9	5	5	16	49.3		3.8
10440	1976	3	26	22	28	31.3		3.5
10470	1974	5	21	7	42	38		3.9
10500	1973	7	24	0	48	38		3.9
10590	1967	3	24	17	38	38		3.5
10610	1965	10	24	12	16	57		4.3
10640	1964	5	28	20	52	3		3.9
10660	1964	3	11	19	19	8		4.3
10760	1933	9	24	23	55	5		4.3
10800	1928	1	27	3	13	0		4
10810	1927	8	13	1	0	51		3.5
10820	1923	11	9	13	22	0		3.9
20007	1946	5	30	3	41	0	5.5	6
20009	1946	1	25	17	32	0	5.8	6.1
50980	2003	5	6	21	59	43	3.6	3.7
51191	2004	2	23	17	31	20		4.6
51872	2005	11	12	19	31	16		3.9
52697	2006	12	8	16	48	39		3.2

Table 10. Calibration dataset 3.

Event Number	Year	Month	Day	Hour	Minute	Second	Mw(bestmag)	Catalogue-02 Magnitude
11	1774	9	10	15	30	0		5.9
22	1755	12	9	13	45	0		6.1
29	1901	10	30	14	49	0		5.3
613	1910	5	26	6	12	0		4.8
623	1881	1	27	13	20	0		5
814	1905	4	29	1	59	0	5.1	5.7
853	1880	7	4	8	20	0		5.2
891	1911	11	16	21	25	48	5.5	5.8
945	1915	8	25	2	15	0	4.6	4.9

Event Number	Year	Month	Day	Hour	Minute	Second	Mw(bestmag)	Catalogue-02 Magnitude
947	1924	4	15	12	50	0	5.2	5.5
960	1925	1	8	2	45	0	4.8	5
1020	1881	7	22	2	45	0		5.8
1029	1885	4	13	10	25	0		5
1058	1954	5	19	9	35	0	5.3	5.4
1060	1960	3	23	23	10	0	5	5.3
1071	1971	9	29	7	18	52	4.9	5.1
1080	1917	12	9	21	40	0		5
1086	1978	9	3	5	8	32	5.5	5.15
1090	1980	7	15	12	17	22.1	4.8	4.9
1098	1991	11	20	1	54	18.6	4.7	4.6
1117	1855	7	25	11	50	0		6.4
1157	1964	3	14	2	39	0	5.3	5.7
1646	1954	7	29	4	40	27		4.3
10590	1967	3	24	17	38	38		3.5
10610	1965	10	24	12	16	57		4.3
10640	1964	5	28	20	52	3		3.9
10660	1964	3	11	19	19	8		4.3
10760	1933	9	24	23	55	5		4.3
10810	1927	8	13	1	0	51		3.5
20007	1946	5	30	3	41	0	5.5	6
20009	1946	1	25	17	32	0	5.8	6.1

Table 11. Calibration dataset 4.

eventno	Year	Month	Day	Hour	minute	Mw	source
814	1905	4	29	1	59	5.1	Ms (Bernardi)
239	1905	12	25	17	5	4.7	Ms (Bernardi)
891	1911	11	16	21	25	5.5	Ms (Bernardi)
945	1915	8	25	2	13	4.6	Ms (Bernardi)
947	1924	4	15	12	49	5.2	Ms (Bernardi)
960	1925	1	8	2	45	4.8	Ms (Bernardi)
1036	1929	3	1	10	32	5	Ms (Bernardi)
1038	1933	8	12	9	58	4.6	Ms (Bernardi)
1039	1935	6	27	17	19	5.6	Ms (Bernardi)
1055	1943	5	28	1	24	5.4	Ms (Bernardi)
20009	1946	1	25	17	32	5.8	Ms (Bernardi)
20003	1946	1	26	3	15	4.7	Ms (Bernardi)
20007	1946	5	30	3	41	5.5	Ms (Bernardi)
1058	1954	5	19	9	35	5.3	Ms (Bernardi)
1060	1960	3	23	23	10	5	Ms (Bernardi)
946	1961	8	9	13	10	4.9	Ms (Bernardi)
1061	1964	2	17	12	20	4.8	Ms (Bernardi)
1157	1964	3	14	2	39	5.3	Ms (Bernardi)
1070	1968	6	27	15	43	4.6	Ms (Bernardi)
1068	1968	8	19	0	36	4.7	Ms (Bernardi)
1071	1971	9	29	7	18	4.9	Ms (Bernardi)
1086	1978	9	3	5	8	5.5	Ms (Bernardi)
1090	1980	7	15	12	17	4.8	Ms (Bernardi)
1098	1991	11	20	1	54	4.7	Ms (Bernardi)
1108	1994	12	14	8	56	4.3	Regional moment tensor inversion

10140	1996	3	31	6	8	4.2	Regional moment tensor inversion
1102	1996	7	15	0	13	4.6	Ms (Bernardi)
10180	1997	11	22	4	56	3.6	Regional moment tensor inversion
10220	1999	2	14	5	58	4	Regional moment tensor inversion
10240	1999	12	29	20	42	4.9	Local moment tensor inversion
311	2001	2	23	22	19	3.4	Local moment tensor inversion
310	2001	3	17	0	29	3.4	Local moment tensor inversion
1345	2001	7	17	15	6	4.7	Local moment tensor inversion
1782	2002	4	29	15	14	3.5	Local moment tensor inversion
50973	2003	3	22	13	36	3.9	Local moment tensor inversion
50977	2003	4	29	4	55	3.4	Local moment tensor inversion
50980	2003	5	6	21	59	3.6	Local moment tensor inversion
51030	2003	7	17	2	27	3.5	Local moment tensor inversion
51039	2003	7	18	11	1	3.5	Local moment tensor inversion
51051	2003	8	1	3	20	3.7	Local moment tensor inversion
51075	2003	8	22	9	21	3.6	Local moment tensor inversion
51077	2003	8	22	9	30	3.5	Local moment tensor inversion
51184	2004	2	18	14	31	3.2	Local moment tensor inversion
51260	2004	6	21	23	10	3.3	Local moment tensor inversion
51278	2004	6	28	23	42	3.4	Local moment tensor inversion
51346	2004	11	24	22	59	5	Local moment tensor inversion
51355	2004	12	5	1	52	4.5	Local moment tensor inversion
51437	2005	5	12	1	38	3.7	Local moment tensor inversion
51764	2005	9	8	11	27	4.4	Local moment tensor inversion
54351	2008	1	21	16	40	3.7	Local moment tensor inversion

Table 12. Dataset used for the magnitude to standardized intensity calibration.

5 Some examples of the macroseismic parameterization of historical earthquakes

In this chapter we present some examples of historical earthquakes. The figures show:

- The intensity field; in red: the catalogue, minimum magnitude, and minimum RMS locations. The underlying yellow line indicates the movement of the respective epicenter as a function of depth (stability indicator).
- The intensity field, plotted as a function of epicentral distance, overlaying the theoretical *ECOS-09* attenuation curves at different fixed depth levels and using the assessed magnitudes at the corresponding depth. The results shown are derived with the following strategies: dataset 2, all intensities and three highest intensity levels, both with fixed depth (blue curve) and variable depth; dataset3 alpine, all intensities, variable depth. The different theoretical attenuation curves correspond to: 1→3 km; 2→ 6km; 3→ 10km; 4→ 15km; 5→ 20km.

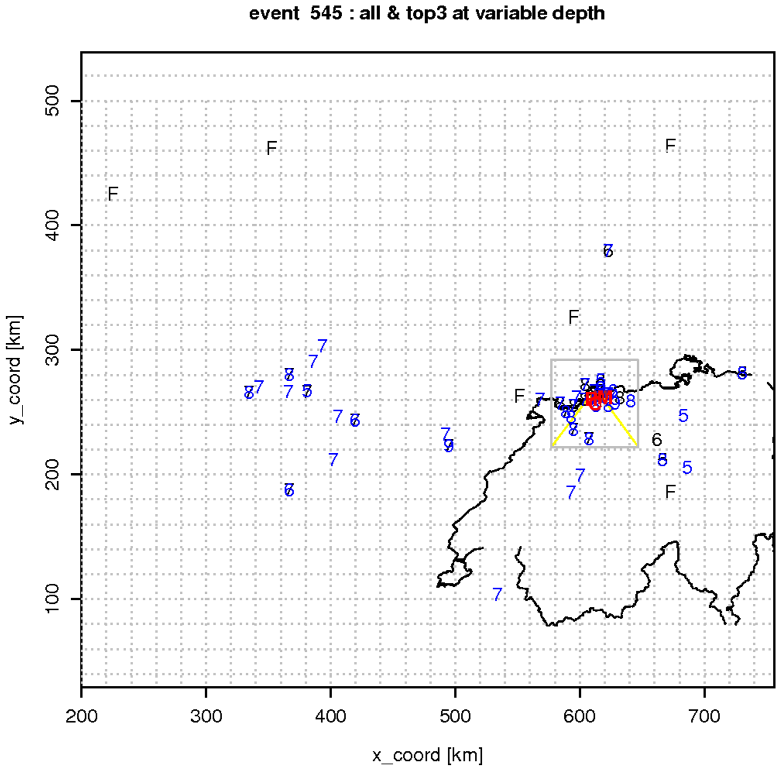
event 545 : all & top3 at variable depth
y_coord [km]
x_coord [km]
200
300
400
500
600
700
100
200
300
400
500

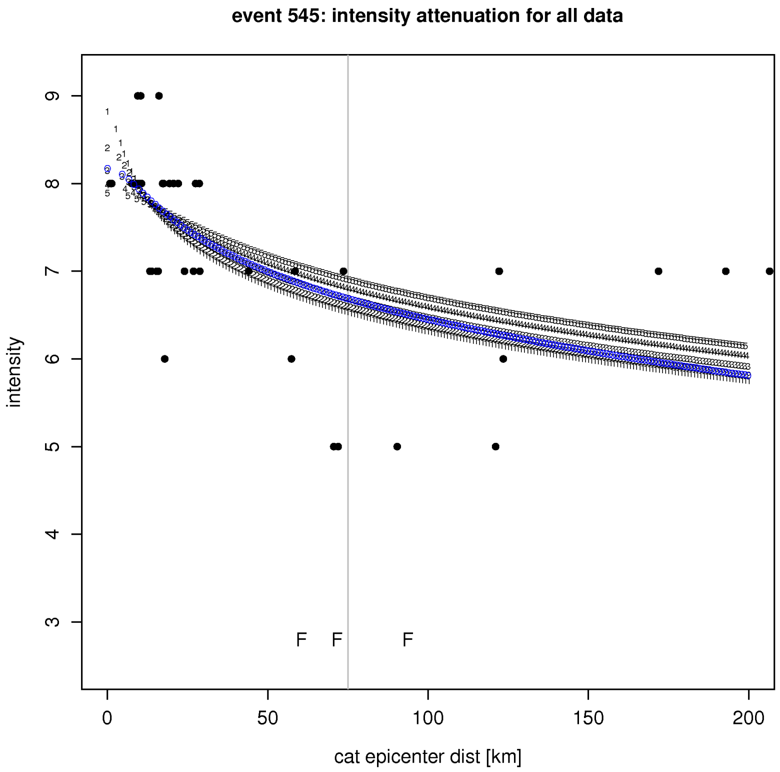
event 545: intensity attenuation for all data
intensity
cat epicenter dist [km]
0
50
100
150
200
3
4
5
6
7
8
9

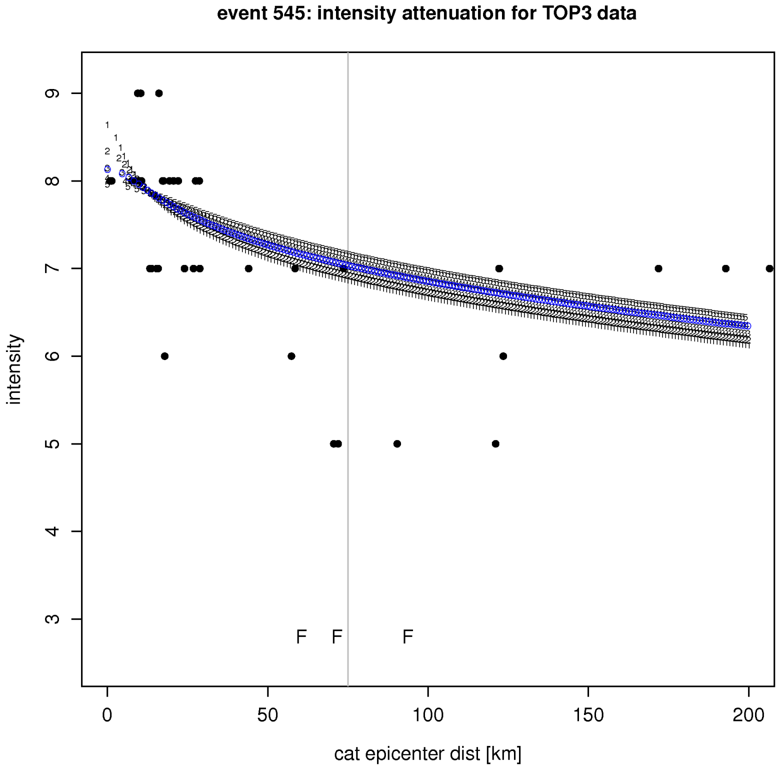

Event 545 (1356.10.18): Assigned magnitude 6.6, no depth.

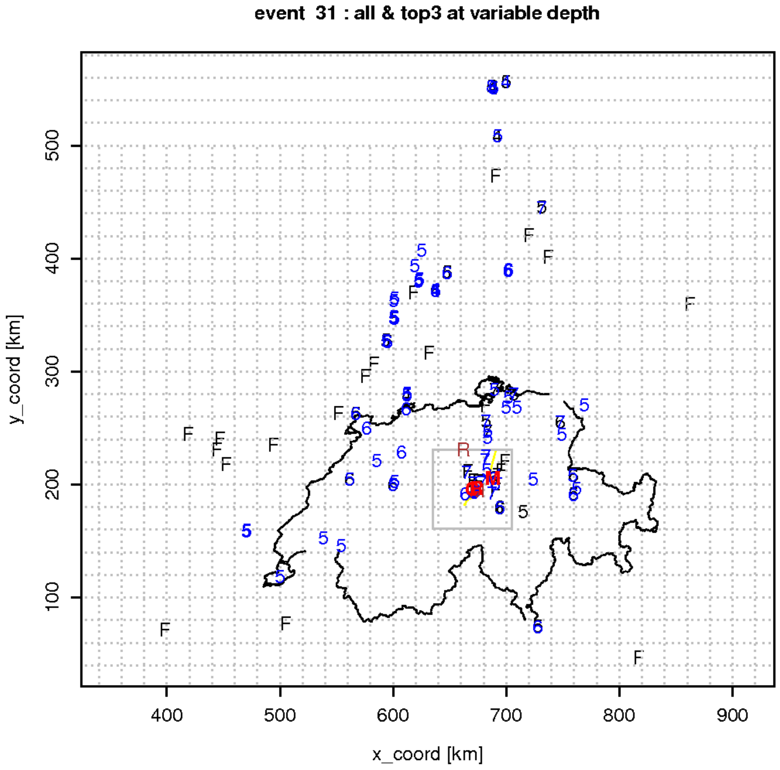

event 31 : all & top3 at variable depth
y_coord [km]
x_coord [km]

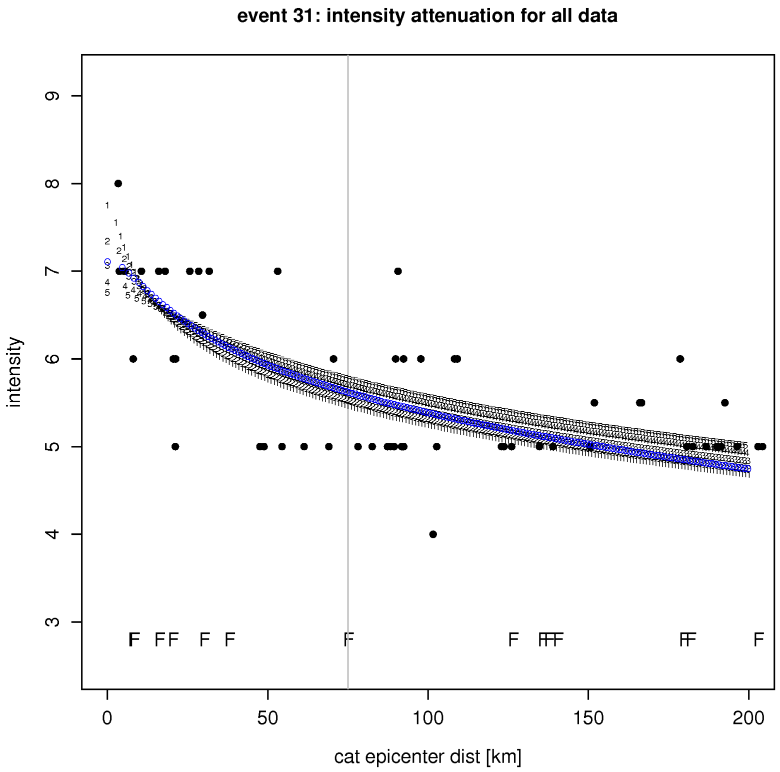

event 31: intensity attenuation for all data
intensity
cat epicenter dist [km]

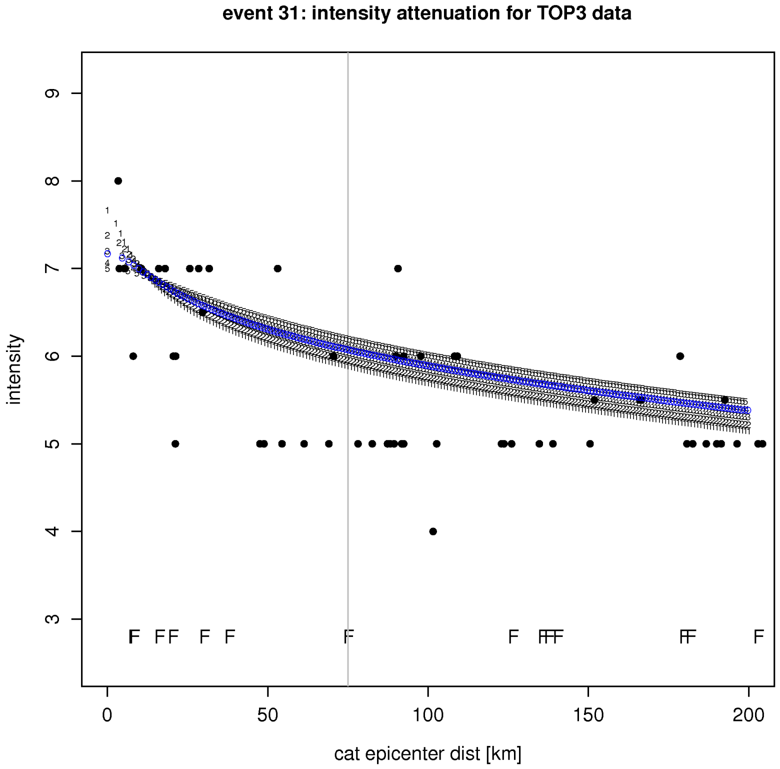

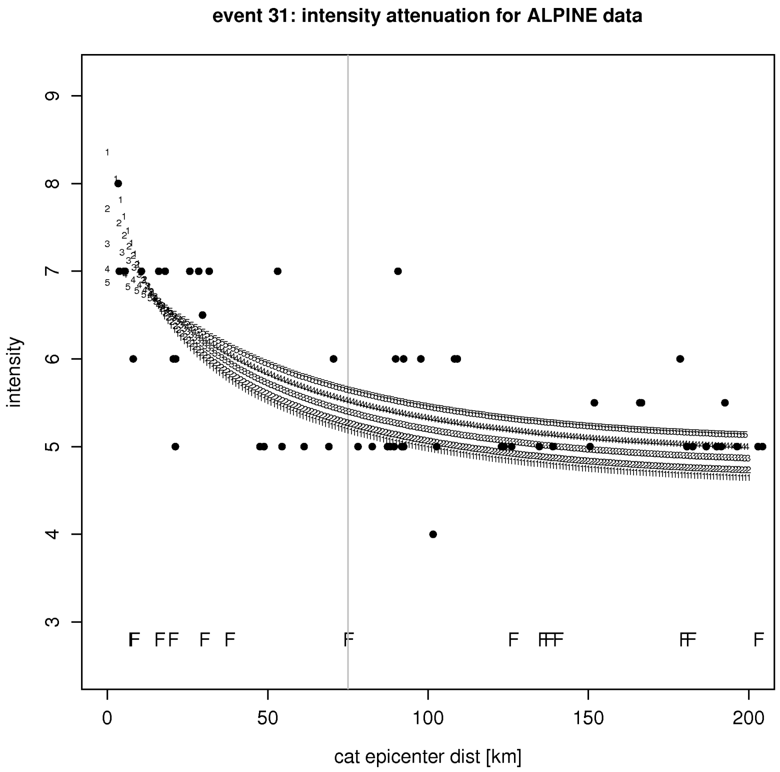

Event 31 (1601.09.18): Assigned magnitude 5.9, depth 10km.

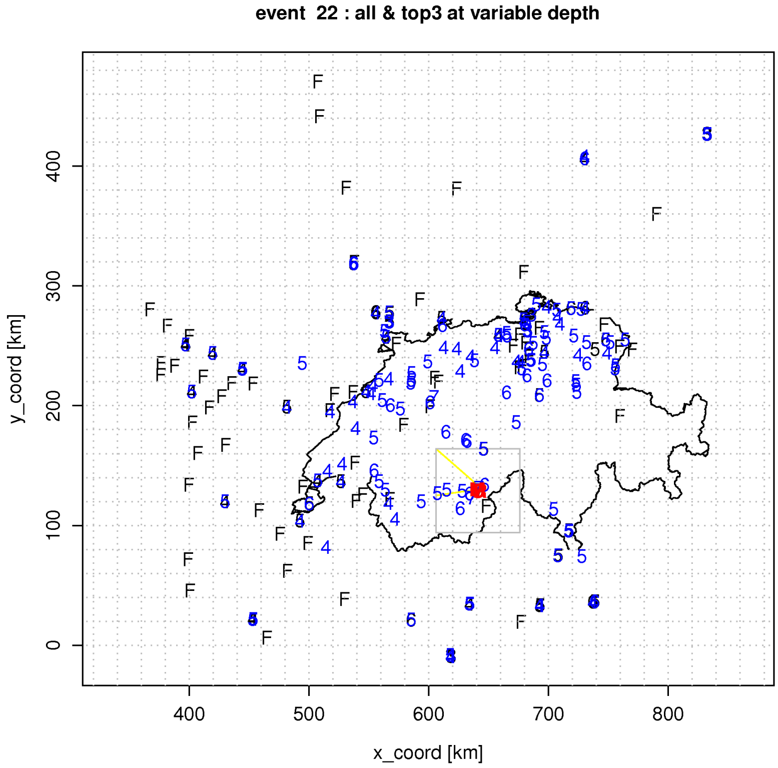
event 22 : all & top3 at variable depth
y_coord [km]
x_coord [km]

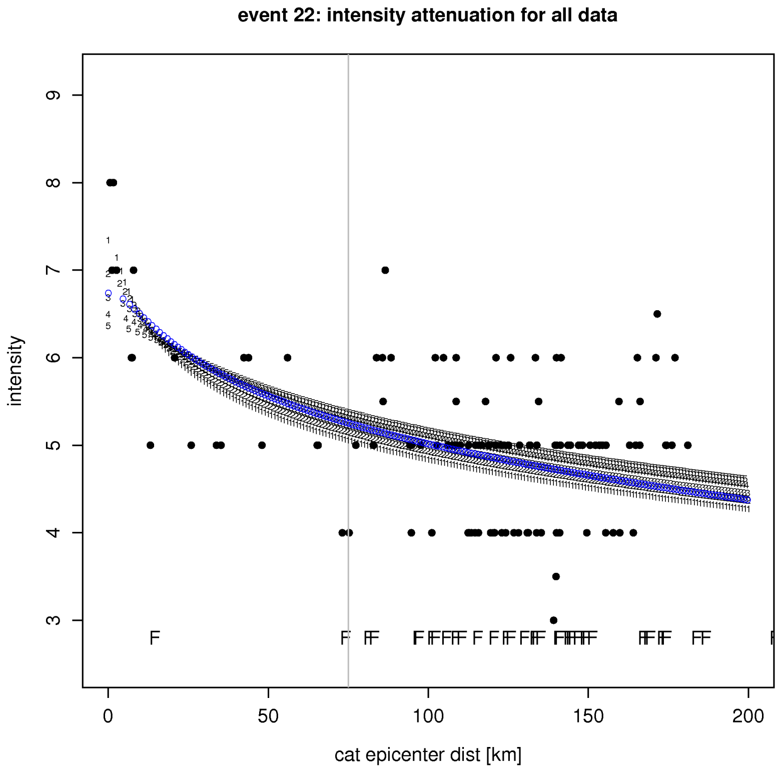
event 22: intensity attenuation for all data
intensity
cat epicenter dist [km]

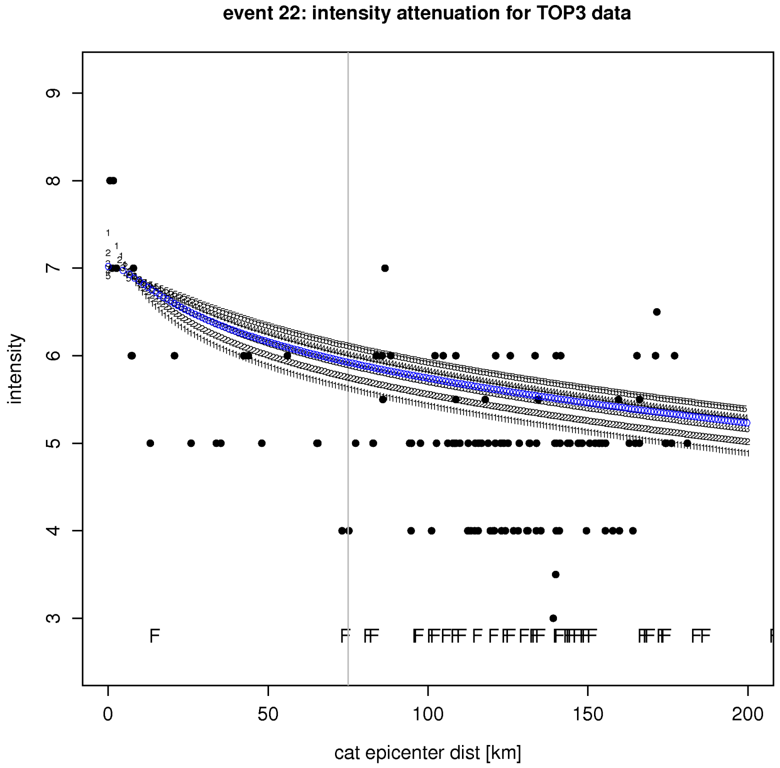

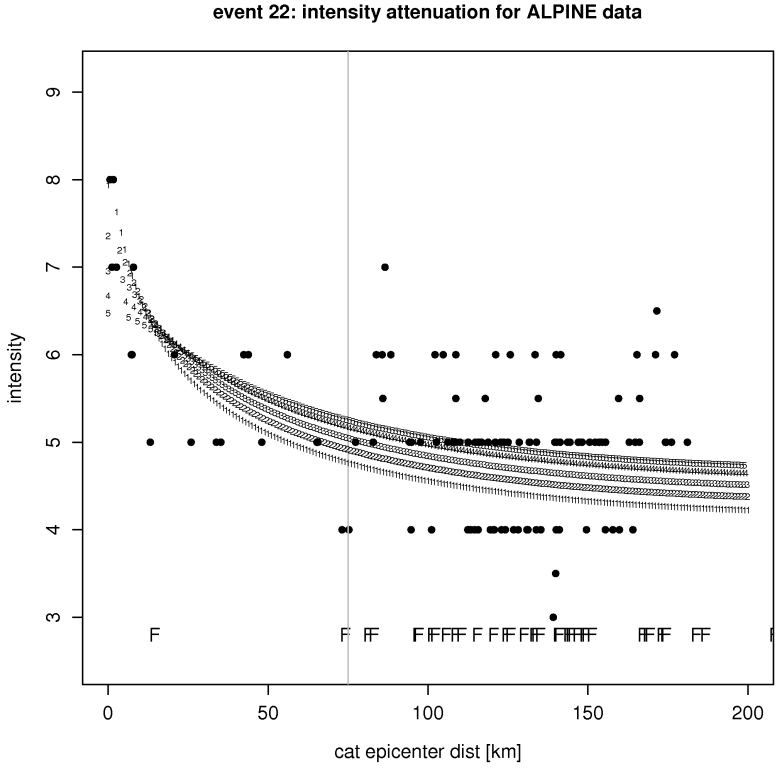

Event 22 (1755.12.09): Assigned magnitude 5.7, no depth.

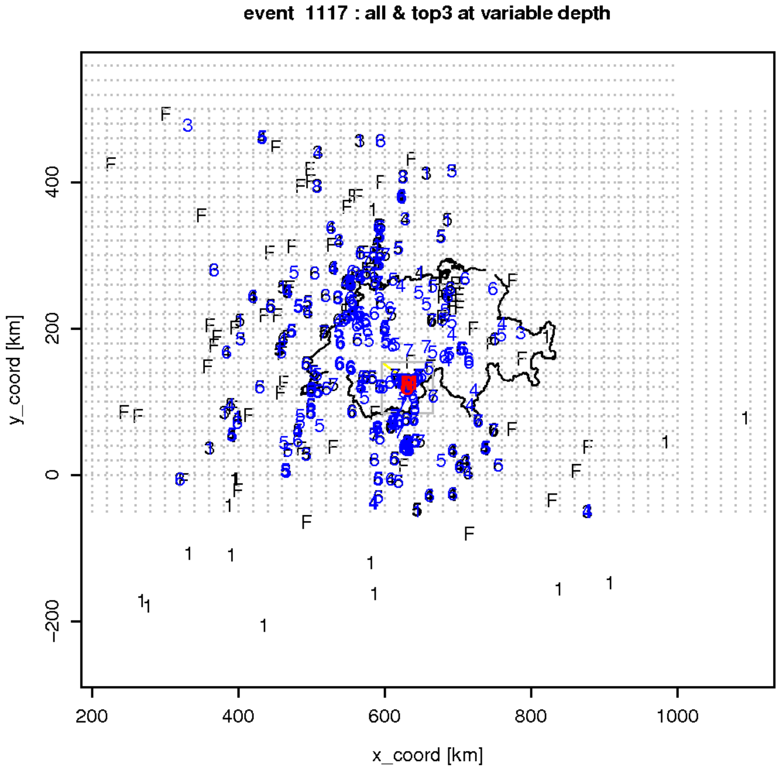
event 1117 : all & top3 at variable depth
y_coord [km]
x_coord [km]

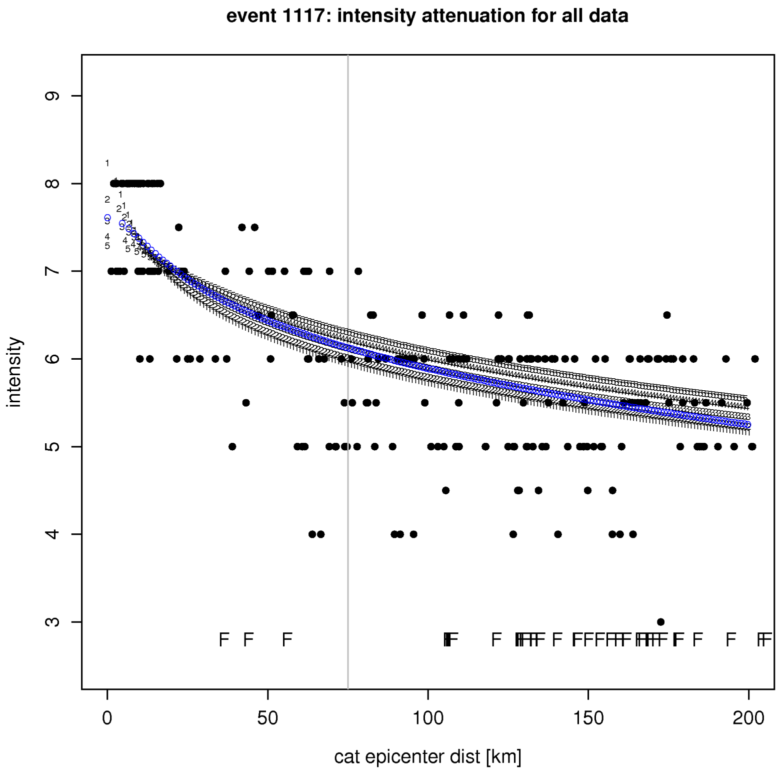
event 1117: intensity attenuation for all data
intensity
cat epicenter dist [km]

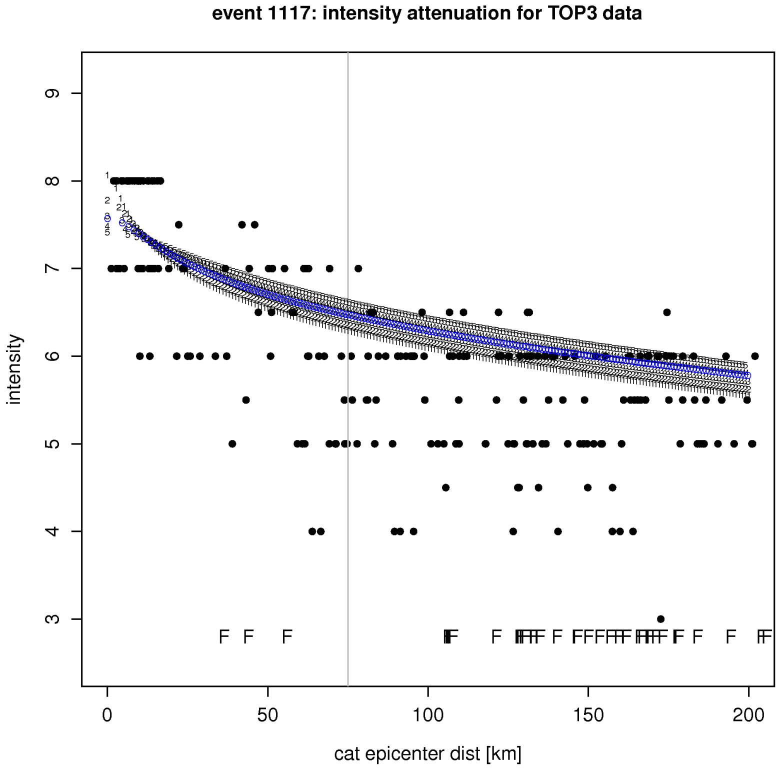

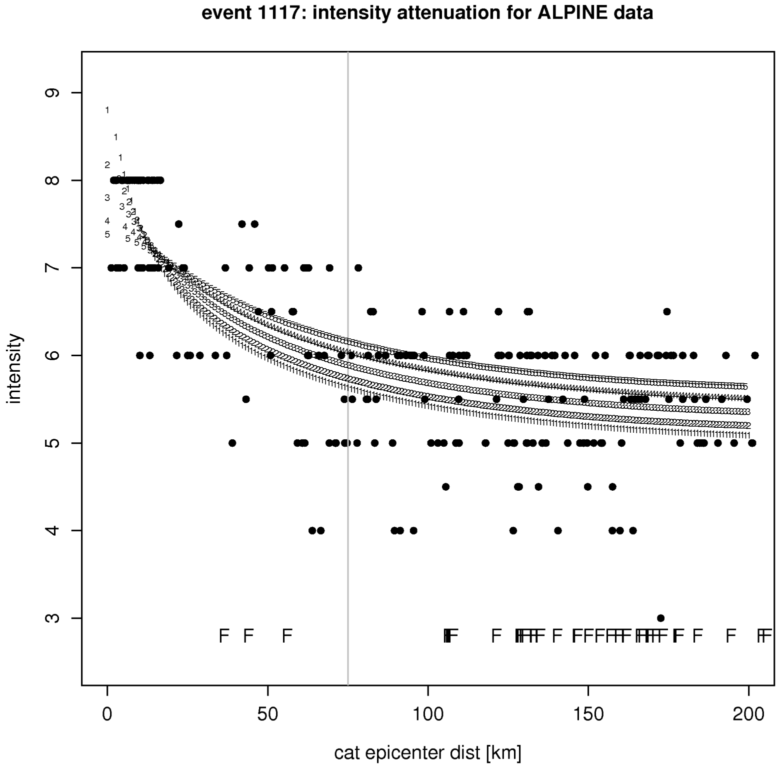

Event 1117 (1855.07.25): Assigned magnitude 6.2, depth 10 km.

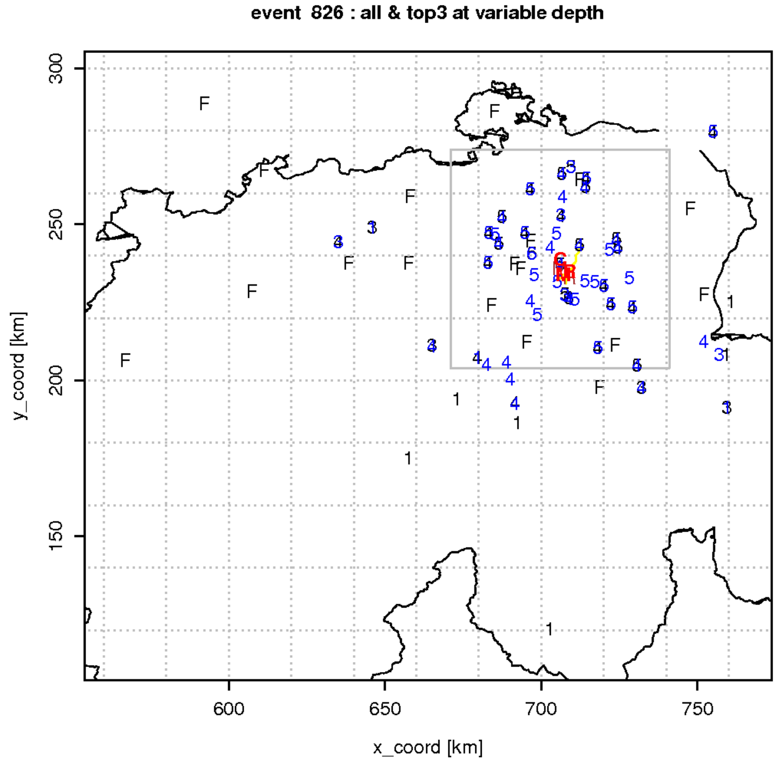
event 826 : all & top3 at variable depth
y_coord [km]
x_coord [km]
150
200
250
300
600
650
700
750

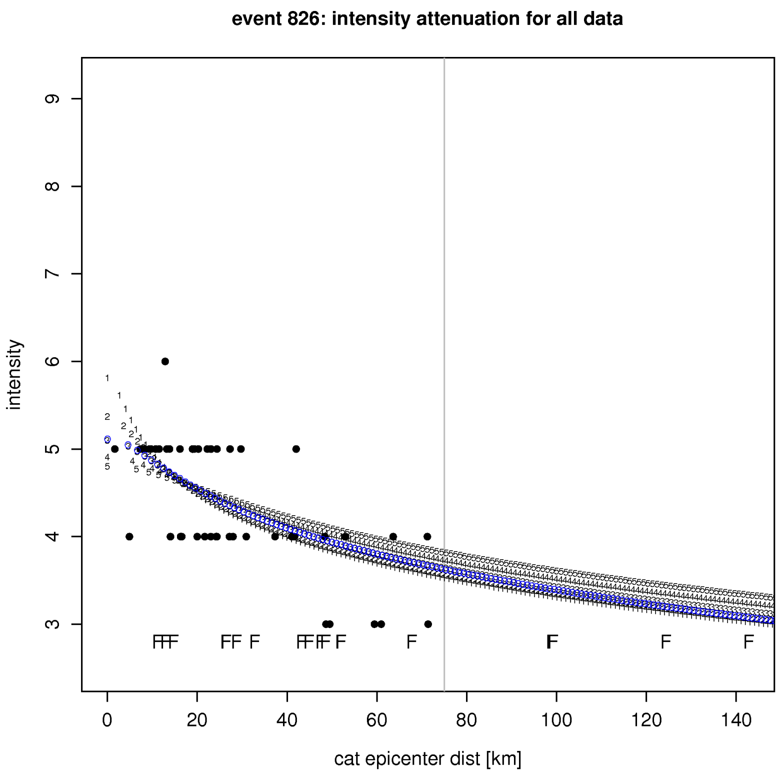
event 826: intensity attenuation for all data
intensity
cat epicenter dist [km]
3
4
5
6
7
8
9
0
20
40
60
80
100
120
140

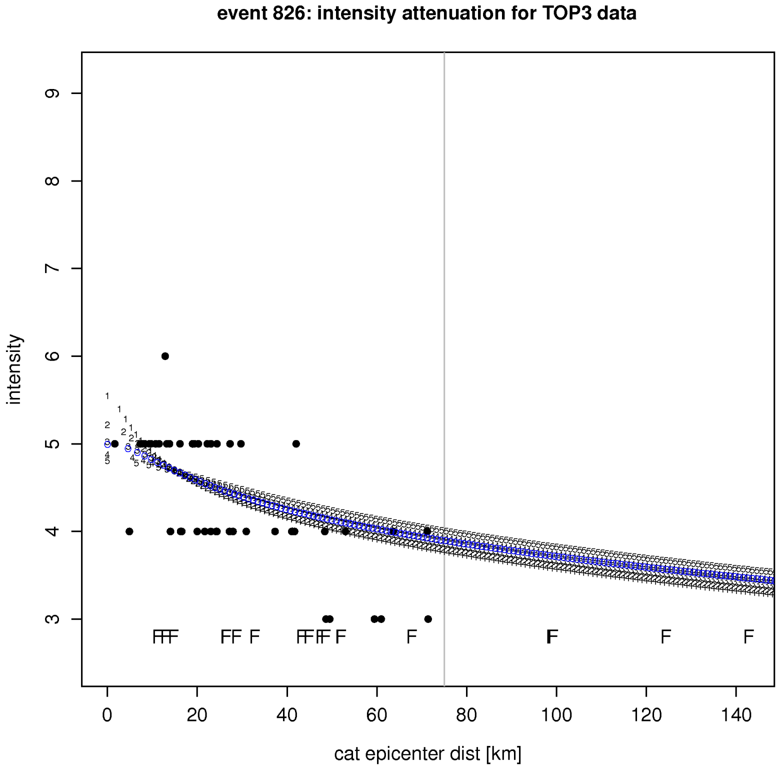

Event 826 (1877.05.02): Assigned magnitude 4.4, no depth.

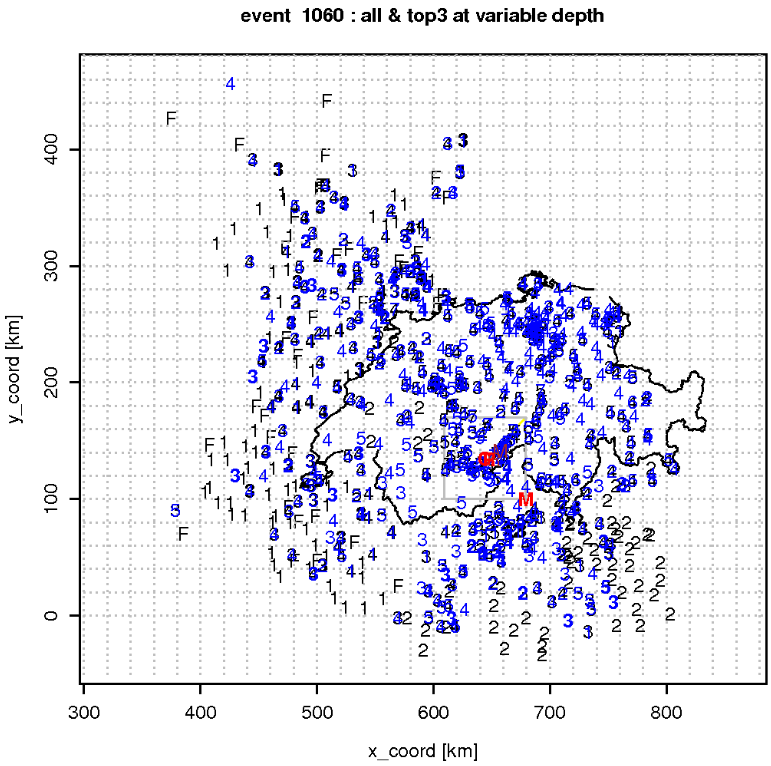

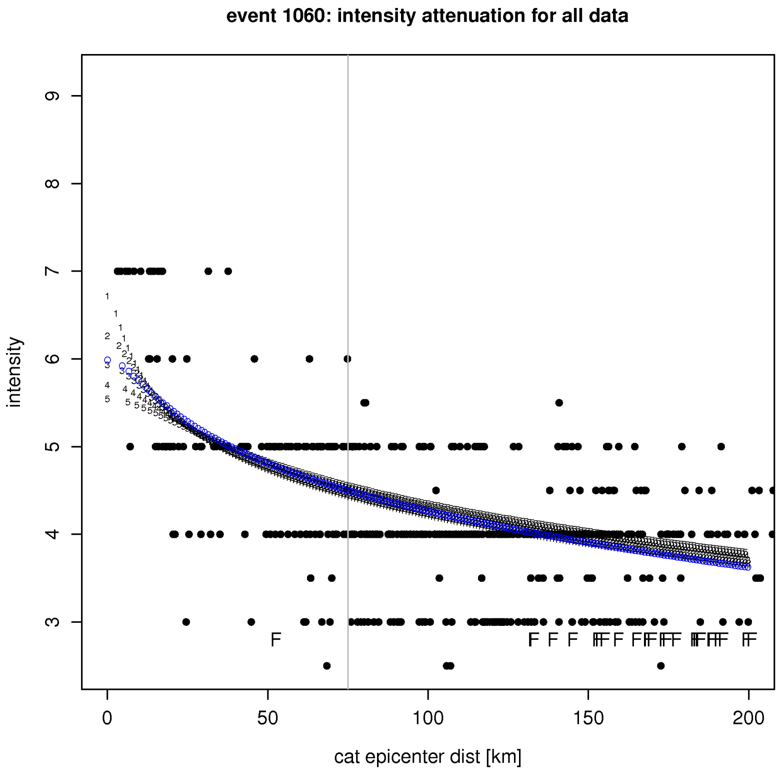
event 1060: intensity attenuation for all data
intensity
cat epicenter dist [km]
0
50
100
150
200
3
4
5
6
7
8
9
F

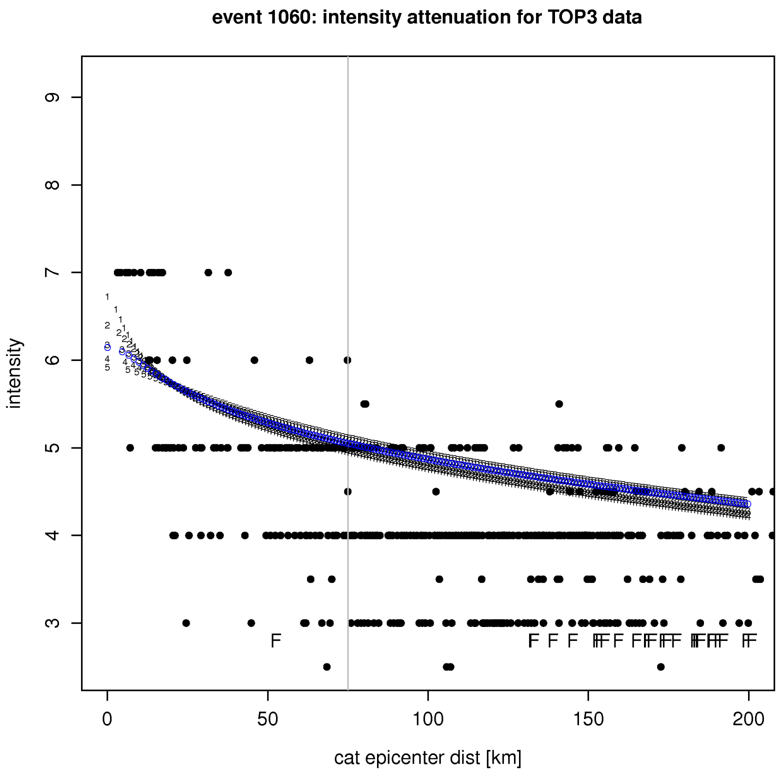
event 1060: intensity attenuation for TOP3 data
intensity
cat epicenter dist [km]
0
50
100
150
200
3
4
5
6
7
8
9
F

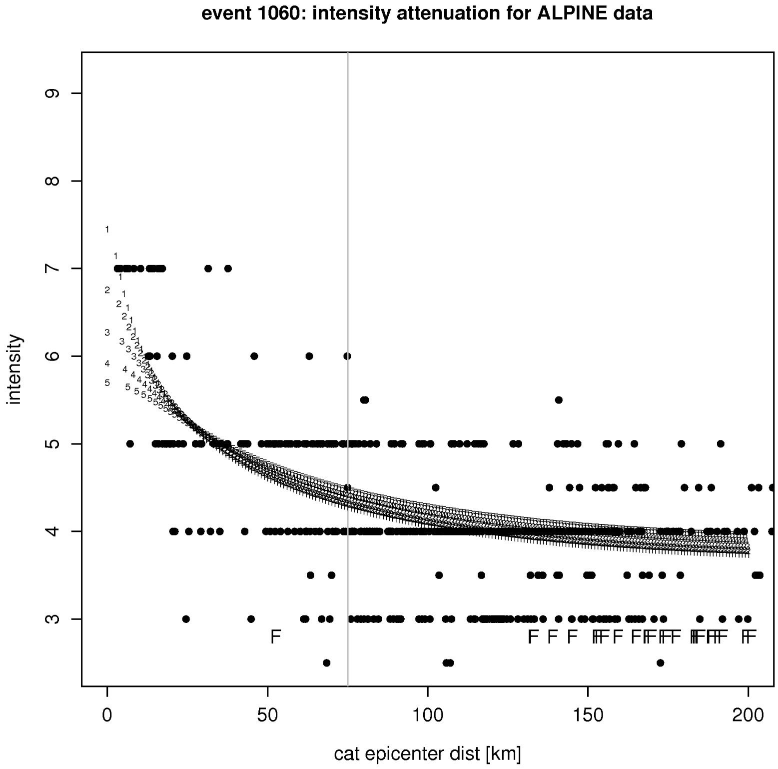

Event 1060 (1960.03.23): Assigned magnitude 5.0, depth 5km.

6 References

Ambraseys, N. (1985). Intensity-attenuation and magnitude-intensity relationships for Northwest European earthquakes. *Earth Eng. Struct. Dyn.*, **13**, 733-778.

Bakun, W. H., and C.M. Wentworth (1997). Estimating earthquake location and magnitude from seismic Intensity data, *Bull. Seism. Soc. Am.*, **87**, 1502–1521.

Bakun, W. H and O. Scotti (2006). Regional intensity attenuation models for France and the estimation of magnitude and location of historical earthquakes, *Geophys. J. Int.*, **164**, 596–610.

Bernardi, F., J. Braunmiller, and D. Giardini (2005). Seismic moment form regional surface-wave amplitudes: amplications to digital and analog seismograms, *Bull. Seism. Soc. Am.* **95**, 408-418.

Blake, A. (1941). On the estimation of focal depth from macroseismic data. *Bull. Seism. Soc. Am.* **31** (3). 225-232.

Braunmiller, J., N. Deichmann, D. Giardini, S. Wiemer, and the SED Magnitude Working Group (2005): Homogeneous Moment-Magnitude Calibration in Switzerland. *Bull. Seism. Soc. Am.* **95**, No. 1, Feb. 2005.

Fäh, D., D. Giardini, F. Bay, F. Bernardi, J. Braunmiller, N. Deichmann, M. Furrer, L. Gantner, M. Gisler, D. Isenegger., M.J. Jimenez., P. Kaestli, R. Koglin, V. Masciadri, M. Rutz , C. Scheidegger, R. Schibler, D. Schorlemmer, G. Schwarz-Zanetti, S. Steimen., S. Sellami, S. Wiemer, and J. Wossner (2003). Earthquake catalogue of Switzerland (ECOS) and the related macroseismic database. *Eclogae Geol. Helv.*, **96**, 219-236.

Gasperini, P. (2001). The attenuation of seismic intensity in Italy: a bilinear shape indicates the dominance of deep phases at epicentral distances longer than 45 Km. *Bull. Seism. Soc. Am*. **91**, 826-841.

Gómez Capera A.A. (2006). Seismic hazard map for the Italian territory using macroseismic data. *Earth. Sci. Res. J.*,**10-**2, 67-90.

Hinzen K.G. and M. Oemisch (2001). Location and magnitude from seismic intensity data of recent and historic earthquakes in the Northern Rhine Area, Central Europe. *Bull. Seism. Soc. Am*, **91**,1, 40-56.

Kövesligethy, R. (1906). Mathematikai és Természettudomanyi Értesitö. **24**. 349-368 (in Hungarian).

Kovesligethy, R. von. (1907) 'Seismischer Stärkegrad und Intensität der Beben', *Gerlands Beitr. Geophys*. **8.**

Musson, R., Jiménez, MJ. And Gómez Capera AA (2008). Macroseismic estimation of earthquake parameters. *British Geological Survey Open report*, OR/08/004, 55pp.

Shebalín, N.(1968), Método de utilización de datos ingeniero-geológicos en la zonificación sísmica. En:Zonificación sísmica de la U.R.S.S. *Nauka*. 95-111.

Swiss Seismological Service, (2002). ECOS - Earthquake Catalog of Switzerland. ECOS Report to PEGASOS, Version 31. 3. 2002, Appendix A: ECOS Database. SED, Zürich. http://histserver.ethz.ch/.

APPENDIX D-1

Site amplification factors for intensity attenuation; A case study for Switzerland

Philipp Kästli and Donat Fäh,
Swiss Seismological Service, CH-8092 Zurich

Unpublished
November 2008

Abstract

Local soil conditions can notably affect earthquake ground motion. This is often seen in macroseismic intensity fields where sites located on soft sediments show higher intensities than neighbouring locations do. To map expected macroseismic site amplification for Switzerland, we statistically analysed differences between observed macroseismic intensity and intensity estimates based on the Swiss attenuation relations, using macroseismic data from 221 earthquakes. Two regional attenuation relations were used (Alps and Foreland), each of them with two parameter sets for deep and shallow sources. The subsoil conditions of the localities were described by a combination of geological and tectonic characteristics. We categorized site conditions using a standardized size for the area around the centre of each settlement. Typical intensity amplifications of the site classes were calculated from the median intensity residuals between observed and calculated intensities.

Median observed amplifications relative to well-compacted sediments vary between about +0.7 intensity units for some eroded maritime sedimentary rocks and organic soils, and about –0.3 intensity units for Alpine flysch. Many crystalline rock classes could not be characterized, since there are too few settlements on them. Variability within one site class is large, and reaches values in the range of about one intensity unit. Some investigated villages show remarkable intensity anomalies for all analysed earthquakes.

Our analysis has some limitations where settlements are not regularly distributed within one soil class. A good example occurs in alluvial plains, where most settlements are located at the edges of the sedimentary basins. Moreover, the regional attenuation relations that we used account for some site effects. This was due to different averages in site conditions intrinsic to the data employed for deriving the Alps and Foreland attenuation relation. We therefore suggest that macroseismic attenuation relations should be developed from combined assessments of attenuation and site amplification.

Two case studies of recent smaller events in Basel and the Valais show that scenario calculations based on Swiss attenuation relations and macroseismic site amplification predict intensities that deviate no more than one intensity unit from those observed at about 90 % of the sites. These case studies cover only observed intensities up to intensity V. However, the underlying attenuation relations and site amplification factors were derived from observations with intensities up to VIII in some cases. We therefore suggest using the presented site amplification factors for earthquakes with magnitudes between 3 and 5.5.

Keywords: intensity, site amplification, geological soil classification, macroseismic attenuation, earthquake scenario, Switzerland

1 Introduction

It is evident from theory and observation that on soft soils, earthquake ground motion is amplified relative to hard rock sites at a similar distance from the seismic source. Elevated ground motion leads to a higher earthquake impact and higher observed intensity and more damage. However, it is not easy to predict the effects of a particular earthquake in a specific locality with no investigations at the site. Such effects depend on many factors: shear wave velocity and composition of the material, layer thickness, groundwater level, velocity contrast between sediments and bedrock, three-dimensional geological configuration and finally vulnerability of structure (e.g. Rodriguez Marek et al. 1999). Each earthquake also produces a particular ground motion relative to its tectonic situation, source depth and mechanism, and

directivity and characteristics of the rupture process. However, those parameters are usually not known before or immediately after an earthquake.
Estimates of amplifications in terms of macroseismic intensity are an important input for reliable ground motion maps and scenario simulations, especially for areas such as Switzerland with very variable local geology (Figure 1). Intensity is convenient, since it relates directly to damage and yields hazard values, which are relevant to planners and insurers. To estimate the geographical distribution of the amplification effects, there are three common ways:

1. Defining intensity site amplification for soil classes (or topographic features) with reference to measured or modelled ground motion. The conversion from ground motion to intensity is often expressed by parameters such as peak ground acceleration (PGA) or peak ground velocity (PGV) (e.g. Wald et al. 1999). However, the ability of different ground motion parameters to represent intensity varies over the intensity scale. Moreover, the relationship between ordinal intensity and a continuous ground motion parameter is neither linear nor open to extrapolation (Kästli & Fäh, 2006).
2. Detecting intensity amplification on a site-by-site basis, from statistical analysis of past intensity assignments at that site (e.g. Gallipoli et al. 2003). Although this method may provide useful results that can be reproduced for the sites considered, it does not necessarily link amplification to known soil characteristics. As a result we cannot extrapolate the results in space.
3. Deriving intensity amplification by soil class from historical macroseismic data (e.g. Fäh 1985). What are typical differences between observed intensities and those estimated from attenuation relations? A precondition for this method is a long track record of macroseismic intensities consistently assigned.

In this paper we will apply the third procedure and compare to results from the second method for Swiss site with clear intensity anomalies. The model is tested by comparison to observations for two recent earthquakes.

2 Task and methods

Our main goal is to quantify site amplification for typical soil and rock classes in Switzerland using method three above. Site amplification factors are defined with respect to the Swiss macroseismic attenuation relations (SED, 2002; Fäh et al., 2003).
The Earthquake Catalog of Switzerland (ECOS02) provides a uniform estimate of the moment magnitudes Mw for all historical and instrumental events. The historical events were assessed following the proposal of Bakun & Wentworth (1997). This uniform earthquake size estimate in terms of magnitude required a magnitude/intensity calibration based on a calibration dataset of earthquakes in the 20th century for Switzerland and adjacent areas, and the development of macroseismic attenuation relations (Fäh *et al.* 2003). The relations can be summarized as follows:

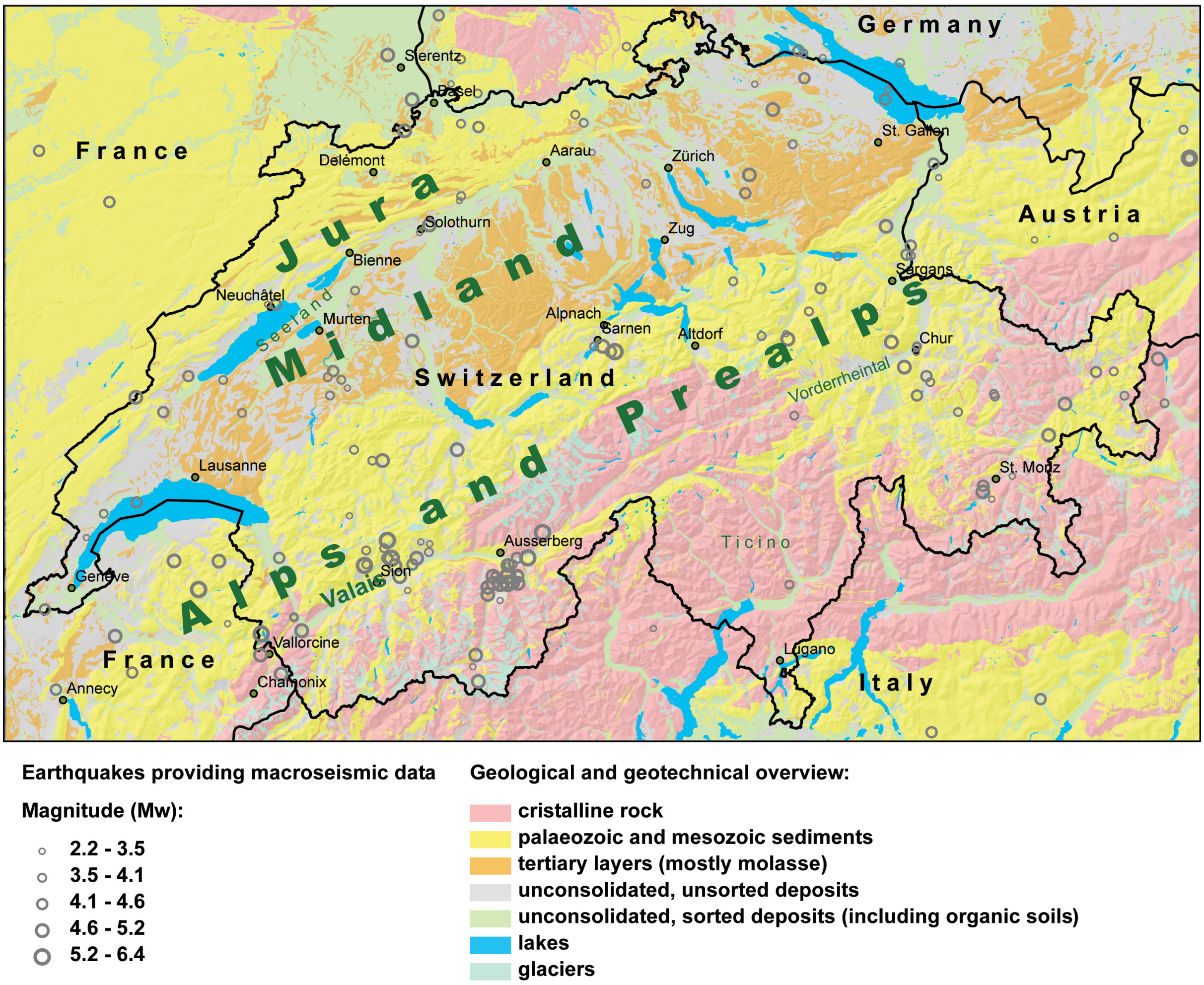

Figure 1: Basic geological overview of Switzerland. The epicentres of felt earthquakes since 1850 are shown as circles. Macroseismic intensities from these events were used in our analysis. Place names mentioned in the text are provided.

For sites in the range up to 55 km epicentral distance, the following attenuation model is used:

Shallow events:	$I_{exp} = 1.27 * M_w - 0.043 * D + 0.096$
Deep events:	$I_{exp} = 1.44 * M_w - 0.030 * D - 1.73$

I_{exp} is the EMS98 Intensity value (European Macroseismic Scale (Grünthal, 1998)) at the site; D is the distance (km) from the source location to the site. The constants were derived from the calibration set of events in the magnitude range up to Mw 6.1.
For sites in the 55-200 km distance range the attenuation relations are as follows:

Shallow foreland events:	$I_{exp} = 1.27 * M_w - 0.0115 * D - 1.65$
Shallow alpine events:	$I_{exp} = 1.27 * M_w - 0.0064 * D - 1.93$
Deep foreland events:	$I_{exp} = 1.44 * M_w - 0.0115 * D - 2.76$
Deep alpine events:	$I_{exp} = 1.44 * M_w - 0.0064 * D - 3.04$

For magnitudes above Mw=5.5 it is recommend using only the relation for deep events. The calculated intensities are valid for soils of class B (well consolidated sediments) according to the Swiss building code SIA 261 (SIA 2003) and Eurocode 8 (Commission of the European Communities 1998).

To compute soil specific amplification factors, three data sets are compared:

a) Intensity data points (IDPs) at the Swiss village or city district level, observed since 1850, for earthquakes with a maximal observed intensity of at least V on the European Macroseismic Scale (EMS-98) (see Figure 1);
b) Expected macroseismic intensity for these sites and the specific earthquakes computed with the Swiss macroseismic attenuation laws summarized above (Fäh et al. 2003);
c) Soil characterisation of the locations, expressed by the geological as well as the geotectonic classification of the Geological and Tectonic Maps of Switzerland 1:500'000 (Geologische Karte der Schweiz / Geotektonische Karte der Schweiz, Bundesamt für Landestopographie, 2006).

The Swiss Seismological Service (SED) has collected macroseismic information for all significant earthquakes in Switzerland and neighbouring countries. This dataset with roughly 35'000 EMS-98 intensity assignments covers 720 earthquakes and 17'000 settlements in and around Switzerland. For our study we selected from this database IDPs that

1) refer to sites within Switzerland, of which the surface geology as well as the coordinates of the settlements are homogeneously established;
2) refer to 221 earthquakes after 1850 with maximum intensities larger than intensity IV. The moment magnitudes of these events range from 2.7 to 6.4, with a median of 4.3. The epicentre location uncertainty is smaller than 10 km for 64 % of the events, and up to 20 km for the others.
3) have “medium” or higher quality following ECOS quality definitions (SED, 2002): each intensity assignment is based on the reports of at least four independent eyewitnesses or comparable sources.

To assign a soil or rock class to a settlement or zip code area, we defined all settlements as circles with a diameter of 500 m around the manually selected centre of the area densely covered with buildings. This is summarized in Figure 2. Inside each circle, the soil classes according to the geological and geotechnical maps of Switzerland were reviewed to characterize geological properties and soil variability. For our statistical analysis only those locations with one soil class covering more than 80% of the area within a circle were selected. Alternatively, calculations were performed using those sites with at least 95 % homogeneous soil conditions. They provided neither a better explanation of the intensity residuals nor significantly different amplification results for individual site classes.

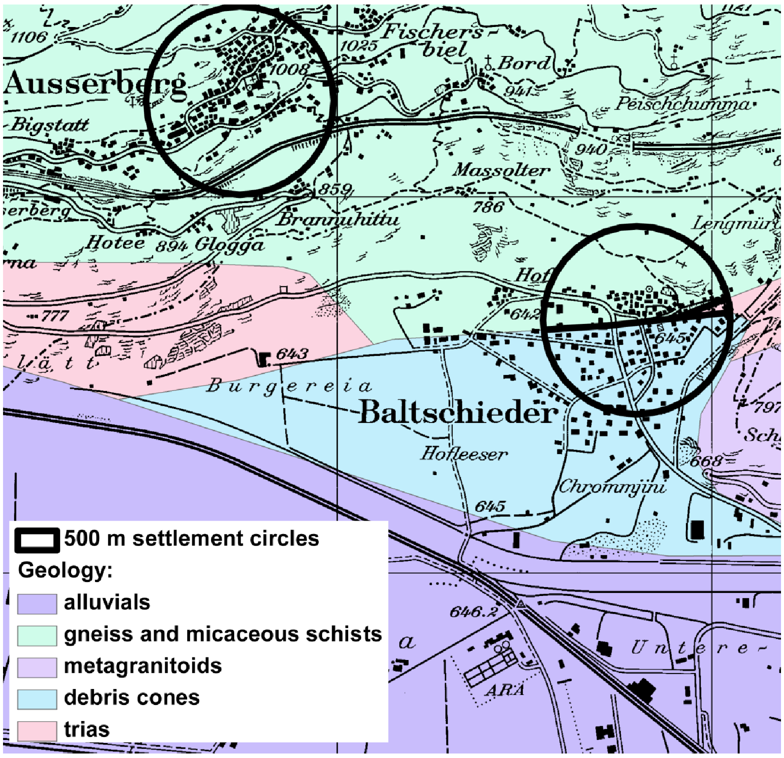

Figure 2: Example of the analysis procedure. While intensity residuals of Ausserberg were used to characterise the amplification behaviour of gneiss and micaceous schists, those of Baltschieder were discarded. There we could not assign the residual to a single soil type. The location of Ausserberg is shown in Figure 1.

As a next step, the difference between the observed and the computed intensity was calculated for every IDP. This difference (residual) is interpreted as the effect of the local site amplification in that spot. Then, sites were grouped according to their geologic, geotechnical, or combined features and checked for consistent and statistically significant coincidences between intensity residuals and soil characteristics:

1. Median residuals were calculated for every combination of a geological soil class with a geotectonic unit of the second of three geotectonic aggregation levels of the Geological Map of Switzerland (our “primary classes”).
2. The various primary classes were grouped manually into larger units wherever geologically and geotechnically similar soil types showed similar amplification behaviour. Since the geology contributes more to the statistical explanation of local amplification patterns, we used it as the main feature to aggregate results.
3. Remaining geologic primary classes were grouped by their tectonic unit if this significantly contributed to a homogeneous description of the data. In other words, several geologic subclasses of a tectonic unit were grouped if they showed the same amplification pattern.

Our result is a classification based on geological and tectonic features of Swiss subsoil conditions. The resulting classes have different macroseismic site amplification factors. The assigned amplification values were calculated as the median of the intensity residuals of all IDPs per soil class within Switzerland. The results are given in Table 1 and Figure 3.

For two soil classes, organic soils and soft silts and sands of quaternary sediments, the methodology above gave distorted results. Consequently, their amplification behaviour was assessed based on slightly modified considerations:

Historically, organic soils were avoided for settlements, and spot tests showed that many of the IDPs supposedly lying on organic soils were in fact on their edges, or contained small, only recently settled areas of organic soil. To avoid a bias, the amplification factor for organic soils was derived from a limited area around the lakes of Neuchâtel, Bienne and Murten, including the Aare valley down to Solothurn (see Figure 1 for the localities). There, we have extended areas of organic soils that allow us to estimate the macroseismic soil amplification factor for this particular soil type. We assume that this locally derived amplification factor can be applied to all Swiss sites with organic soils.

Within the class of soft quaternary silts and sands, settlements were distributed unequally. Given flooding risks, central floodplains remained unsettled until the middle 20^{th} century. Most settlements contributing to the amplification value of this soil class are near valley edges or on upper terraces. For these alluvial plains, we derived the amplification factor from all settlements, but as will be discussed further on, we recommend another interpretation scheme for applying results to typical floodplains.

3 Results

3.1 Amplification results for different soil classes

Table 1 summarized the derived residuals (the difference between observed and computed intensities) for all geologic and geotechnical soil classes for which sufficient data is available. These residuals are additive to the expected intensity from the attenuation model. There is a slight statistical correlation between intensity residuals and magnitude, but analyses based on linear models and estimations of their quality (Akaike 1974) have shown that both the direction and level of the interaction between intensity residuals and magnitude vary between different branches (alpine/forland, deep/shallow) of the attenuation model. Thus, such correlations are supposed artefacts of the non-continuous attenuation model and are not analysed further with reference to site effects. Since residuals are differences between values on an ordinal scale (observed intensities are given in integers) and a continuous regression function, we do not expect them to follow a normal distribution. We describe their distribution with non-parametric statistics as far as possible. In this context, the standard deviation of the mean residual is also rather a hint to the computed median's significance than a quantitative measure.

Table 1: Intensity residuals for different geologic and geotechnical soil classes (in EMS98 intensity units) obtained from the analysis of the macroseismic data points. Bold fields of the 50%-percentile indicate medians whose deviation from 0 is statistically significant at a 95% level.

(geological unit)	Geotectonic/regional restriction	Additional explanation	Amplification behaviour	# of IDP	25% percen-tile	50% percen-tile	75% percen-tile	Median standard deviation	Sd(mean)
a) Crystalline									
Gneis and micaceous schists			+	69	-0.48	**0.48**	0.83	1.02	0.14
b) Paleozoic									
Perm, Verrucano	Sediment cover	Remaining sediment covers of the central alpine syncline	+	18	0.21	**0.72**	1.5	1.05	0.24
c) Mesozoic									
c.1 Jura and northern Switzerland									
Lacustrine Limestones	Jura, Mesozoic and Epivariszic platforms	Limestone and Dolomite, medium phase also with thicker layers of marl	+	49	0.28	**0.74**	1.13	0.65	0.09
Keuper		Deposits of coastal areas and lagunes: heterogeneous layers of limestone, gypsum, marl	+	15	0.26	**0.75**	1.29	0.75	0.19
Dogger	Jura, mesozoic and epivariszic platform	sandstone	+	49	-0.05	**0.47**	0.84	0.66	0.14
Malm, Jura	Mesozoic and epivariszic platform		+	83	0.22	**0.49**	1.19	0.81	0.1
Malm, Jura	Alpine nappes		0	38	-0.37	**-0.05**	0.54	0.66	0.15
Lower Cretaceous	Inner jura	Marls and mudstones	+	33	-0.28	**0.64**	0.92	1.1	0.22
	Other facies of inner jura		+	27	-0.24	**0.9**	0.93	0.92	0.21
c.2 Northern Pre-alps									
Malm & lower Cretaceous	Alpine nappes	Malm: High share of compact, nearly pure (“white”) calcium carbonate rocks	0	39	-0.36	-0.03	0.60	0.67	0.14

d) Tertiary									
d.1 Tertiary of Swiss midland and northern Switzerland									
Ruppelien, lower saltwater molasse	Tertiary grabens	Fine-grain sandstones, marls and clay	+	26	0.19	**0.47**	0.78	0.48	0.11
Aquitanien, lower freshwater molasses	Midland molasse		+	132	-0.35	**0.52**	1.19	1.19	0.1
Chattien/lower freshwater molasse	Jura and midland molasse	sandstones, marls and clay (grain size decreases from the northern Pre-alps towards the Jura)	+	63	0.02	**0.58**	0.97	0.76	0.12
Burdigalien, Helvetien of the Allgäu region. Upper saltwater molasse	Midland molasse	sandstones, marls and clay (grain size decreases from the northern Pre-alps towards the Jura)		95	-0.47	**0.56**	1.11	1.15	0.13
Upper feshwater molasse		sandstone interbedded with marl and siltstone. Grey marl is the dominant lithology		257	-0.17	**0.6**	1	0.75	0.07
	Other facies of midland molasse		+	65	-0.26	**0.47**	0.87	0.82	0.12
d.2 Tertiary of the Northern Prealps									
Flysch	Alpine and prealpine area		-	49	-0.96	**-0.31**	0.36	0.97	0.14
Chattien, lower freshwater molasse	Subalpine molasse	Dominant conglomerates, intersected with sandstones	0	52	-1.19	0.06	0.66	1.11	0.17
e) Pleistocene									
e.1 moraines									
Moraine on flysch		Alps and Pre-alps	0	33	-1.51	0.14	0.52	1.03	0.22
Moraine on subalpine molasse		Alps and Pre-alps	0	28	-0.7	0.1	0.62	1.04	0.25
Moraines, incl. recent moraines	Alpine nappes	Alps and Pre-alps	0	137	-0.61	0.14	0.85	1.08	0.10

Moraines, including recent moraines	Midland molasses and Jura	Foreland	+	846	-0.48	**0.39**	1.01	1.01	0.04
e.2 non-glacial deposits									
Older fluvioglacial gravel terrasses			+	21	0.21	**0.73**	1.27	0.80	0.22
Loess, loess loam and weathered loams			+	58	0.22	**0.72**	1.27	0.78	0.11
Fluvioglacial and glaciolakustric gravels (terraces)			+	931	-0.14	**0.47**	1.06	0.89	0.03
Late pleistocene landslide deposits	Thick late Pleistocene landslide deposits		0	19	-0.95	-0.02	0.57	1.1	0.24
f) Holocene									
Alluvials	Jura, Mesozoic/Epivariszic Platform, Midland molasses		+	249	-0.31	**0.41**	1.06	1	0.07
Alluvials	Big alluvial plains		+	419	-0.33	**0.33**	1.05	1.03	0.05
Alluvials	Wildhorn nappes	Area of Stans, valleys of Sarner and Engelberger Aa; with high share of lake sediments	+	52	-0.19	**0.32**	0.9	0.81	0.14
Alluvials	Buendnerschiefer nappes	Hinterrheintal and other small areas of Graubünden	0	15	-0.59	-0.02	0.42	0.81	0.21
Alluvials	Other alpine nappes	Small areas along steep alpine river, throughout the alps	0	78	-1.00	0.00	0.72	1.21	0.15
Hill foot debris			+	51	-0.32	**0.46**	1.09	1.05	0.17
Postglacial landslides			(+)	53	-0.45	0.23	0.68	0.81	0.15
Debris cones of rivers		Mostly cones of steep contributory rivers and ravine grabens in the alpine and pre-alpine main valleys	0	369	-0.78	0.09	0.79	1.2	0.06
organic soils		(based on regional studies of the Seeland region)	+	62	-23	**0.72**	1.39	1.22	0.15
	Thick quarternary deposits in general		(+)	10	-0.2	**0.48**	0.52	0.32	0.17

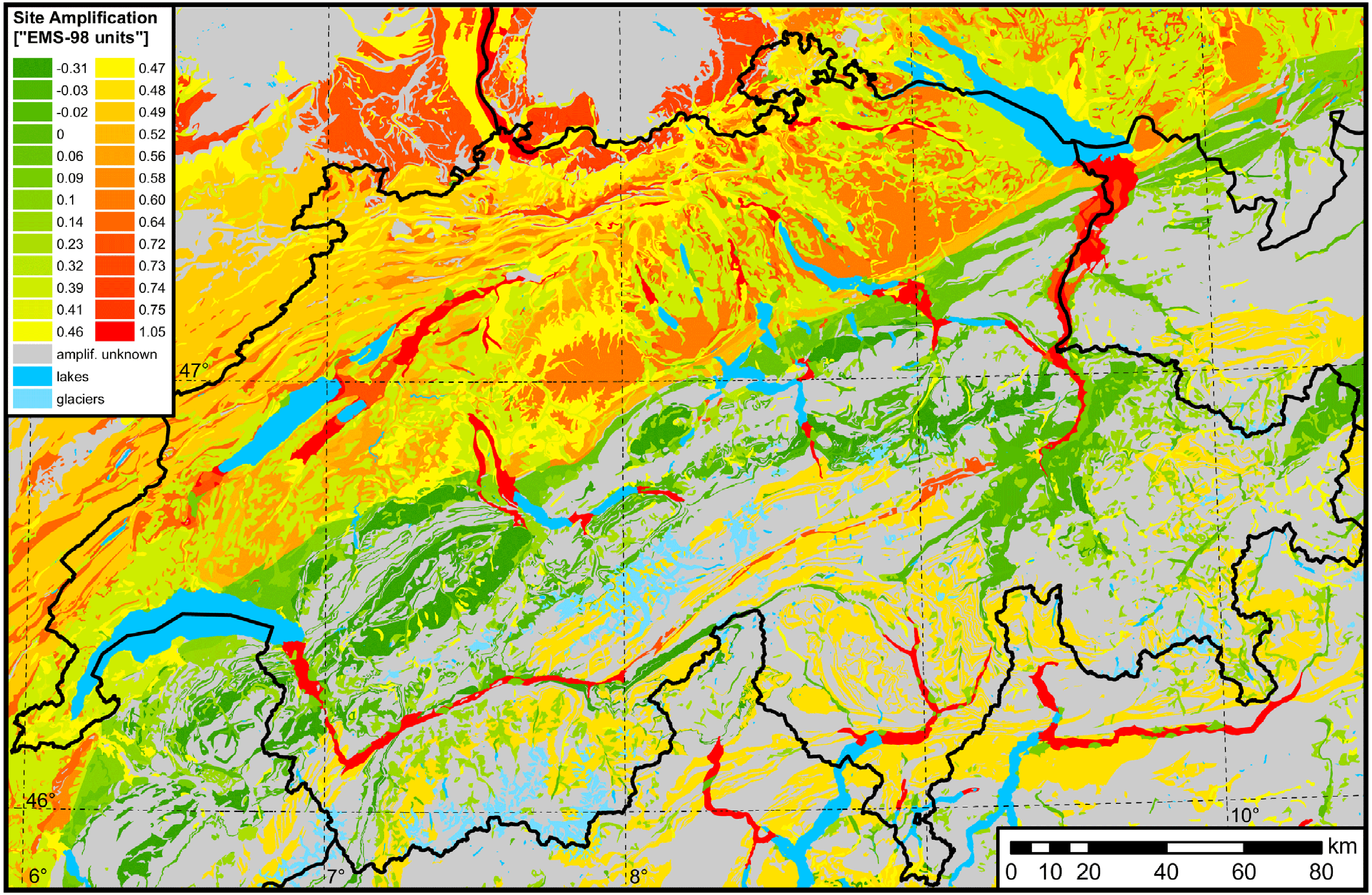

Fig. 3. Site amplification map for Switzerland obtained from the analysis of macroseismic data. This map shows the median values derived from the statistical analysis. For big floodplains we used the 75th-percentile as the best amplification estimation (see text).

Crystalline bedrock (site class group a in table 1)

While rock sites a usually assumed to cause no amplification effects, macroseismic data provide no way to derive site (de-)amplification for rock sites, since there are not enough settlements on different types of crystalline bedrock to allow statistically significant results. The exceptions are gneiss and micaceous schists. They are common in central Switzerland, the southern side-valleys of the Valais region and in the Ticino where our intensity data are best (see Figure 1 for the locations). Here, the data show a typical elevation of 0.48 intensity units. We have no mechanical explanation for this behavior, except a possible weathering of the uppermost layer. A more probable interpretation could be that the used attenuation relations do not correctly describe the far field attenuation behavior in the Ticino region. We lack near field observations there due to its low seismicity. For the large areas of crystalline rocks without sufficient macroseismic data to derive the amplification behaviour, we think that "no amplification" is still a reasonable assumption.

Paleozoic deposits (site class group b in table 1)

Paleozoic deposits of the central alpine syncline (upper Valais and Vorderrheintal) show a relatively high amplification of 0.72 (+- 0.24) intensity units. One possible explanation would be heterogeneities within these sediments (e.g. deeply weathered surface layers vs. unweathered underlying strata). Single-site analyses using geophysical methods already started in the Valais may provide closer insight.

Fine grain maritime mesozoic and tertiary deposits (fine-grain classes of groups c and d: limestone, marl, flysch)

All Mesozoic deposits of the Jura and northern Switzerland show relatively high site amplification. These sediments mix hard limestone formations with soft marl layers. Observed amplification is higher on facies with a high share of soft layers and heterogeneous layering (e.g. Keuper) than on geological classes with a high share of compact limestone rocks (e.g. Malm), However, the compact limestone areas are often in locations on steep rock areas or karst with little soil formation and are therefore only sparsely populated. Settlements are concentrated rather on the marl sites, often with deep loamy topsoil. Thus, we assume that the higher amplification in the Jura region might not be typical for the whole area, but valid for the sites of most villages and settlements.

In the limestone Pre-alps, we do not observe this phenomenon: The prealpine Malm-dominated nappes do typically not show any site amplification. At the moment, it is not obvious whether this is explained by a lower share of marl in the local limestone layers or other factors such as a higher grade of geological metamorphizationduring the formation of the Alps. Also, we do not have a mechanical interpretation for the observed deamplification in all flysch sites. It may be common for many rocky sites of the Alps to lead to lower intensities than those expected for well compacted sediments; however, most of them are hardly settled and thus no intensity residuals are available for analysis. Here, flysch is an exeption: It forms fertile, agriculturally productive soils and is settled densely enough to be well reflected in the macroseismic data.

Tertiary Molasse Deposits (site class group d in table 1)

The main tertiary deposits, the molasses of the Swiss midland and the northern Pre-alps, are left by rivers flowing from the Alps north. While in the Prealps, the main deposits are stable conglomerates: northern deposits are dominated by sand and siltstone with different states of consolidation. Generally, no site amplification is observed on hard Prealpine conglomerates, but finer grained tertiary deposits of the midland show site amplifications of 0.47 to 0.6 intensity units. In this case we can also assume that the state of weathering is key.

Pleistocene and Holocene Deposits (groups e and f)

Moraines are well compacted, although not cemented, with a very heterogeneous mixture of grain sizes ranging from silt to big stones. According to the data, they do not tend to amplify ground shaking. However, the different behavior of moraines on midland molasses (amplification similar to uncovered midland molasse) from moraines on Pre-alpine molasses and Alpine nappes (no significant amplification) may indicate that amplification is due to layers below the moraines.

For deposits not compacted by a glacier, we observe two tendencies:

1. Heterogeneous deposits, such as big landslides and debris cones, show little or no amplification, while sorted sediments such as river and hill foot deposits may cause median amplifications of 0.3 to 0.7 intensity units.

2. Among sorted sediments, coarse grain deposits or those from steep rivers in the alpine area, show less amplification than fine-grained midland river sediments (alluvial sediments on midland molasses, + 0.4 intensity units) and finest grain lake and aeolic sediments (loam and loess, > +0.7 intensity units). Amplification observed on alluvial sediments of the Wildhorn nappes supports this observation. Although alpine, they are widely dominated by lake deposits of Lakes Lucerne, Alpnach and Sarnen.

One soil class, the big alluvial plains, needs further discussion:

Data from big Holocene floodplains show lower site amplifications than we might expect with a medium value of only 0.33 intensity units. However, water saturated, very unstable sand and silt layers are common here, and earthquake ground motion measurements, as in the lower Valais area, show amplifications up to a factor of ~10 between soft sediments and bedrock (corresponding to about 1-2 intensity units) for the central Rhone valley (Roten et al., 2008). We suppose that the low amplification detected in the macroseismic data comes from the location of the ancient settlements at the edges of the valley floor on more compact sediment layers of upper terrasses or even partly on hard rock sites, due to the danger of flooding. Only recently, in the last few decades, settlements (and more often industrial facilities) were constructed on former flood plains. These sites are supposed to experience high amplification of earthquake ground motion, but they are not well represented in the macroseismic dataset. Therefore, we recommend assigning a site amplification of +1.05 intensity units (corresponding to the 75th percentile of observed intensity residuals) for typical floodplains rather than the median of historical data. This recommendation applies especially for stronger earthquakes above magnitude 4 – 4.5, which provide enough energy at lower frequencies to excite the fundamental frequency of resonance in sedimentary basins and basin-edge generated surface waves of significant amplitude. The recommendation needs verification in future earthquakes.

3.2 Discussion of the reference site condition

By comparing macroseismic intensities of recent events to recorded ground motion within the same settlement, a conversion equation between ground motion parameters (peak ground acceleration and velocity, Housner intensity) and macroseismic intensity was recently derived (Fäh et al., 2005; Kästli and Fäh, 2006). Fäh et al. (2005) applied this ground-motion intensity conversion to the values of the Swiss ground motion attenuation relation (Bay et al., 2003; 2005). The ground motion recordings used in the Swiss ground motion attenuation relation are from sites of the Swiss National Seismic Network. All seismometers from the sites used are placed on good quality bedrock. Some stations are also located in tunnels and galleries. This ground motion attenuation relation is therefore valid for good quality rock conditions. It was estimated that the reference ground condition has shear-wave velocities of about 1500m/s in the upper 30m. This unweathered rock is usually not settled; it differs considerably from the reference ground condition of the macroseismic attenuation relation. As a consequence, we observe that the intensities calculated for hard rock sites are 0.75 to 1.25 intensity units below those of the macroseismic attenuation relation for magnitudes in the range 4.2 to 6.2 and epicentral distances larger than 20km (see Figure 4). The differences observed at distances smaller than 20km point to an inconsistency in the formalism to describe near-source attenuation for macroseismic data and ground motion parameters (especially the handling of hypocentral depth), which needs to be improved in future ground motion attenuation studies.

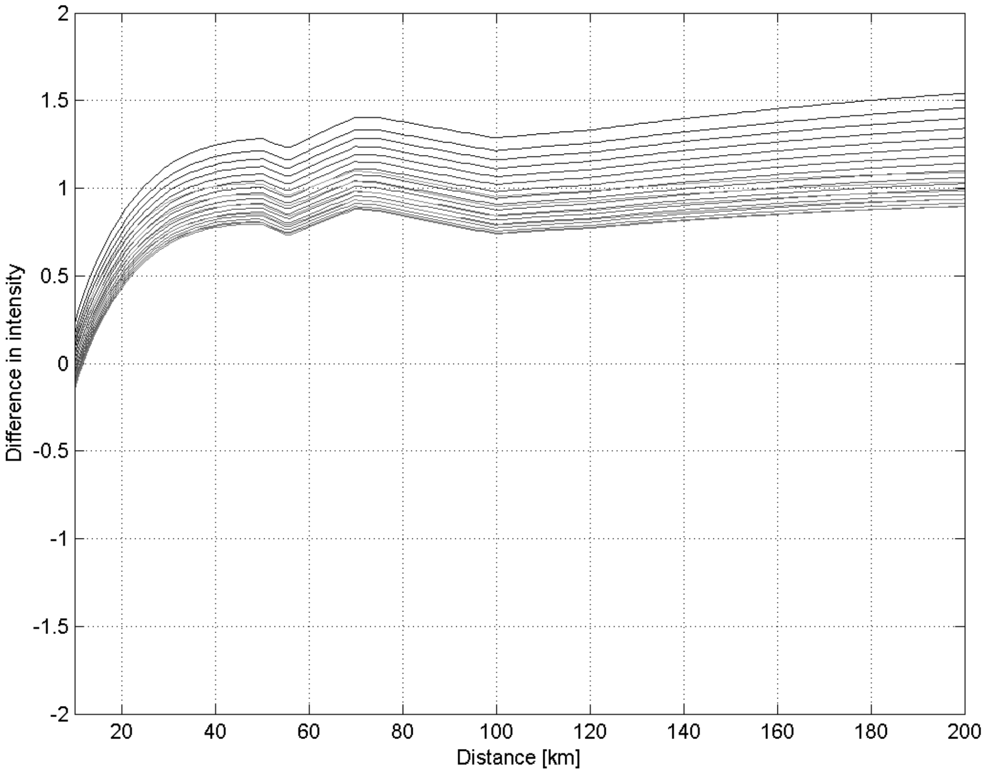

Figure 4: Difference between the macroseismic attenuation model for Switzerland (for deep events) and intensities computed from the Swiss ground motion attenuation model for sites in the Swiss Foreland (modified from Fäh et al., 2005). Single lines show different magnitudes of the events in the range Mw=4.2 and 6.2. The difference first decreases and then increases with increasing magnitude.

3.3 Comparing results to studies based on regional data

The intensity residuals found in our study are very similar to Beer's findings (1997) for soft soils in the Swiss Foreland as well as for sites on marl in the Sub-alpine Rhine valley, Central Switzerland and the region around Solothurn (Figure 5). Fäh (1985) detected amplification effects of 0.5 intensity units or more for Pleistocene gravel and Holocene river sediments, while an effect on clay sites was not detectable. His dataset consisted of macroseismic intensity points from northern and eastern Switzerland. Fäh's reference soil behaviour corresponds to sites more affected by site amplification than SIA soil class B. As a result, rock sites (mostly limestone) show negative amplification effects of about 0.5 intensity units.
Fäh (1985) as well as Beer (1997) show that within sedimentary basins, the groundwater level is a good indicator for site amplifications. For sites with groundwater depth smaller than 9 m, intensity residuals are roughly one intensity unit higher than on those with a groundwater level below 30 m. This effect can be shown only on a local scale, since groundwater levels are not mapped homogeneously throughout Switzerland.

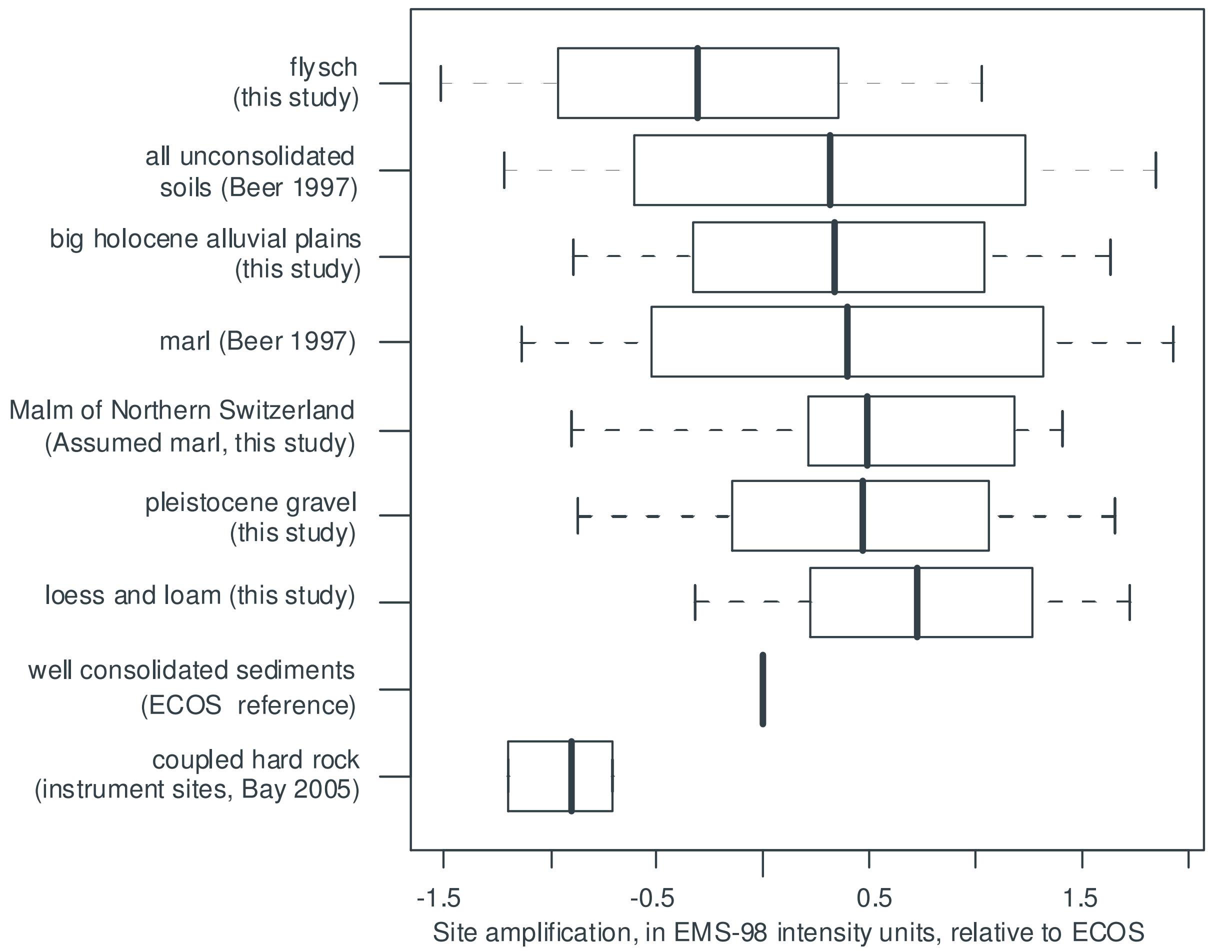

Figure 5: Typical intensity residuals for different geotechnical soil classes. Boxes cover the median average deviation (this study), or one standard deviation in the case of hard rock conditions (Fäh et al., 2005) and Beer's work (1997). Whiskers delimit 90%-quantile or 90%-confidence intervals, respectively.

3.4 Results for specific localities

Site by site characterizations based on intensity residuals (without grouping or extrapolation) can be applied for settlements with intensity observations for at least 8-10 earthquakes. Figure 6 shows settlements with statistically increased or reduced macroseismic intensities during past earthquakes (for a detailed listing, see Appendix). Significance levels are derived using a binomial model (in case of less than 10 earthquake reports per site) an a normal model (more than 10 earthquake reports) - they provide rather a qualitative indication for site effects than a quantitatively reliable probability.

In some cases the results of such single site studies are well explained by the known geological features such as fine lake sediments (e.g. Lucerne), high groundwater levels, or 2D/3D ground motion amplification effects (e.g. some sites in the Valais). In others, we still lack an explanation. The density of points is driven by the density of villages with sufficient IDP's available. We might expect that for villages with heterogeneous site conditions the tendency is towards the positive intensity anomalies, however varying also in time due to the expansion of the settlement areas.

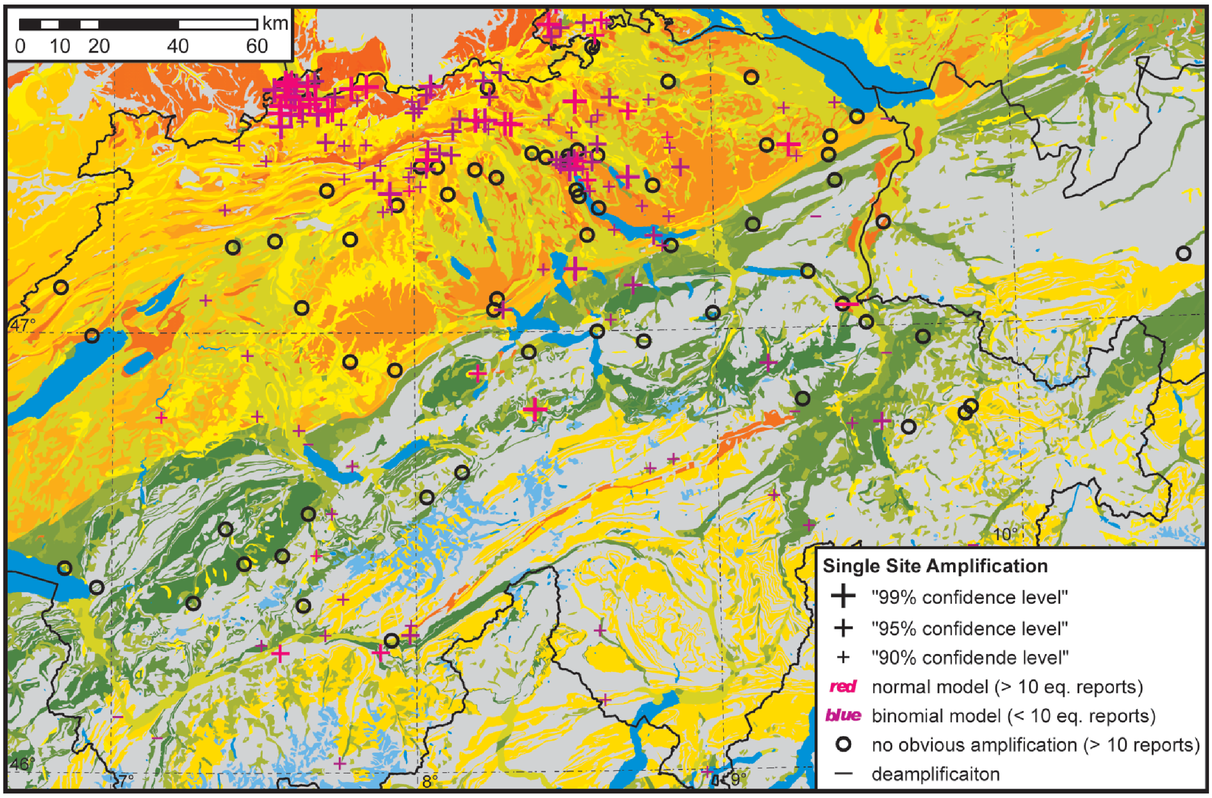

Figure 6: Settlements with a macroseismically detectable site amplification (+), no obvious amplification (o), or a detectable deamplification (–). While for sites with ten and more intensity reports, the amount of the amplification is tested for significance (normal model), for sites with less observations the confidence statement just refers to the sign of the amplification/deamplification (binomial model). Background: Site amplification map for Switzerland based on geological classification as shown in Figure 3.

3.5 *Regional effects and regionalization*

From previous research based on the old geotechnical map of Switzerland (Schweizerische Geologische Kommission 1967), we find indications for regional effects overlaying site effects. We therefore tested this hypothesis and repeated the analysis based on the new maps individually for 2, 3 or 6 sub-regions of Switzerland (see Table 2). However, given the availability of intensity assignments for amplification analysis of the same or similar geological soil conditions, we found no significant regional effects. We suppose that the regional effects in former studies were due to confounding with the influence of other, non-resolved parameters, such as sediment grain size, share of marl in mixed rocks etc.
In some cases, e.g. alpine lower freshwater molasses vs. midland lower freshwater molasses, our regionalisation coincides with the areas of typologically similar facies in the geological map. There we need additional research and possibly geophysical investigation to characterize the surface material and to answer the question whether different amplification behaviour is related to the properties of these facieses or to other, regional factors.

<table>
<tr><td rowspan="2">Alpine and Pre-alpine area
South of the line Lausanne – St. Margrethen</td><td></td><td>1. Western Alps
West of Solothurn</td></tr>
<tr><td></td><td>2. Eastern Alps
East of Solothurn</td></tr>
<tr><td rowspan="4">Foreland area
North of the Line Lausanne – St. Margrethen</td><td rowspan="2">Jura
North of the line La Dôle – Neuchâtel – Bienne – Brugg</td><td>3. Western Jura
West of Solothurn</td></tr>
<tr><td>4. Eastern Jura
East of Solothurn</td></tr>
<tr><td rowspan="2">Midland
Between Jura and Alps</td><td>5. Western midland
West of Solothurn</td></tr>
<tr><td>6. Eastern midland
East of Solothurn</td></tr>
</table>

Table 2 : Regionalization criteria used to test results for regional effects. See also Figure 7.

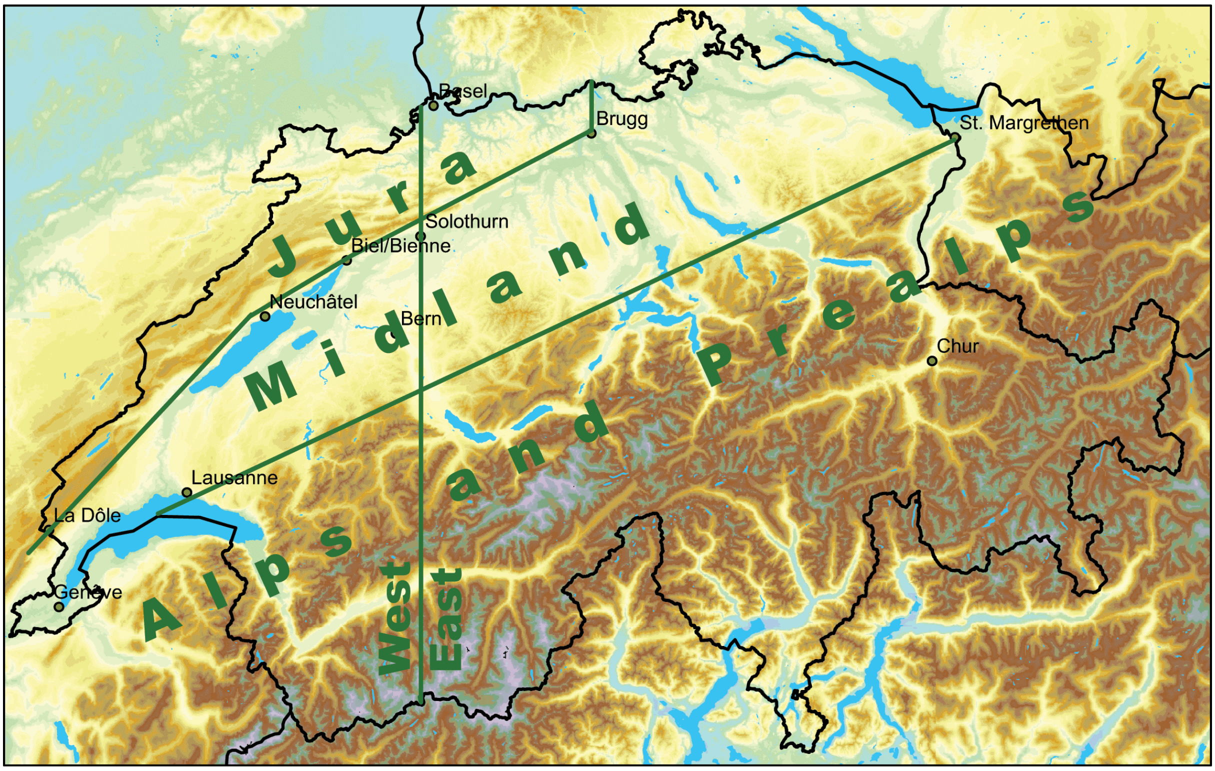

Figure 7: Regionalization criteria used to test results for regional effects. See also Table 2.

3.6 Overall mean amplification

Compared to the Swiss macroseismic attenuation relations, the analysed macroseismic dataset shows a mean overall amplification of 0.25 intensity units. Why? The attenuation relations describe the difference between alpine and foreland intensity attenuation as a function of the the epicentre location, without considering that systematic differences in soil condition exist between the typical felt area of alpine and forland events. This finding has been recognized in instrumental recordings (Bay et al., 2003): Seismic stations on rock in the foreland have in the mean a factor of 2 larger amplitudes when compared to Alpine stations.

Since the calibration dataset for attenuation relations contains the larger events of the 20th century, a typical alpine calibration event has many, mostly far-field IDPs in the foreland, and a typical foreland calibration event has many, mostly far-field IDPs in alpine areas. As a result, the attenuation relations tend to have lower intensities in the far-field attenuation of foreland events. They have higher intensities in the far-field attenuation of alpine events. The macroseismic dataset of our study has a larger number of foreland data than the dataset that was used for calibrating the attenuation relations (see Table 3). Therefore, the overall observed intensity is higher than expected from the attenuation relations. However, this finding only affects our interpretation of the reference site condition or zero point of site amplification. It does not affect the differences in expected intensities between different soil types.

Spatial distribution of IDPs (this study)				Spatial distribution of IDPs (ECOS calibration events)		
	No. IDP alpine	No. IDP foreland			No. IDP alpine	No. IDP foreland
Epicentre location alpine	4118	2449		Epicentre location alpine	1050	982
Epicentre location foreland	1047	6152		Epicentre location foreland	374	1206

Table 3: Spatial distribution of IDPs of earthquakes with epicentres in the alpine area, and the foreland, respectively: comparison of the base data of this study with those from the calibration events used to derive the intensity attenuation relations.

4 Application for recent earthquakes

To check the performance of intensity estimations based on magnitude, source depth, and local site conditions, we performed two case studies to compare modelled intensities with those derived from macroseismic questionnaires. In addition, intensities were estimated from recorded peak ground velocity at the stations of the Swiss seismic networks.
The first event is the earthquake of September 8, 2005(11:27 UTM) with its epicentre near Vallorcine in the French Alps: roughly 5 km from the French/Swiss border. The magnitudes are Ml = 4.9 and Mw = 4.5. The focal depth is about 7 km. The shaking was widely felt in the Chamonix region as well as in the Valais and caused rock falls, small landslides, and some minor damage to several settlements.
The second event was the induced earthquake of December 8, 2006, triggered by water injections during a deep heat-mining project (hot dry rock method) in the city of Basel (Deichmann et al. 2007). This event had a magnitude of Ml = 3.4 (Mw = 3.0) and a focal depth of 4.5 km. Due to its low depth and the densely populated area, this event caused notable public concern and about 2000 reports of small damage.
For both events, observed intensity was assessed using two methods:
Macroseismic intensity was derived from questionnaires collected with passive sampling (reports to a form on the website of the Swiss Seismological Service: http://www.seismo.ethz.ch/info/) as well as active sampling (personally addressed mailing) and semi-active sampling (mailing of paper questionnaires to stores, municipal and postal offices of the affected area for redistribution). Only intensity assignments of medium or good quality were used. *Instrumental intensity* was derived from peak ground velocities measured at permanent strong motion and broadband stations as well as from semi-permanent seismometers using the conversion rules discussed in Kästli & Fäh (2006). While strong motion sensors are often placed in settled areas, many of the broadband seismic stations from the Swiss digital network, especially in the alpine area are placed directly on hard rock; some are placed in caverns, some in places with strong topography, rising the question of possible 2d- and 3d-effects. However, as no macroseismic amplification/deamplification information is available for these individual sites, they are just handled as standard rock (no station correction). This may add some scatter especially in the case of the Vallorcine event. The instrumentally derived intensity observations were compared to an intensity estimation map based on the Swiss intensity attenuation relations and the site amplifications derived from the macroseismic data. For the Basel event, the attenuation relation for "shallow foreland events" was used. The intensity estimation map of the Vallorcine event is based on a weighted intermediate of estimates for "shallow alpine" and "deep alpine" events. For geological soil

classes with no site amplification defined from macroseismic data (mostly the unsettled alpine rock types), an amplification of zero was assumed.
A general overview of the observed and modelled intensity maps is given in Figures 8 a) and b). For a quantitative analysis, the observed intensities were compared to the mean expected intensities within a circle with a radius of 50 m around the instrument site (for PGV-derived intensities) or 250 m around the settlement centre (for macroseismic intensities). The comparison generally shows good agreement between observation and our model.
The average differences between observed and calculated macroseismic intensities are moderate (Figure 9): 0.3 intensity units for the Vallorcine event and 0.23 intensity units for the Basel event (instrumental intensity: 0.09 / 0.04). 44 of 72 observed macroseismic intensities are predicted correctly by the model: for 25 sites the predicted intensity differs by 1 unit from the observed intensity. Deviations are higher at low intensities (<= III) and may also result from erroneously assigned observed intensities: From five eyewitnesses in a village all reporting not to have felt an event, for example, an intensity I (earthquake not felt) can not be distinguished clearly from an intensity III (earthquake felt by 10-15% of the population).
The macroseismic field of the Basel event is affected not only by site effects, but also by distinct source radiation (Ripperger et al., 2008). The low values of the intensities in the south-east of Basel are due to reduced radiation of energy in that direction.
The relatively high bias of the macroseismic model in case of Basel may partially be a magnitude scaling effect: 36 vents with good moment magnitude detection with Mw 2.4…5.2 in and around Switzerland show a medium relationship of the SED local magnitude to the moment magnitude of Mw = Ml – 0.2 (Fäh et al. 2003), and this rule was applied for many events used for deriving the ECOS intensity attenuation, if Ml, but not Mw was known from instrumental measurements. Ml of the Basel event was 3.4. If, instead of the measured Mw = 3.0, an Mw = Ml-0.2 was used for the attenuation part of the intensity model, we would result in an overall model offset of 0.02 intensity units, and a near-source intensity estimation of 4.5, explaining perfectly the two groups of (integer) intensity IV and V observations in the epicentral area (see fig. 9a).For intensities derived from PGV, the deviations of the model are slightly higher (31 out of 65 are correct, another 28 with 1 unit deviation). Based on the data available, it is not obvious whether this is due to propagating errors from the PGV-to-intensity relationship or from site effects at the seismic stations. However, the error of the macroseismic intensity estimation is not distance-dependent, a finding which supports our attenuation relations (see Figure 9b).

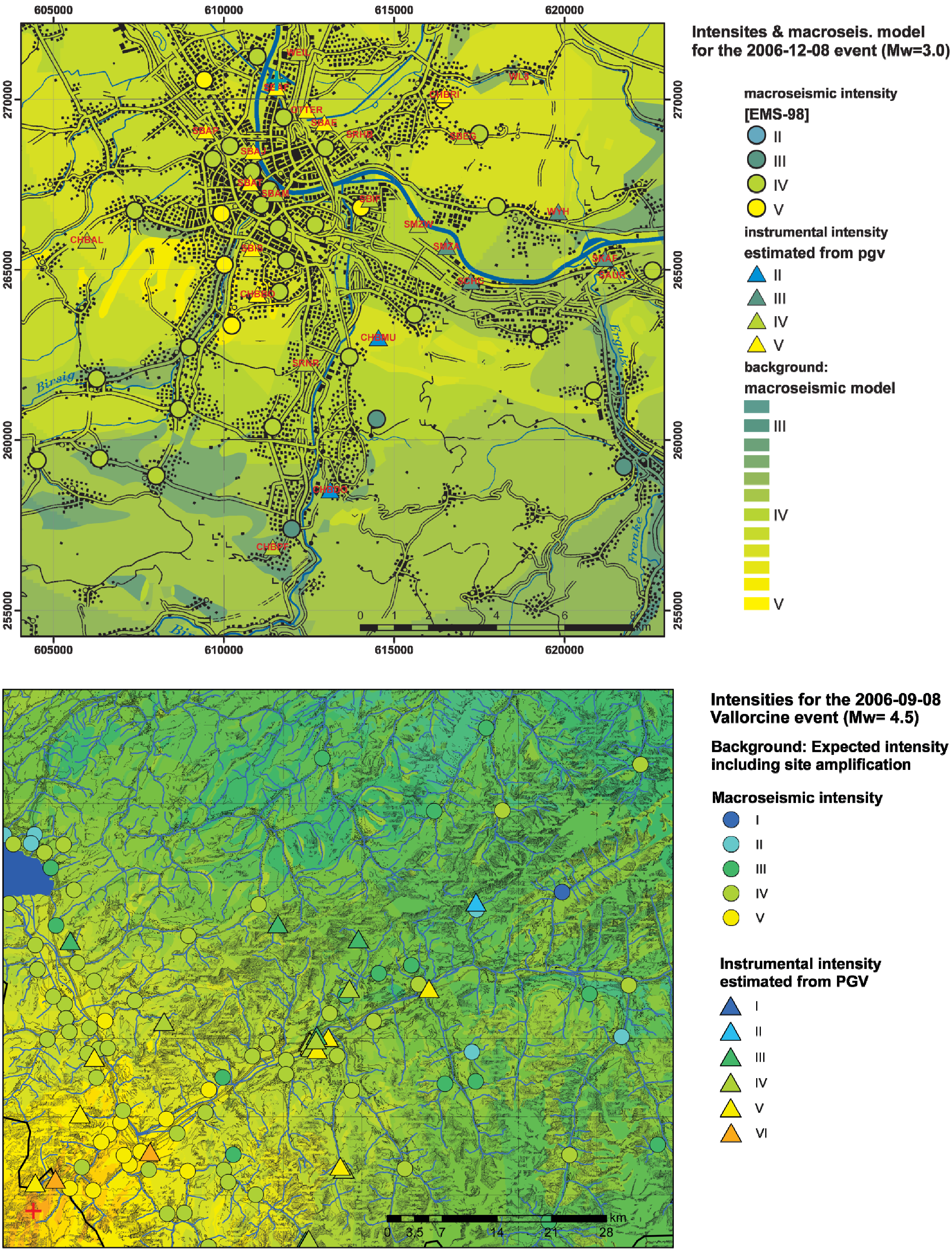

Figure 8a/b): Comparison of intensity estimations derived from magnitude, distance and site amplification to intensity values derived from questionnaires and PGV measurements for a) the 2005-09-08 Vallorcine event and b) the 2006-12-08 Basel event.

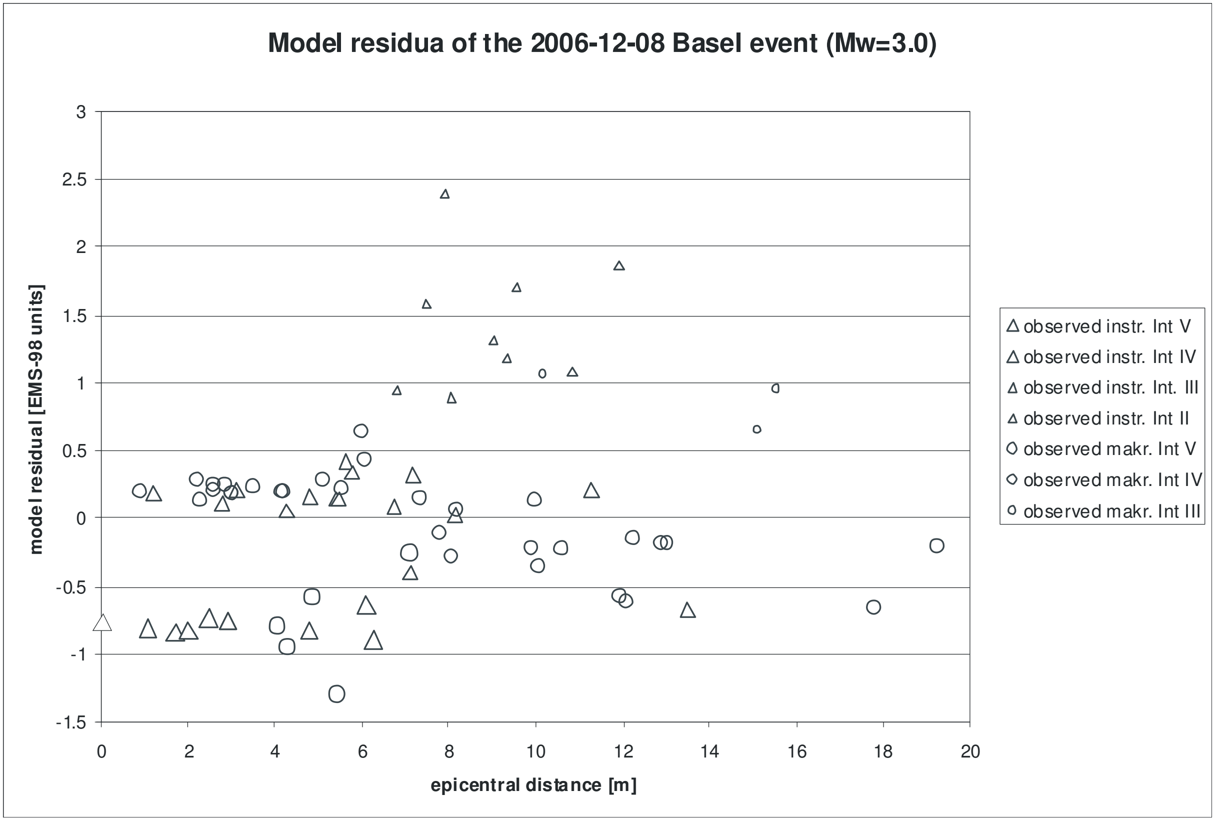

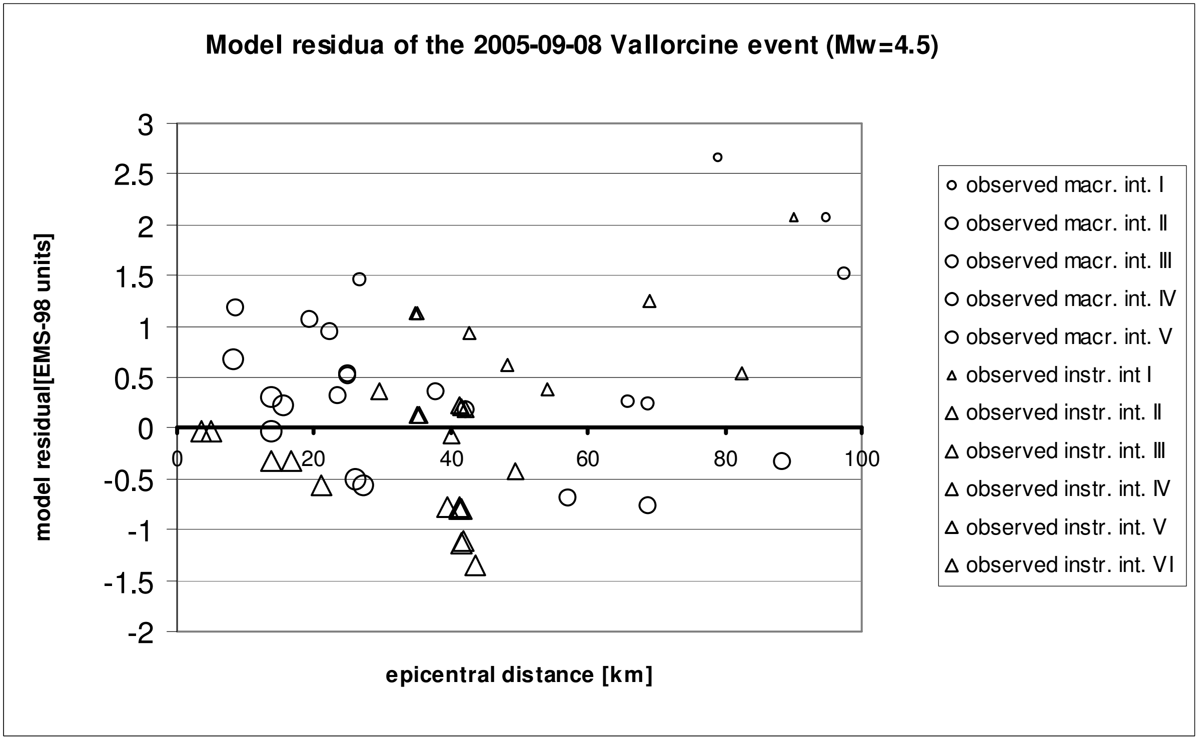

Figure 9a/b: Plot of distance versus difference between expected minus observed intensity; separated by event and by source of the intensity data (macroseismic observations, intensity derived from PGV).

5 Discussion

The Swiss macroseismic attenuation laws are valid for sites with consolidated sediments. We have found site amplifications of 0.3 to 0.75 EMS-98 intensity units to be typical for a set of geological soil classes describing different types of mostly soft sediments. For each class we provide the median values as well as error bounds. We found an influence of the sediment grain size, the compaction and cementation of deposits, the grade of sorting in loose sediments, the share of marl in mixed rocks and the related state of weathering. Thick layers of holocene sediments are not well covered by the analysed dataset.

If conservative hazard estimates should be calculated from the site amplifications described above, we recommend using the 75th-percentile amplification as a predictor rather than the median. This choice will account for a considerable spatial variance of amplification behaviour observed within most soil classes. For the amplification factors of typical Holocene alluvial sites, we recommend using the 75th-percentile for *all* site amplification calculations.

Although the new geological map 1:500’000 of Switzerland allows us to derive homogeneous amplification factors for single soil classes beneath most settlements, it still omits many aspects that proved important for site amplification at individual locations. These are, among others, the sediment layer thickness, heterogeneity of sediments, groundwater level, contrast in wave-velocity between bedrock and sediments, shape of the bedrock, and surface topography. In Switzerland, with its heterogeneous geology and small-scale structures, these factors vary considerably in space. As a result, describing site amplification simply by geological and geotechnical characteristics of the topmost layer may prove less effective than in places with homogeneous sedimentary basins. Still soil amplification estimates derived from geology and macroseismic data are currently the best data available for most parts of Switzerland. However geographical resolution is still limited in many regions. On a regional scale, information can be improved by assessing single-site intensity deviation, by using the results of microzonation studies, or by studying the local history of macroseimic reports.

The set of attenuation relations already contains a regionalisation of Switzerland (explicitly with the terms “alpine” and “foreland” as well as implicitly with the epicentral depth classification, since typical epicentral depth varies between different regions of Switzerland). Although this classification refers to the epicentre location and not the location of the IDP, there may be some confounding between characteristics of the attenuation relations and site effects, since epicentres are spatially correlated to their macroseismic fields, and intensity attenuation is derived from IDPs not corrected for local site amplification. As a result, the geology-specific site amplification factors presented here are valid only for Switzerland and the nearest adjacent areas, and their absolute values are valid only with reference to the used attenuation relations. If applied to other regions or relative to other attenuation laws, they might under- or overestimate site amplification effects. We suggest that a next generation of macroseismic attenuation relations should be developed from combined assessments of attenuation and site amplification.

Two case studies, with observed macroseismic intensities up to V, were modelled based on magnitude, intensity attenuation and site amplification. Observed intensities were predicted with a maximal error of one intensity unit in more than 95 % of the cases. Such models are presently implemented in a shakemap tool, and might be used for earthquake loss scenarios. The macroseismic attenuation relation as well as site amplification are both calibrated with intensities up to VIII in some cases. We therefore suggest using the presented site amplification factors for earthquakes with magnitudes between 3 and 5.5. However, we presently lack independent real world data to assess the model performance against a larger, damaging earthquake.

6 Acknowledgements

We would like to thank Syed Mohammed Baqir Bukhari for his help with relocating the settlement barycentres, and our English editor, Dr. Kathleen J. Jackson, for the language review.

References

Akaike, H. 1974. A new look at the statistical model identification. IEEE Transactions on Automatic Control 19(6), 716-723.

Ambraseys, N. N. 1985. Intensity-attenuation and magnitude-intensity relationships for western European earthquakes. *Earthquake Eng. Struct. Dyn.* 13, 733-778.

Bakun, W. H. & Wentworth, C. M., 1997. Estimating earthquake location and magnitude from seismic Intensity data, *Bull. Seism. Soc. Am.*, 87, pp. 1502–1521.

Bay, F., D. Fäh, L. Malagnini, and D. Giardini 2003. Spectral shear-wave ground motion scaling for Switzerland. *Bull. Seism. Soc Am.*,Vol.93, 414-429.

Bay, F., S. Wiemer, D. Fäh, and D. Giardini 2005. Predictive ground motion scaling in Switzerland: Best estimates and uncertainties. *J. Seismol.* 9, 223-240.

Beer, Ch. 1997. Erdbebengefährdung in Abhängigkeit vom Geologischen Untergrund. In: *Beiträge zur Geologie der Schweiz, Geotechnische Serie Nr. 92*. Zürich, Schweizerische Geotechnische Kommission.

Bundesamt für Landestopographie 2006. Geologische Karte der Schweiz im Massstab 1:500'000; Vektordatensatz. Bern, Bundesamt für Landestopotraphie.

Bundesamt für Landestopographie 2006. Tektonische Karte der Schweiz im Massstab 1:500'000; Vektordatensatz. Bern, Bundesamt für Landestopotraphie.

Commission of the European Communities 2001. Eurocode 8: Design of structures for earthquake resistance. Part 1: General rules, seismic actions and rules for buildings. Bruxelles, Commission of the European Communities, European Committee for Standardization.

Deichmann N., C. Bachmann, F. Bethmann, J. Ernst, K. Evans, D. Fäh, D. Giardini, M. Häring, S. Husen, P. Kästli, M. Mai, J. Ripperger, U. Schanz, S. Wiemer 2007. Seismicity Induced by Water Injection for Geothermal Reservoir Stimulation 5 km Below the City of Basel, Switzerland. In: *EOS, Trans. AGU, Fall Meet. Suppl., Abstract V53F-08*

Fäh, D., D. Giardini, F. Bay, F. Bernardi, J. Braunmiller, N. Deichmann, M. Furrer, L. Gantner, M. Gisler, D. Isenegger, M.J. Jimenez, P. Kästli, R. Koglin, V. Masciadri, M. Rutz, C. Scheidegger, R. Schibler, D. Schorlemmer, G. Schwarz-Zanetti, S. Steimen, S. Sellami, S. Wiemer, J. Wössner, 2003. Earthquake Catalogue Of Switzerland (ECOS) And The Related Macroseismic Database. *Eclogae geol. Helv.* 96, 219-236.

Fäh, D. 1985. Seismische Mikrozonierung der Schweiz. Diploma Thesis at the Institute of Geophysics. Zürich, Swiss Federal Institute of Technology.

Fäh, D., P. Kästli, S. Steimen 2005. Earthquake Scenarios and Shake-Maps based on Ground Motion and Macroseismic Information. Lisbon, Mundiconvenius.

Fritsche, F., Fäh D. in prep. The 1946-Earthquake in the Valais: Historical and Geophysical Studies with Respect to Damage Fields and Site-Effects.

Gallipoli M. R., M. Mucciarelli, D. Albarello, V. Lapenna, M. Schiattarella, G. Calvano 2003: Hints about site amplification effects comparing macroseismic hazard estimate with microtremor measurements: the Agri valley (Italy) example. *J. Earthq. Eng.* 7, 51-72.

Gasparini, P. 2001. The attenuation of seismic Intensity in Italy: a bilinear shape indicates the dominance of deep phases at epicentral distances longer than 45km. *Bull. Seism. Soc. Am.*, 91, 826-841.

Grünthal, G. 1998. European Macroseismic Scale 1998. *Cahiers du Centre Européen de Géodynamique et de Séismologie, volume 15*. Luxembourg, Centre Européen de Géodynamique et de Séismologie.

Kästli, P., D. Fäh 2006. Rapid estimation of macroseismic effects and shake maps combining macroseismic and instrumental data. Proceedings of the *First European Conference on Earthquake Engineering and Seismology* (ECEES), Genève (CD ROM).

Kästli, P, M. Gisler, D. Fäh 2006b . Expert judgement versus automatic and statistical analysis of macroseismic questionnaires. Proceedings of the *First European Conference on Earthquake Engineering and Seismology* (ECEES), Genève (CD ROM).

Medvedev S. V., W. Sponheuer, V. Karnik 1964. Seismic intensity Scale. *Adac. Sci. USSR, Sov. Geophys. Comm.*

Rodriguez Marek A., J. D. Bray, N. A. Abrahamson 1999. Empirically Based Geotechnical Seismic Site Classification. In: W. M. Elliott, P. McDonough. Optimizing Post-Earthquake Lifeline System Reliability (Proceeding of the 5th U.S. conference on Lifeline Earthquake Engineering. *Technical council on Lifeline Earthquake Engineering Monograph No. 16.*

Roten, D., Fäh, D., Olsen, K.B & Giardini D., 2008. A comparison of observed and simulated site response in the Rhone valley. Geophysical J. Int., 173, 3, 958-978.

Schweizerische Geologische Kommission 1967. Vereinfachte geotechnische Karte der Schweiz 1:200'000. Bern, Kümmerly & Frey.

SED (Schweizerischer Erdbebendienst) 2002. ECOS - Earthquake Catalog of Switzerland. Zurich – online at http://www.seismo.ethz.ch, Swiss Seismological Service, ETHZ.

SIA 2003. Einwirkungen auf Tragwerke - SIA Norm 261. Zürich, Schweizerischer Ingenieure- und Architektenverband.

Wald, D. J., V. Quitoriano, T. H. Heaton, H. Kanamori 1999. Relationship between Peak Ground Acceleration, Peak Ground Velocity, and Modified Mercalli Intensity for Earthquakes in California, *Earthq. Spectra* 15, 557-564.

Appendix: Amplification behaviour of individual settlements

Table 7a/b): typical intensity residuals for a set of Swiss settlements.
(+)/+ / ++: positive deviation of the detected intensities from expected intensities calculated from attenuation is significant nominally at a 90 / 95 / 99 % probability level.
(–)/–/– – : negative deviation, significant at a 90 / 95 / 99 % probability level.
While in case of 10 and more intensity assignments, a normal model is used (indicating that the average intensity deviation is different from zero), sites with sparse data were tested with a binomial model (testing just for the sign of the residual). Significance levels are more hints for possible amplification effects than real probabilities, as the testing strategy does not account for multiple testing, nor (in case of the normal model) for the fact that the observed standard deviation of the residuals may not represent their true variability.

a) All sites with 10 and more intensity assignments available (significance hint based on a normal model)						
Zip	place name	average intensity deviation	# intensity assignments	# intensity higher than expected	# intensity lower than expected	significance hint
5000	Aarau	0.58	35	30	5	++
9000	St. Gallen	0.20	31	19	12	
4600	Olten	0.39	30	23	7	++
8400	Winterthur	0.38	29	19	10	+
8200	Schaffhausen	0.39	28	17	11	+
6300	Zug	0.51	27	21	6	+
4410	Liestal	0.48	26	21	5	+
5400	Baden	0.39	24	20	4	++
8000	Zürich	0.41	24	17	7	+
6010	Kriens	0.04	21	11	10	
8610	Uster	0.46	21	17	4	+
8134	Adliswil	0.62	20	14	6	++
1700	Fribourg	0.36	20	14	6	(+)
4500	Solothurn	0.18	20	10	10	
4000	Basel	0.08	19	11	8	
7180	Disentis/Muster	0.35	19	13	6	
3860	Meiringen	0.35	19	11	8	
4102	Binningen	0.56	18	17	1	++
8750	Glarus	0.12	18	12	6	
8802	Kilchberg/ZH	0.45	18	11	7	
4900	Langenthal	0.34	18	12	6	
4133	Pratteln	0.85	18	17	1	++
4127	Birsfelden	0.12	17	11	6	
7270	Davos Platz	0.22	17	8	9	
8953	Dietikon	0.14	17	11	6	
8600	Dübendorf	0.25	17	10	7	
6390	Engelberg	0.75	17	13	4	++
9100	Herisau	0.33	17	12	5	
4313	Möhlin	0.65	17	14	3	++
2000	Neuchâtel	0.39	17	10	7	

8212	Neuhausen am Rheinfall	0.54	17	13	4	+
4153	Reinach BL	0.45	17	15	2	+
3920	Zermatt	0.37	17	12	5	
6460	Altdorf	0.37	16	10	6	
7310	Bad Ragaz	-0.27	16	5	11	
4051	Basel	0.62	16	12	4	++
8640	Rapperswil SG	0.31	16	12	4	
6370	Stans	0.09	16	9	7	
3930	Visp	0.37	16	11	5	+
9630	Wattwil	0.25	16	9	7	
5430	Wettingen	0.46	16	14	2	++
4800	Zofingen	0.30	16	10	6	
3715	Adelboden	-0.19	15	7	8	
4144	Arlesheim	0.35	15	12	3	(+)
8840	Einsiedeln	0.11	15	12	3	
6410	Goldau	0.09	15	10	5	
3818	Grindelwald	0.40	15	9	6	
8280	Kreuzlingen	0.90	15	13	2	++
3954	Leukerbad	-0.23	15	8	7	
4104	Oberwil BL	0.65	15	12	3	++
4123	Allschwil	0.51	14	12	2	+
7050	Arosa	0.15	14	7	7	
8180	Bülach	0.83	14	12	2	++
7260	Davos Dorf	0.02	14	7	7	
9230	Flavil	0.37	14	9	5	
8215	Hallau	0.82	14	11	3	++
3718	Kandersteg	0.50	14	10	4	(+)
3550	Langnau im Emmental	0.23	14	8	6	
8952	Schlieren	-0.04	14	6	8	
6430	Schwyz	0.27	14	10	4	
3800	Unterseen	0.52	14	10	4	+
1800	Vevey	-0.10	14	8	6	
8820	Wädenswil	0.05	14	10	4	
8620	Wetzikon ZH	0.41	14	8	6	
9500	Will SG	0.11	14	7	7	
6340	Baar	0.24	13	8	5	
4057	Basel	0.55	13	9	4	+
4054	Basel	0.41	13	10	3	
9200	Gossau SG	0.63	13	11	2	++
2300	La Chaux-de-Fonds	0.34	13	9	4	
3775	Lenk im Simmental	0.19	13	8	5	
6014	Littau	0.43	13	9	4	
4142	Münchenstein	0.49	13	11	2	++
4310	Rheinfelden	0.83	13	11	2	++
5032	Rohr AG	0.41	13	10	3	
6060	Sarnen	0.58	13	11	2	+
3770	Zweisimmen	-0.11	13	6	7	
4055	Basel	0.24	12	7	5	
4053	Basel	0.35	12	10	2	(+)

4103	Bottmigen	1.06	12	11	1	++
3400	Burgdorf	0.18	12	7	5	
2540	Grenchen	0.37	12	8	4	
8853	Lachen SZ	0.20	12	7	5	
5080	Laufenburg	0.61	12	11	1	+
8706	Meilen	0.18	12	8	4	
4132	Muttenz	0.50	12	11	1	++
4665	Oftringen	0.61	12	11	1	+
9400	Rorschach	0.21	12	7	5	
7320	Sargans	-0.88	12	2	10	—
5012	Schönenwerd	0.10	12	8	4	
3960	Sierre	0.72	12	8	4	+
4106	Therwil	0.62	12	11	1	++
8304	Wallisellen ZH	0.75	12	10	2	++
5610	Wohlen AG	-0.04	12	7	5	
8004	Zürich	0.08	12	8	4	
9050	Appenzell	0.08	11	8	3	
4058	Basel	0.35	11	9	2	
4056	Basel	0.89	11	10	1	++
6500	Bellinzona	-0.07	11	6	5	
3900	Brig	0.24	11	7	4	
5200	Brugg AG	0.69	11	10	1	++
6440	Brunnen	0.28	11	7	4	
7075	Churwalden	0.29	11	9	2	
4657	Dulliken	0.54	11	10	1	+
6020	Emmenbrücke	-0.12	11	5	6	
8500	Frauenfeld	0.02	11	6	5	
4402	Frenkendorf	0.39	11	10	1	++
5070	Frick	0.32	11	9	2	
3714	Frutigen	0.41	11	7	4	
4460	Gelterkinden	0.57	11	9	2	++
8340	Hinwil	0.33	11	7	4	(+)
4303	Kaiseraugst	0.21	11	9	2	
6403	Küssnacht am Rigi	-0.22	11	4	7	
5600	Lenzburg	0.06	11	7	4	
8315	Lindau	-0.04	11	5	6	
1920	Martigny	-0.37	11	5	6	
8887	Mels	-0.04	11	5	6	
6436	Muotathal	-0.04	11	5	6	
4125	Riehen	0.90	11	10	1	++
8803	Rüschlikon	0.38	11	8	3	
9053	Teufen AR	0.19	11	8	3	
5726	Unterkulm	0.46	11	8	3	
8880	Walenstadt	0.45	11	6	5	
8006	Zürich	0.56	11	9	2	+
8037	Zürich	0.22	11	8	3	
5330	Zurzach	0.60	11	9	2	(+)
4710	Balsthal	0.19	10	6	4	
4052	Basel	0.41	10	9	1	+
3011	Bern	0.36	10	8	2	

5312	Döttingen	0.51	10	7	3	
9642	Ebnat-Kappel	-0.09	10	6	4	
6182	Eschholzmatt	0.12	10	5	5	
7017	Flims Dorf	0.14	10	5	5	
4414	Füllinsdorf	0.68	10	9	1	++
3785	Gsteig b. Gstaad	-0.06	10	5	5	
1820	Montreux	0.15	10	6	4	
8462	Rheinau	0.10	10	5	5	
8630	Rüti ZH	0.26	10	8	2	
5745	Safenwil	0.78	10	8	2	(+)
7220	Schiers	-0.16	10	4	6	
8226	Schleitheim	0.73	10	9	1	++
5034	Suhr	0.42	10	7	3	
8488	Turbenthal	0.52	10	7	3	(+)
8570	Weinfelden	0.26	10	6	4	
8702	Zollikon	0.71	10	8	2	+
8050	Zürich	-0.04	10	5	5	

b) sites with less than 10 intensity assignments available, but indices for site amplification (significance hint based on binomial model)

Zip	place name	average intensity deviation	# intensity assignments	# intensity higher than expected	# intensity lower than expected	Significance hint
8852	Altendorf	0.49	9	7	2	(+)
9220	Bischofszell	0.44	9	7	2	(+)
6330	Cham	0.37	9	7	2	(+)
8157	Dielsdorf	0.51	9	7	2	(+)
8127	Forch	0.45	9	7	2	(+)
8606	Greifensee	0.49	9	7	2	(+)
8700	Küsnacht ZH	0.74	9	7	2	(+)
4415	Lausen	0.55	9	7	2	(+)
6003	Luzern	0.88	9	8	1	+
8213	Neunirch	0.63	9	8	1	+
7500	St. Moritz	-0.71	9	2	7	(–)
4802	Strengelbach	0.78	9	7	2	(+)
4632	Trimbach	0.46	9	7	2	(+)
4612	Wangen b. Olten	0.40	9	8	1	+
8005	Zürich	0.38	9	8	1	+
8048	Zürich	0.48	9	8	1	+
8910	Affoltern am Albis	-1.01	8	1	7	–
6780	Airolo	1.23	8	7	1	+
4059	Basel	0.36	8	8		++
8494	Bauma	1.26	8	7	1	+
8305	Dietlikon	0.91	8	7	1	+
5412	Gebenstorf	0.59	8	8		++
5082	Kaisten	0.92	8	7	1	+

5314	Kleindöttingen	0.53	8	7	1	+
5035	Unterentfelden	0.79	8	7	1	+
5012	Wöschnau	0.55	8	7	1	+
8047	Zürich	0.67	8	7	1	+
4147	Aesch BL	0.83	7	7		++
3803	Beatenberg	0.77	7	6	1	(+)
8627	Grüningen	0.58	7	6	1	(+)
4434	Hölstein	0.16	7	6	1	(+)
6900	Lugano	0.24	7	6	1	(+)
3962	Montana-Vermala	0.78	7	6	1	(+)
3904	Naters	0.80	7	6	1	(+)
5013	Niedergösgen	0.67	7	6	1	(+)
8153	Rümlang	0.76	7	6	1	(+)
7188	Sedrun	0.84	7	6	1	(+)
7132	Vals	0.81	7	6	1	(+)
4803	Vordemwald	0.73	7	6	1	(+)
8032	Zürich	0.48	7	6	1	(+)
8051	Zürich	0.65	7	6	1	(+)
8045	Zürich	0.70	7	7		++
6493	Hospental	1.19	6	6		+
4654	Lostorf	1.03	6	6		+
5107	Schinznach Dorf	0.76	6	6		+
8730	Uznach	-1.76	6		6	–
5303	Würenlingen	0.56	6	6		+
8057	Zürich	0.60	6	6		+
8222	Beringen	0.86	5	5		+
4126	Bettingen	0.65	5	5		+
8767	Elm	0.59	5	5		+
9473	Gams	-0.82	5		5	–
5073	Gipf-Oberfrick	0.96	5	5		+
3902	Glis	0.70	5	5		+
5024	Küttingen	0.85	5	5		+
8413	Neftenbach	1.12	5	5		+
5102	Rupperswil	0.65	5	5		+
5224	Unterbözberg	0.88	5	5		+
8217	Wilchingen	1.13	5	5		+
4417	Ziefen	1.11	5	5		+
8044	Zürich	0.57	5	5		+
9320	Arbon	1.18	4	4		(+)
5413	Birmenstorf AG	0.53	4	4		(+)
6658	Borgnonoe	1.42	4	4		(+)
6675	Cevio	2.03	4	4		(+)
4658	Däniken SO	1.01	4	4		(+)
4143	Dornach	0.91	4	4		(+)
8132	Egg b. Zürich	1.07	4	4		(+)
5074	Eiken	0.82	4	4		(+)
4458	Eptingen	0.83	4	4		(+)

3916	Ferden	0.32	4	4		(+)
3945	Gampel	0.86	4	4		(+)
1204	Genève	0.67	4	4		(+)
3626	Hünibach	-1.17	4		4	(–)
3723	Kiental	0.67	4	4		(+)
4245	Kleinlützel	0.90	4	4		(+)
5742	Kölliken	0.97	4	4		(+)
7031	Laax GR	-1.38	4		4	(–)
4438	Langenbruck	0.94	4	4		(+)
8426	Lufingen	1.04	4	4		(+)
5242	Lupfig	0.49	4	4		(+)
3250	Lyss	0.77	4	4		(+)
4312	Magden	0.65	4	4		(+)
7436	Medels im Rheinwald	1.94	4	4		(+)
2740	Moutier	0.51	4	4		(+)
8425	Oberembrach	0.55	4	4		(+)
9424	Rheineck	-0.85	4		4	(–)
3132	Riggisberg	0.72	4	4		(+)
8427	Rorbas	0.47	4	4		(+)
6343	Rotkreuz	1.43	4	4		(+)
1922	Salvan	-1.11	4		4	(–)
8203	Schaffhausen	1.00	4	4		(+)
7419	Scheid	1.03	4	4		(+)
6215	Schwarzenbach b. Beromünster	0.16	4	4		(+)
1933	Sembrancher	-0.61	4		4	(–)
3613	Steffisburg	1.38	4	4		(+)
4246	Wahlen b. Laufen	0.80	4	4		(+)
8542	Wiesendangen	0.61	4	4		(+)
8492	Wila	0.97	4	4		(+)
9658	Wildhaus	-1.12	4		4	(–)
5210	Windisch	0.55	4	4		(+)
4443	Wittinsburg	0.91	4	4		(+)
7205	Zizers	-0.99	4		4	(–)